The Dissertation Committee for Yi-Bo Wang certifies that this is the approved version of the following dissertation:

Pulmonary Delivery of Brittle Matrix Powders Produced by Thin Film Freezing

Committee:

Robert O. Williams III, Supervisor

James W. McGinity

Jay I. Peters

Hugh D. Smyth

Alan B. Watts

Zhengrong Cui

Pulmonary Delivery of Brittle Matrix Powders Produced by Thin Film Freezing

By

Yi-Bo Wang, B.S.;M.S.

Dissertation

Presented to the Faculty of the Graduate School of

The University of Texas at Austin

in Partial Fulfillment

of the Requirements

for the Degree of

Doctor of Philosophy

The University of Texas at Austin

December 2013

Dedication

To my loving and supportive family, my wife Grace Wang,
my father Mr. Jian Wang and mother Mrs. Yanbin Xu

Acknowledgement

First of all, I would like to express my sincere appreciation to my supervising professor, Dr. Robert O. Williams III for providing me the opportunity to work under his guidance for the past four and a half years. Thank you for sharing your extensive knowledge of pharmaceutics with me throughout my graduate study. I am grateful for his suggestive guidance, incessant encouragement, caring and understanding mentorship. I would like to thank Dr. Alan B. Watts, for his constructive suggestions, experimental ideas, and substantial guidance to my research and scientific writing. I greatly appreciated Dr. Jay I. Peters, for bringing his in-depth clinical expertise into my research and many insightful suggestions on my papers. This dissertation would not have been possible without their persistent help. I would also like to extend my gratitude to the other members of my committee, Dr. James W. McGinity, Dr. Hugh D. Smyth and Dr. Zhengrong Cui, for their guidance and encouragement on my coursework, research and writing throughout my graduate education.

I am genuinely thankful to many other faculty members in the College of Pharmacy who have assisted me in the last four and a half years. Dr. Salomon Stavchansky, thank you for giving me the opportunity to TA for your pharmacokinetics class. It was a valuable experience and did help a lot for my PK data analysis. Dr. Hugh Smyth, thank you for giving me the opportunity to become a student leader with the AAPS student chapter and letting me TA for compounding lab. Dr. Jason McConville, thank you for

sharing your knowledge and experience of dissolution testing and pulmonary drug delivery with me. To other professors whom I have learned from in the classroom, Dr. Cui Zhengrong, Dr. Janet Walkow, Dr. Maria Croyle, Dr. Krishnendu Roy, Dr. Carlton Erickson, Dr. Christopher Frei, Dr. Ananth Annapragada and Dr. John Koleng, thank you as well.

I would also like to acknowledge the staff in the College of Pharmacy, Yolanda Abasta, Stephanie Crouch, Claudia McClelland, Belinda Lehmkuhle, Jay Hamman, John Reineke, Jim Baker, Joe Adcock, Herman Schwarzer and Sharla Brewer, for the support they gave to all the graduate students.

I give thanks to my fellow graduate students in pharmaceutics for their assistance, friendship and guidance: Dr. Nicole Beinborn, Dr. Hélène Lirola, Dr. Meimei Zhang, Dr. Houli Li, Dr. Stephanie Bosselmann, Dr. Kevin O'Donnell, Dr. Bo Lang, Dr. Thiago Carvalho, Dr. Javier Morales, Dr. Sumalee Thitinan, Dr. Shih-fan Jang, Dr. Justin Hughey, Dr. Yoen-Ju Son, Sha Liu, Ping Du, Ju Du, Simone Carvalho, Justin Keen, Ryan Bennett, Soraya Hengsawas, Siyuan Huang, Chris Brough, Xin Hua, Shengnan Tan, Ashkan Yazdi, Nihal Bandara and Matt Herpin.

To those at UTHSC in San Antonio that have assisted me in quantification of tacrolimus in the whole blood and lung tissue: Dr. Martin Javors and Gregory Friesenhahn, your work was critical to my research.

Finally, I'd like to thank my loving and supportive family. My dear wife, Grace, I am grateful for her unconditional love, understanding, patience and endless encouragement for me to pursue my dream. My father Jian and mother Yanbin, who have been

unreservedly supportive for my graduate study in the US financially and spiritually. I am thankful to my mother-in-law, Lihua, for being a mother to me when my parents are not around. Lastly, I appreciate the care and support from all my friends in Austin.

Pulmonary Delivery of Brittle Matrix Powders Produced by Thin Film Freezing

Yi-Bo Wang, Ph.D

The University of Texas at Austin, 2013

Supervisor: Robert O. Williams III

Recently, the portfolio of compounds approved for inhalation therapy has expanded rapidly for lung disease therapies. The rationale for this delivery approach includes a more targeted and localized delivery to the diseased site with reduced systemic exposure, potentially leading to decreased adverse side effects. We have proposed that brittle matrix powders prepared by thin film freezing (TFF) are a suitable platform for pulmonary drug delivery which can achieve high lung concentrations while limit the corresponding systemic levels associated with toxicity, and enhanced physicochemical and aerodynamic properties can be obtained by varying TFF processing parameters.

In Chapter 2, the in vitro and in vivo performance of an amorphous formulation prepared by TFF and a crystalline micronized formulation produced by milling was compared for Tacrolimus (TAC). TFF processed matrix powders was capable of achieving deep lung delivery due to its low density, highly porous and brittle characteristics. When emitted from a Miat® monodose inhaler, TFF processed TAC formulations exhibited a fine particle fraction (FPF) of 83.3% and a mass median

aerodynamic diameter (MMAD) of 2.26 μm. Single dose 24-h pharmacokinetic studies in rats demonstrated that the TAC formulation prepared by TFF exhibited higher pulmonary bioavailability with a prolonged retention time in the lung, possibly due to decreased clearance (e.g., macrophage phagocytosis), compared to the micronized TAC formulation. Additionally, TFF formulation generated a lower systemic TAC concentration with smaller variability than the micronized formulation following inhalation, potentially leading to reduced side effects related to the drug in systemic circulation.

Chapter 3 investigated the impact of processing parameters in the TFF process on the physicochemical and aerodynamic properties of the resulting formulations. All of these enhanced powder properties resulted from higher freezing rate contributed to a better aerodynamic performance of the obtaining formulations. Moreover, a decreasing trend of FPF was observed for these TFF powders when the initial solid concentrations increased. The variation of the freezing rate and initial solid loading in the TFF process enabled the production of formulations with enhanced physicochemical properties and improved aerodynamic performance.

Table of Contents

List of Tables ix
List of Figures xi
Chapter 1 : The Impact of Pulmonary Diseases on the Fate of Inhaled Medicines 1
1.1 Abstract 1
1.2 Introduction 2
1.3 Lung physiology and pathophysiology 4
1.4 Drug deposition altered by lung diseases 7
1.4.1 Present State of Art 7
1.4.2 Modeling of aerosol deposition and associated lung diseases 12
1.5 Drug absorption affected by lung diseases 20
1.6 Pulmonary clearance influenced by lung diseases 26
1.6.1 Mucociliary clearance and impact of lung diseases 26
1.6.2 Alveolar macrophage uptake 31
1.6.3 Clearance modeling 34
1.7 Clinical Aspects 35
1.8 Concluding Remarks 37
1.9 References 37
Chapter 2 : In Vitro and In Vivo Performance of Dry Powder Inhalation Formulations: Comparison of Particles Prepared by Thin Film Freezing and Micronization 54
2.1 Abstract 54
2.2 Introduction 55
2.3 Materials and methods 59
2.3.1 Materials 59
2.3.2 Preparation of micronized TACMAN and TFF TACMAN 59
2.3.3 Differential Scanning Calorimetry (DSC) 61
2.3.4 Powder X-ray Diffraction (XRD) 61
2.3.5 Attenuated Total Reflectance-Fourier Transform Infrared Spectroscopy (ATR-FTIR) 62
2.3.6 Scanning Electron Microscopy (SEM) 62
2.3.7 Brunauer–Emmett–Teller (BET) specific surface area analysis 62
2.3.8 Geometric particle size measurement 63
2.3.9 In vitro aerosol performance 63

2.3.10 In vivo pulmonary dosing in rats 65
2.3.11 Quantification of TAC concentration in the lung and blood 66
2.3.12 Pharmacokinetic and statistical analysis 68
2.4 Results and discussion 68
2.4.1 Crystallinity 68
2.4.2 Molecular interactions investigated by ATR-FTIR 71
2.4.3 Morphology, geometric particle size and aerodynamic properties 72
2.4.4 Pharmacokinetic analysis of micronized TACMAN verses TFF TACMAN 76
2.5 Conclusion 81
2.6 References 81
Chapter 3 : Effect of Processing Parameters on the Physicochemical and Aerodynamic Properties of Respirable Brittle Matrix Powders Produced by Thin Film Freezing 88
3.1 Abstract 88
3.2 Introduction 89
3.3 Materials and Methods 92
3.3.1 Materials 92
3.3.2 Formulation Preparation 92
3.3.3 Differential Scanning Calorimetry (DSC) 93
3.3.4 Powder X-ray Diffraction (XRD) 93
3.3.5 Powder Bulk Density and Porosity 94
3.3.6 Brunauer–Emmett–Teller (BET) specific surface area analysis 94
3.3.7 Aerodynamic Performance 94
3.3.8 Geometric Particle Size Measurement 96
3.3.9 Mechanical Testing 96
3.4 Results and Discussion 97
3.4.1 Formulations prepared by different freezing processes 97
3.4.2 TFF powders prepared at different initial solid concentrations 102
3.5 Conclusion 105
3.6 References 106
Tables 109
Figures 128
Appendices 162

Appendix A: Prior Arts for Inhaled Tacrolimus 162
A.1 Purposes 162
A.2 Methods 162
A.3 Results 162
Appendix B: Optimization of Fine Particle Fraction (FPF) of TFF TACMAN (1:1) by Acoustic Mixing 163
B.1 Purposes 163
B.2 Methods 163
B.3 Results 164
Appendix C: Determination of Patient and Device Dependence of TFF TACMAN .. 166
C.1 Purposes 166
C.2 Methods 166
C.3 Results 167
C.4 References 168
Appendix D: Physical Stability of TFF processed powders 169
D.1 Purposes 169
D.2 Methods 169
D.3 Results 169
Appendix E: Residual Solvent Analysis of TFF-processed Powders by Thermogravimetric Analysis (TGA) 171
E.1 Purposes 171
E.2 Methods 171
E.3 Results 171
E.4 References 172
Appendix F: Aerodynamic properties of micronized TACMAN (1:1) 173
F.1 Purposes 173
F.2 Methods 173
F.3 Results 174
Appendix G: Determination of Tacrolimus Concentrations in the Bronchoalveolar Lavage (BAL) Fluid 174
G.1 Purposes 174
G.2 Methods 174
G.3 Results 175

G.4 References 176
Appendix H: Mechanical Testing of TFF Processed Powders by Texture Analyzer using Different Selection of Probes 177
H.1 Purposes 177
H.2 Methods 177
H.3 Results 177
Appendix I: Mechanical Testing of TFF Processed Powders Prepared at Different Freezing Rates by Texture Analyzer 179
I.1 Purposes 179
I.2 Methods 179
I.3 Results 180
Appendix J: Theoretical Modeling of the Freezing Rate of Formulations Prepared by Different Freezing Processes 181
J.1Purposes 181
J.2 Methods 181
J.3 Results 181
J.4 References 185
Bibliography 186
Vita 210

List of Tables

Table 1.1 Current inhaled pharmaceuticals for treatment of lung diseases (a) and systemic applications on the market or undergoing clinical studies. 109

Table 1.2 Most commonly occurring lung diseases, their definitions, causes, symptoms and pathophysiology. 111

Table 1.3 Advanced technologies for production of dry powder formulations designated for inhalation. 112

Table 1.4 Particle deposition equations at different flow conditions for the three deposition mechanisms. 113

Table 1.5 List of input and output parameters for aerosol deposition models. 114

Table 1.6 Breathing pattern of adults at two different conditions, sedentary and light activity. 115

Table 1.7 The impact of lung diseases on the fate of inhaled medicines for each of these processes. 116

Table 2.1 Specific surface area (SSA), geometric particle size distribution of micronized TACMAN (1:1) and TFF TACMAN (1:1). Values are expressed as mean±SD (n=3). 117

Table 2.2 Lung pharmacokinetic parameters of TFF TACMAN (1:1) and micronized TACMAN (1:1) following single dose exposure to dry powder aerosols generated from a rotating brush generator. All the parameters were calculated based on average lung concentration (n=5). 118

Table 3.1 Physicochemical properties of TFF RHOMAN (-140°C), TFF RHOMAN (-50°C) and shelf lyophilized RHOMAN. 119

Table 3.2 Bulk density and calculated aerosolized particle density based on measured geometric and aerodynamic diameters of TFF RHOMAN prepared by different freezing processes. 120

Table 3.3 Bulk density and calculated aerosolized particle density based on measured geometric and aerodynamic diameters of TFF RHOMAN prepared at different solid concentrations (0.5%, 1%, 5% and 10%). 121

Table A.1 Summary of prior arts of inhaled Tacrolimus. 122

Table B.1 Aerodynamic parameters of TFF TACMAN before and after acoustic mixing. 123

Table C.1 Aerodynamic parameters of TFF TACMAN (1:1) using three different DPIs, Handihaler®, Aerolizer® and Miat® monodose inhaler. 124

Table C.2 Aerodynamic parameters of TFF TACMAN (1:1) using three different DPIs, Handihaler®, Aerolizer® and Miat® monodose inhaler at low, medium and high flow rate that generated by patients clinically. 125

Table E. 1 Residual solvent amount of TFF processed powders immediately after preparation, stored for a week in a desiccator at room temperature (25℃, <15% RH) and in a humidity chamber placed in a heated oven (40°C, >90%RH). 126

Table J.1 Density and thermal properties used to calculated thermal diffusivity (α) for water and ice. 127

List of Figures

Figure 1.1 Model of airways described by Weibel. Reprinted with permission from Lee et al. AAPS J 11, 414-423 (2009). 128

Figure 1.2 Schematic illustration of lung physiology at cellular and extra-cellular levels. Reprinted with permission from Ungaro et al. *J Pharm Pharmacol* 64, 1217-1235 (2012). 129

Figure 1.3 The impact of lung diseases on aerosol particle depostion and absorption. .. 130

Figure 1.4 Computational modeling of the branching network of airways in the human lung. Only generations 0 (trachea) to 12 are illustrated. Reprinted with permission from Martonen etal. *Adv Eng Softw* 28, 359-364 (1997). 131

Figure 1.5 Dose-normalized PF-00610355 concentration (C)-time profile following the first inhalation dose in healthy volunteers (HV), patients with asthma and COPD (chronic obstructive pulmonary disease). Reprinted with permission from Diderichsen et al. *Clin Pharmacokinet* 52, 443-452 (2013). 132

Figure 1.6 Aerosol particles subject to dissolution, absorption and mucociliary clearance spontaneously. Reprinted with permission from Edsbacker et al. *Pulmonary Pharmacology & Therapeutics* 21, 247–258 (2008). 133

Figure 2.1 Illustration of RBG and nose-only dosing apparatus for rats..... 134

Figure 2.2 DSC profiles of (from top to bottom) micronized bulk TAC, micronized bulk MAN, physical mixture of micronized TAC and MAN (1:1), TFF TAC only, TFF MAN only and TFF TACMAN (1:1). 135

Figure 2.3 X-ray powder diffraction patterns (from the top to bottom): micronized bulk TAC, micronized bulk MAN, physical mixture of micronized TAC and MAN (1:1), TFF TAC only, TFF MAN only and TFF TACMAN (1:1). 136

Figure 2.4 Attenuated total reflectance Fourier transform infrared spectroscopy of (from the top to bottom): micronized bulk TAC, micronized bulk MAN, physical mixture of micronized TAC and MAN (1:1), TFF TAC only, TFF MAN only and TFF TACMAN (1:1)..... 137

Figure 2.5 SEM images of micronized TACMAN (a) and TFF TACMAN (b) under different magnification: top (2.70KX, scale bar=10 μm) and bottom (25.00KX, scale bar=1 μm). 138

Figure 2.6 Aerodynamic diameter distribution of TFF TACMAN when emitted from a Miat® monodose inhaler at a flow rate of 90 L/min. 139

Figure 2.7 TAC concentration in the rat lungs plotted as percentage of initial dose following exposure to dry powder aerosols generated from a rotating brush generator. TFF TACMAN (open cycle) and Micronized TACMAN (solid square). 140

Figure 2.8 TAC concentration in whole blood following single dose exposure to dry powder aerosols generated from a rotating brush generator. TFF TACMAN (open cycle) and Micronized TACMAN (solid square). 141

Figure 3.1 Nucleation and growth of particles between frozen ice chips with high cooling rate in thin film freezing (TFF) formulation frozen at -140°C (left); with medium cooling rate in TFF formulation frozen at -50°C (middle); with low cooling rate in shelf lyophilized formulation (right). Amorphous ice particles are represented as white domains and solute precipitate as solid dots or gray regions. Adapted with permission from Engstrom et al. *Eur J Pharm Biopharm* 65 (2007) 149–162. .. 143

Figure 3.2 DSC of bulk Rhodamine B, bulk mannitol, Physical Mixture of RHOMAN (1:99), TFF RHOMAN (-140°C), TFF RHOMAN (-50°C) and shelf lyophilized RHOMAN. 144

Figure 3.3 X-Ray Diffraction of TFF RHO, TFF MAN, TFF RHOMAN (-140°C), TFF RHOMAN (-50°C) and shelf lyophilized RHOMAN. 145

Figure 3.4 Aerodynamic properties of TFF RHOMAN (-140°C), TFF RHOMAN (-50°C) and shelf lyophilized RHOMAN determined by Next Generation Impactor (NGI) equipped with Miat Monodose Inhaler at flow rate of 90 L/min. 146

Figure 3.5 Geometric particle size distribution of aerosolized TFF RHOMAN (-140°C), TFF RHOMAN (-50°C) and shelf lyophilized RHOMAN powders determined by Sparytac® equipped with Miat Monodose Inhaler at flow rate of 90 L/min. 147

Figure 3.6 Nucleation and growth of particles between frozen ice chips with low solid concentration in TFF formulations (A); with high solid concentration in TFF formulations. Amorphous ice particles are represented as white domains and solute precipitate as solid dots or gray regions. Reprinted with permission from Engstrom et al. *Eur J Pharm Biopharm* 65 (2007) 149–162. 148

Figure 3.7 Aerodynamic properties of TFF RHOMAN prepared at different solid concentrations (0.5%, 1%, 5% and 10%) determined by Next Generation Impactor (NGI) equipped with Miat Monodose Inhaler at flow rate of 90 L/min. 149

Figure 3.8 Geometric particle size distribution of aerosolized TFF powders prepared at different solid concentrations (0.5%, 1%, 5% and 10%) determined by Sparytac® equipped with Miat Monodose Inhaler at flow rate of 90 L/min. 150

Figure 3.9 Linear regression of the resulting bulk density of TFF powders to initial solid concentrations. 151

Figure 3.10 Mechanical testing of TFF RHOMAN prepared at different solid concentrations (0.5%, 1%, 5% and 10%) determined by Texture Analyzer..... 152

Figure B.1 Acoustic mixer and mixing mechanisms. 153

Figure D.1 DSC of TFF TACLAC stored at 25°C/15%RH at time 0, 1 month, 3 months and 6 months. 154

Figure D.2 DSC of TFF TACLAC stored at 30°C/75%RH at time 0, 1 month, 3 months and 6 months. 155

Figure D.3 DSC of TFF TACMAN stored at 25°C/15%RH at time 0, 1 month, 3 months and 6 months. 156

Figure D.4 DSC of TFF TACLAC stored at 30°C/75%RH at time 0, 1 month, 3 months and 6 months. 157

Figure F. 1 Aerodynamic properties of micronized TACMAN when emitted from a Miat® monodose inhaler at a flow rate of 90 L/min. 158

Figure G.1 TAC concentration in the BAL fluid following single dose exposure to dry powder aerosols generated from a rotating brush generator. TFF TACMAN (open cycle) and Micronized TACMAN (solid square). 159

Figure H. 1 Immersion-force-curve of TFF RHOMAN (1%) determined by texture analyzer using different testing probes. 160

Figure I.1 Mechanical testing of TFF RHOMAN (-140°C), TFF RHOMAN (-50°C) and slow shelf frozen RHOMAN powders determined by Texture Analyzer..... 161

Chapter 1 : The Impact of Pulmonary Diseases on the Fate of Inhaled Medicines

1.1 Abstract

The portfolio of compounds approved for inhalation therapy has expanded rapidly for treatment of lung diseases. To assess the efficacy and safety of inhaled medicines, a better understanding of their fate in the lungs is essential; especially in diseased lungs where a change in anatomical structure, ventilation parameters and breathing pattern may occur. In this article, the impact of lung pathophysiology factors on the fate of inhaled medicines is reviewed, and discussed in the context of aerosol deposition, dissolution, absorption and clearance. Special emphasis is given to computational modeling of aerosol deposition and clearance taking disease factors into consideration. In silico modeling can be used as a valuable tool to characterize the biopharmaceutics and pharmacodynamics of inhaled medicines, or assess risks associated with inhaled environmental pollutants for patients with pulmonary diseases. The deposition pattern of aerosol particles is greatly altered by different lung diseases based on both experimental data and model simulation. The fate of inhaled medicines after deposition primarily depends on the site of aerosol deposition. Therefore, when developing inhalation products for treatment of lung diseases, the dosing regimen, safety and pharmacokinetic studies should be conducted on patients with lung diseases, in addition to healthy subjects.

1.2 Introduction

Treatment of lung diseases by drug inhalation has a long history beginning in the early 1950s when the first inhaled drug for asthma therapy emerged. Over the past 60 years, significant inhalation products have been developed not only for the treatment of asthma, but also for other pulmonary diseases, such as chronic obstruction pulmonary diseases (COPD), cystic fibrosis, pneumonia, to name a few. The rationale for such treatments includes more localized and targeted delivery with minimum systemic exposure. More recently, systemic delivery of drugs administered by inhalation has gained attention due to advantages including: 1) enormous surface area of the lungs; 2) good epithelial permeability; 3) extensive vascularization; 4) faster onset of action compared to the oral route; 5) avoidance of first pass metabolism (Patton and Byron, 2007). Therefore, a variety of inhalation products are under development for treatment of systemic diseases.

Table 1.1 briefly summarizes the current inhalation products on the market or undergoing clinical studies, their drug classification and therapeutic usage. As listed in this table, majority of the inhalation products available on the market are locally acting drugs for treatment of lung diseases. These drugs are delivered to the lungs to either relieve the airway constriction or reduce inflammation and infection, which are mainly bronchodilators, corticosteroids and antibiotics. Most of the inhaled products designed to exert a systemic effect are still in clinical development, including fast-onset analgesics, peptides and proteins. Despite the rapid development of inhaled drugs for systemic

delivery, the inhalation market is still dominated by products for treatment of lung diseases.

Understanding the fate of inhaled drugs in the lungs is essential for determining the therapeutic efficacy of inhaled pharmaceuticals for treatment of lung diseases. Recently published reviews have categorized the fate of inhaled medicines in healthy lungs into four processes, including deposition, dissolution, absorption and clearance.(Forbes et al., 2011; Niven, 2011; Olsson et al., 2011; Todoroff and Vanbever, 2011; Yang et al., 2008b; Zhang et al., 2011). However, none of these reviews have considered the impact of diseased lung pathophysiology on each of these processes in the respiratory tract. A series of questions were posed by Patton et al. regarding how lung diseases affect the biopharmaceutics and pharmacodynamics of inhaled medicines (Patton et al., 2010). Still remarkably little is known in this field. If such questions are addressed, the pace of development of therapeutics for treating lung diseases may be accelerated. This review focuses on the fate of inhaled drugs in the lungs and the impact of lung pathophysiology on their fate. Aerosol drug deposition, dissolution, absorption and clearance are discussed in terms of how each process is influenced by pulmonary diseases. Computational modeling of aerosol deposition and clearance is discussed in detail as a powerful tool to predict the therapeutic efficacy of inhaled pharmacological drugs and risks associated with inhaled environmental aerosols.

1.3 Lung physiology and pathophysiology

The lungs are composed of a series of branching airways, which can be classified into two parts: the conducting zone and the respiratory zone, as described by Weibel's airway model (Fig.1.1) (Weibel, 1963). The conducting zone (generations 0 to 16) comprises of the trachea, bronchi, bronchioles and terminal bronchioles, which are responsible for conducting air to the respiratory regions of the lung (Weibel, 1963). There are no alveoli in the conducting zone and the walls are too thick for diffusion; accordingly, no gas exchange occurs in this region (West, 2007). The total volume of the conducting zone is about 150 mL for a healthy human, and is also referred as the anatomic dead space (West, 2007). The terminal bronchioles branch into respiratory bronchioles, which have alveoli occasionally embedded within their walls. The respiratory bronchioles continuously branch into alveolar ducts and alveolar sacs, which are completely covered by alveoli. The respiratory bronchioles, alveolar ducts and alveolar sacs constitute the respiratory zone (generations 17 to 23), which facilitates gas exchange between airspaces and blood capillaries (Weibel, 1963). The length of the respiratory zone is only a few millimeters, but it composes most of the lung with a total volume of 2.5 to 3 L (West, 2007).

Different types of epithelium line in different regions of the lung (Fig.1.2). In human bronchi, epithelia are composed of columnar basal, ciliated, brush and goblet cells (about 60 μm in height) (Patton and Byron, 2007). There is a surface gel-aqueous layer lined on top of the cells. This layer is composed of a luminal mucus layer (consisting of 95%

water, 2% mucin, polymer, salts, proteins, and lipids), and a periciliary layer underlying the mucus layer with low viscosity to facilitate the cilia beating (Yang et al., 2008b). The coordinate beating of the cilia and the expiratory airflow transport the mucus towards the mouth to clear dust, microorganisms and insoluble particles out of the lungs, and this is referred as mucociliary clearance (Todoroff and Vanbever, 2011). The movement speed of mucus varies in different regions of the airways. It can go up to 20 mm/min in trachea and as slow as 1 mm/min in small peripheral airways (Olsson et al., 2011). When reaching the bronchioles and terminal bronchioles, the same types of cells are present on the epithelium but they are relatively small (around 10 μm in height). The complex gel-aqueous layer lines the entire conducting airways and becomes progressively thinner from the trachea (up to 100 μm) to the bronchi (around 8 μm), and then to terminal bronchioles (about 3 μm) (Patton and Byron, 2007; Ungaro et al., 2012). In the alveolar region, the gel-aqueous layer is replaced by a thin liquid layer (<0.1 μm), which is composed of a pulmonary surfactant film and an aqueous subphase. The pulmonary surfactant consists of 80% phospholipids, 5-10% proteins and 5-10% other lipids (Ungaro et al., 2012). The tall columnar epithelial cells are replaced by thin and broad alveolar type I cells and alveolar type II cells (< 0.1 μm). Alveolar type I cells constitute more than 95% of the alveolar surface, which are adapted for gas exchange and prevent of fluid from entering into the alveoli. Alveolar type II cells are capable of generating into alveolar type I cells and producing surfactants, which allow alveoli to remain inflated at low distending pressures by decreasing surface tension and work of breathing (Todoroff and Vanbever, 2011). Another type of cell that exists in the alveolar region is the alveolar

macrophage. There is no mucus present in the alveolar region implying that mucociliary clearance is not active; therefore the main clearance mechanism in the alveoli is macrophage phagocytosis. Alveolar macrophages reside in the lung lining fluid beneath the surfactant layer (Todoroff and Vanbever, 2011). There are 12-14 macrophages in each of the 500 million alveoli in human lungs, and they only take up 1% of the alveolar surface (Geiser, 2010; Patton and Byron, 2007). However, they are capable of clearing all indigestible particles from the entire surface of the alveoli due to their amoeboid motion (Geiser, 2010).

To better understand the fate of inhaled drugs, adequate knowledge of the movement of blood throughout the lung is critical as well. The blood supplied to the lung can be divided into two portions. The pulmonary arteries carry unoxygenated blood from the right ventricle and branch successively paralleling the bronchi until reaching the terminal bronchioles. In the alveolar region, they branch into capillaries and form a network that covers the alveolar surface to facilitate the diffusion of both oxygen and carbon dioxide. Alveoli are completely enveloped in pulmonary capillaries and the dense network of capillaries provides an excellent environment for gas exchange. The blood-gas barrier between the capillaries and alveoli is extremely thin, with an average thickness of 0.2 to 0.3 μm and a total area of 50-100 m^2 (West, 2007). Beyond that, freshly oxygenated blood from the capillaries goes into small pulmonary veins and eventually drains into the large vein that drains into the left atrium. Also, there is a small portion of systemic blood (via the bronchial circulation) that provides oxygen and nutrients to the larger airways bypassing the pulmonary capillaries. The bronchial circulation thus contributes a small

amount of unoxygenated blood (called venous admixture) to the left ventricle and the systemic circulation. Lymphatic vessels (which drain fluid from the pleural surface and the interstitium) accompany major blood vessels and airways in the lung as well (El-Chemaly et al., 2009).

Lung diseases are some of the most common medical conditions around the world (West, 2012). There are lung diseases predominately affecting the airways (e.g. asthma, COPD, cystic fibrosis), diseases affecting the alveoli (e.g. pneumonia, pulmonary edema, lung cancers) and diseases affecting the surrounding blood vessels and intersitium(e.g. pulmonary embolus, pulmonary hypertension, interstial lung disease) (West, 2012). However, many of these diseases affect more than one compartment of the lung. Table 1.2 summarizes the most commonly occurring lung diseases, their definitions, causes, symptoms and pathophysiology. As mentioned before, very little is known about the impact of lung diseases on the fate of inhaled medicines (Patton et al., 2010). Now, the biopharmaceutics and pharmacokinetics of inhaled drugs in the lungs affected by pathophysiological factors of different lung diseases are discussed for each process: deposition, dissolution, absorption and clearance.

1.4 Drug deposition altered by lung diseases

1.4.1 Present State of Art

The site of aerosol deposition in the respiratory tract is critical when determining the fate of inhaled medicines. Numerous reviews and studies have discussed the basic mechanisms of aerosol deposition in the lung, the size of particles that can be optimally

deposited in the lung, and the factors that affect the deposition efficacy (Patton and Byron, 2007; Rogueda and Traini, 2007; Todoroff and Vanbever, 2011; Yang et al., 2008b). The site of aerosol deposition is determined by the aerodynamic diameter of the aerosol particles. In the oropharynx and large airways (including the trachea and bronchi) where the air velocity is relatively high, large particles (>5 μm) are deposited by inertial impaction because they are unable to follow the change of airstream flow direction. Smaller particles (1–5 μm) are capable of traveling through the upper regions of the lung and deposited in the bronchioles by gravitational sedimentation, where the air velocity is low. In the terminal bronchioles and alveolar region where air velocity is negligible, particles (<0.5 μm) are deposited mainly by diffusion.

In general, two distinct particle size ranges for enhancing alveolar deposition are 1-3 μm (Byron, 1986) and <100 nm (Crampton et al., 2004). The latter size range is rarely used in developing inhalation products partially because it's difficult to generate stable aerosol particles in the range of 50-100 nm (Rogueda and Traini, 2007). It has also been reported that aerosol particles with aerodynamic diameter less than 1 μm can be exhaled up to 80% without deposition due to their low inertial (Heyder et al., 1986). However, aerosol particles deposition in the alveolar region is bi-model. Ultrafine particles (<100 nm) tend to achieve high alveolar deposition fraction (up to 50%) (Yang et al., 2008b), and the deposition efficiency increases as the particle size decreases (Rogueda and Traini, 2007). .

Aerodynamic diameter (D_{ae}) is defined as the diameter of a unit density (ρ_0) sphere, which has the same terminal velocity in still air with the particle. Aerodynamic diameter can be calculated by the equation below:

$$D_{ae} = D_{eq}\sqrt{\rho_p/\rho_0\chi}$$

Where D_{eq} is the geometric diameter of the particle; ρ_p is the particle density and X is the dynamic shape factor derivate from sphere. The dynamic shape factor equals 1.00 for a spherical particle. When particle shape becomes irregular, the dynamic shape factor increases. For instance, the dynamic shape factor is 1.08 for a cube particle, 1.14 for cylinder, 1.57 for sand and 1.88 for Talc (Scheuch and Heyder, 1990). According to the above equation, optimum aerodynamic diameter can also be achieved by generating particles with relatively large geometric size but low particle density or high particle irregularity. Edwards reported use of large porous low density particles to achieve excellent aerodynamic properties (Edwards et al., 1997). Since then, numerical technologies have been proposed to enhance the aerodynamic performance of dry powder formulations (Duddu et al., 2002; Plumley et al., 2009; Richardson and Boss, 2007; Tomashefski Jr. et al., 1993; Vanbever et al., 1999; Watts et al., 2013). As summarized in Table 1.3, the respirable fractions of DPIs prepared by these technologies are significantly higher than that of traditional carrier-based DPIs (10-35%) (Crowder et al., 2002). Besides aerodynamic diameter, the site of aerosol deposition in the respiratory tract is also affected by the anatomy of the airway, breathing pattern, flow rate and tidal volume of the patients (Byron and Patton, 1994).

Godleski group has conducted a series of studies on how different lung diseases altered the aerosol deposition pattern in animal models (Brain et al., 1984; Sweeney et al., 1983; Sweeney et al., 1987; Sweeney et al., 1995). Among all these studies, Insoluble ^{99m}Tc-labeled aerosol particles were utilized to trace the aerosol deposition pattern. Autoradiography imaging was captured on the excised pieces of lung to evaluate aerosol deposition uniformity. A new parameter was introduced in these studies, the Evenness Index (EI), which was calculated by the radioactivity of each individual sample of lung divided by the radioactivity of the entire lung. If the aerosol is uniformly deposited in the whole lungs, the EI would be 1.0 with a Standard Deviation (SD) equal to 0. An EI<1.0 means the sample has less aerosol deposition than the average; to the contrary, an EI>1.0 means that sample receives more than average. Smaller SD indicates that aerosols are more homogenously deposited in the lungs. Rat model with chronic bronchitis (CB) was induced by exposure to sulfur dioxide (SO_2). The control group rats had a more homogenous deposition pattern (SD=0.27) than the CB group rats (SD=0.49). Additionally, CB rats exhibited an enhanced large airway deposition compared with healthy rats because reduction of airway diameter in CB rats may cause increased inertial impaction efficiency in the large airways (Sweeney et al., 1995).

Another lung disease, emphysema was introduced to hamsters by intratracheal elastase installation. Similar to the CB rats, the hamsters with emphysema exhibited less uniform deposition and an enhanced large airway deposition compared to healthy hamsters (Sweeney et al., 1987). Godleski group also studied pulmonary fibrosis, which was induced by a combination of intratracheal bleomycin and O_2 to hamsters. Hamsters

with fibrosis received 60% less particles than the control hamsters in the whole lungs with more heterogeneous distribution. No difference was observed among the diseased group and the control group in terms of breathing pattern, indicating the aerosol deposition pattern was altered primarily by the anatomical change of the airways rather than the breathing pattern.

The difference of particles distribution in these three types of diseased lungs depends on the diseased lesions of the lung. For CB lungs, the diseased lesion is in the large airway not the parenchyma, so aerosol particles mainly deposited in the airway lesion causing large portions of the parenchyma lung have low deposition (Sweeney et al., 1995). In emphysematous lungs, two diseased components may be attributed to the non-uniform distribution of aerosol particles: changes in lung volumes and static pulmonary compliance; change in total pulmonary resistance associated with airways. The increased lung volume and reduced surface area due to destruction of terminal air spaces result in heterogeneous distribution of ventilation, airway closure and enhanced airway deposition (Sweeney et al., 1987). In fibrotic lungs, the diseased lesion primarily occurs in parenchyma rather than airways. The most diseased site retained the smallest amount of particles, because the fibrotic lesions affected the ventilation parameters and the available surface area for deposition (Brain et al., 1984; Sweeney et al., 1983).

Similar radiographic technologies have been used in several clinical studies to investigate the impact of pulmonary disease on aerosol deposition in human lungs. The diseases have been studied include COPD (Brown et al., 2002; Kim and Kang, 1997), asthma (Kim and Kang, 1997), cystic fibrosis (Anderson et al., 1989; Anderson et al.,

1990). As illustrated in Fig.1.3, aerosol particles tend to have higher and non-uniform deposition in the diseased lesions of patients with obstructed lungs compared to healthy subjects. Moreover, the enhancement of deposition efficacy at the diseased site increases with the severity of lung obstruction or lung dysfunction (Anderson et al., 1994; Brown et al., 2001; Itoh et al., 1981; Love and Muir, 1976; Siekmeier et al., 1990). Possible reasons responsible for the enhanced aerosol deposition in patients with obstructed lung diseases are as follows: an increase in upper airway inertial impaction attributed to the reduction of airway diameter resulting from constriction or thickening of mucus; non-uniform ventilation distribution may cause particles to retain in the alveolar region for a longer time; enhanced flow turbulence at the site of obstruction which increases the chance for particle impaction with the airway walls.

1.4.2 Modeling of aerosol deposition and associated lung diseases

To reduce the cost associated with complex animal and clinical studies, mathematical modeling of aerosol deposition in the human respiratory tract has been used to predict deposition and distribution of inhaled pharmaceuticals. However, modeling of aerosol deposition requires a comprehensive knowledge of the geometry of the lungs, the fluid dynamic properties of particles in the airways and the supporting experimental data for model validation. The fundamental theory and airway morphology involved in aerosol deposition modeling, the current existing deposition models and factors affecting the deposition, experimental measurement for particle deposition and model validation was recently reviewed (Martonen et al., 2013).

A very popular analytical model used for simulation of the deposition and distribution of aerosols within the respiratory tract of the lung was proposed by Martonen (Martonen, 1982). Briefly, the human lung is considered as a dichotomous hierarchy of symmetrical tubes. The tracheobronchial airways (TB) are numbered from generation I=0 to 16, and the pulmonary region (P) is numbered from generation I=17-23. P contains three generations of respiratory bronchioles containing some alveoli, three generations of alveolar ducts and alveolar sacs. The angles of bifurcation and gravity within the airways are 70° and 45°, respectively. Two identical sets of 20 airways are present in each generation. The morphology of the lung (Fig.1.4) is described by a supercomputer algorithm (Martonen et al., 1997).

Particle deposition is a function of airway geometries, particle characteristics and breathing conditions. The three major deposition mechanisms have different mathematical expressions when different fluid dynamic patterns are applied to aerosol particles (Martonen et al., 1997). In this model, the entire airway is divided into the large airway (generation 0-4) with turbulence flow; central airway (generation 5-10) and small airway (generation 11-15) with laminar flow at instant rate; alveolar 5 compartment (generation 16-23) with laminar flow of parabolic velocity profile (Martonen et al., 2003). Particle deposition equations depending on different flow conditions and deposition mechanisms are presented in Table 1.4. The cumulative deposition at each generation P(C) can be calculated according to the following equation:

$$P(C) = P(I) + P(S) + P(D) + P(I)P(S)P(D) - P(I)P(S) - P(I)P(D) - P(S)P(D)$$

Tremendous progress has been made in the field of multimodality imaging technologies in the last 20 years. Single Photon Emission Computed Tomography (SPECT) and Positron Emission Tomography (PET) are capable of providing more accurate three-dimensional data on aerosol deposition (Conway et al., 2013). The combination of high resolution computed tomography (HRCT) with data acquired from SPECT or PET provides deposition data more 15 related to anatomy of the lung (Fleming et al., 2011); in addition, HRCT enables the simulation of aerosol deposition based on individual patients rather than generic model (Conway et al., 2013). Therefore, more experimental data can be used for model validation. Moreover, as the advances in deposition modeling, more and more input parameters can be incorporated into the model. Table 1.5 summarizes the available input and output parameters for aerosol deposition 20 modeling.

In this article, we focus on discussing the incorporation of pulmonary disease factors into the aerosol deposition models. Segal et al. used a computer model to evaluate the particle deposition pattern within the lungs of COPD patients compared to healthy patients (Segal et al., 2002). The morphology of COPD lungs are modeled based on both chronic bronchitis (obstructed airways) and emphysema (degeneration of alveoli). Chronic bronchitis (CB) was modeled by reduction of airway diameters and emphysema was modeled by increasing alveolar volumes. For CB lungs, the airway generations 0-16 are narrowed, so the aerosol particles travel in a higher velocity. Therefore, deposition by inertial impaction is remarkably enhanced in the TB region because it's proportional to

the magnitude of the velocity. Moreover, deposition by sedimentation and diffusion is slightly increased. The particles pass through the TB relatively quickly due to accelerated velocity, and the inhalation time is fixed. Thus they tend to resident in the alveolar region for a longer time. Deposition by sedimentation and diffusion are dependent on residence time, hence an increased deposition in generations 17-23 is expected. For emphysema diseased lungs, aerosol deposition slightly decreases because particles must travel a longer distance to deposit on the airway walls due to the increase of alveolar volume.

Martonen et al. simulated asthma based disease parameters on three pathophysiology factors of the human airways: bronchoconstriction of the smooth muscle, inflammation of the airway walls and thickening of the mucus layer (Martonen et al., 2003). The enhancement of aerosol deposition occurred primarily in the region where asthma is located (airway obstruction). Studies with human subjects using SPECT images to trace the aerosol deposition (MMAD=1.8 μm) in healthy and asthmatic groups were conducted to validate the model simulation. In the control group, aerosol particles were uniformly deposited throughout the entire lungs; in the asthmatic group, increased deposition in the central airway and deceased deposition in the peripheral airways were observed, which is correlated with the model simulation results. Another study of has confirmed that regions where bronchoconstriction occurred are the primary sites that the aerosol deposition is enhanced (Sbirlea-Apiou et al., 2004). This study also evaluated the impact of aerosol particle size and the breathing flow rate on enhancement of deposition efficacy. The results illustrated that the enhancement of deposition increased with increased particle size and higher flow rate due to more efficient inertial impaction. These findings might

be viewed as a benefit for site-specific acting drugs targeting the conducting airways (bronchodilators, anti-inflammatory agents, etc.).

Cystic fibrosis (CF) is a genetic disease characterized by hypersecretion of highly viscous mucus, leading to obstructed airway, airway inflammation and infection. Regardless of the initial disease established sites, CF patients will eventually develop obstructive lung disease, which accounts for more than 90% of the death caused by CF (Tomashefski Jr. et al., 1993). The simulation of cystic fibrosis in a mathematical model is represented by reduction in airway diameter, due to thickening of the mucus layer, airway infection and inflammation, or a combination of the three factors. It is well known that in CF, mucous can eventually fill the airways resulting in complete airway obstruction. In studies conducted by Martonen et al., only partial blockage of airways was considered in the model and the term Airway Coefficient (AC) was used to describe the reduction in airway diameter (Martonen et al., 1995; Martonen et al., 1997). The severity of disease was considered in the model as well. AC=1.0 means normal airway without any disease; AC=0.8 represents 20% in diameter reduction; AC=0.6 indicates 40% in diameter reduction. Other parameters added to the model are the ventilation parameters. Table 1.6 gives the breathing pattern of adults at two conditions, sedentary and light activity. The simulated aerosol deposition results demonstrated that under the sedentary breathing condition, particle deposition primarily occurred in the alveolar region of the lung. Moreover, the enhancement of alveolar deposition increased with the severity of disease. The shift of aerosol deposition to the upper airways is more pronounced for larger particle sizes (4 μm) and the light activity breathing condition with high inspiratory

flow rate. The reason can be attributed to the enhanced deposition efficiency by inertial impaction. Therefore, the deposition of inhaled medicines is substantively altered by the degree of airway congestion (severity of disease), and this impact should be considered when designing inhalation therapy protocols with appropriate prescribed breathing regimens.

Lung tumors affecting the airways have been simulated using computer models as well (Farkas and Balásházy, 2007; Martonen and Guan, 2001a, b). Lung carcinomas are classified into two types, sidewall and carinal tumors. For sidewall tumors, the deposition efficiency of large particles (micron-sized) was highly enhanced; on the other hand, nanoparticles tend to have lower deposition efficiency compared with healthy airways. For carinal tumors, enhanced deposition efficiency for micron-sized particles was found and the deposition of nanoparticles was barely affected by the presence of the tumors (Farkas and Balásházy, 2007). Similar to other airway obstructed diseases, the enhancement of aerosol deposition on the tumor sites increases with increasing of aerosol particle size, breathing intensity and tumor size (Martonen and Guan, 2001b).

Aerosol particle deposition is enhanced for diseased lungs most of the time. However, pulmonary diseases may have a negative effect on breathing pattern, which can potentially impact the deposition of inhaled pharmaceuticals. Breathing pattern is typically described in the terms of tidal volume (volume of air inhaled) and flow rate. In general, higher lung deposition has been observed with larger tidal volume because particle-carrying air is capable of penetrating deeper into the lung. Particle deposition in the lung is enhanced with lower flow rate because when the air velocity is low particles

tend to have more time for sedimentation and diffusion (Kim and Hu, 2006; Martonen et al., 2013). Patients with impaired lung functions caused by different lung diseases (COPD, asthma, bronchiectasis etc.) may have very variable spontaneous breathing patterns (tidal volume ranging from 250-2000 mL, flow rate less than 200 to 1000 mL/s). Therefore, they tend to have a lower total lung deposition and greater intersubject and intrasubject variability compared to healthy subjects. When using a controlled slow breathing pattern, higher deposition fraction and smaller intersubject and intrasubject variability were achieved because more time are allowed for aerosol particle sedimentation and diffusion. Thus differences in deposition between healthy subjects and patients were negligible (Brand et al., 2000). A typical 8-10s breath holding after inhalation is recommended on clinical to enhance the deposition of aerosol medicines; however, apparently it's often impossible for patients with severe lung diseases. Nevertheless, when prescribing aerosol medicines, a more slow and deep breathing pattern is recommended to attain the best performance of inhaled medicines, especially for breath-actuated pMDIs and DPIs (Ari et al., 2012).

One of the most promising applications of computational modeling of aerosol deposition is to aid the designing of inhaled pharmaceuticals and the associated devices. In silico models are capable of predicting the optimized particle properties and proper breathing conditions for patients (e.g. velocities, breath holding time) to achieve targeted delivery of aerosols to the diseased lesions of the respiratory tract. Generally, when treating lung diseases, high aerosol deposition in the smooth muscle–lined airways of the lungs is preferred; for systemic applications, enhancing the aerosol deposition in the

pulmonary region (i.e. alveoli) is recommended (Martonen et al., 2013). Moreover, aerosol deposition models can also be used to interpret performance of different devices in clinical studies, such as nebulizers, pMDIs and DPIs (Zhang et al., 2007).

Another application of aerosol deposition modeling is risk assessment of inhaled particulate matter. The U.S. Environmental Protection Agency (EPA) has recently approved several stochastic human exposure models for these purposes, including the Air Pollutants Exposure (APEX) model of EPA's Office of Air Quality Planning(EPA., 2008a), SHEDS-PM and Exposure Model for Individuals (EMI) of EPA's Office of Research and Development (Burke et al., 2001; EPA.). The U.S. EPA office has identified persons suffering from respiratory disease as a sensitive population needing particular consideration in risk assessment of inhaled particulate matter and in the establishment of air pollution standards (Martonen et al., 2013). Therefore, more advanced models of particle deposition that can incorporate a variety of pulmonary diseases are desirable.

In summary, in silico modeling of aerosol deposition and combination of pulmonary disease factors provide a valuable tool for predicting the distribution of therapeutic aerosol in the human respiratory tract. Additionally modeling assists in minimizing the cost of animal and clinical studies by aiding in reasonable design of experiments based on sound scientific hypothesis. Computational modeling is also capable of predicting the inhalation toxicity of air pollutant particles for patients with lung disease. As mentioned by Martonen et al., in silico modeling of aerosol deposition should be utilized in a complementary manner with aerosol therapy protocols (Martonen et al., 2013).

1.5 Drug absorption affected by lung diseases

After deposition, aerosol particles will directly contact with the pulmonary epithelial lining fluid (ELF). The thickness and composition of the ELF are different at different regions of the respiratory tract. Hence, the fate of the deposited aerosol particles depends on the site of deposition, the aqueous solubility and the dosimetry. If the drug is freely soluble in water (e.g. albuterol sulphate, disodium cromoglycate, insulin, calcitonin and tobramycin), it will readily dissolve in the pulmonary lining fluid and be available for absorption or clearance (Patton et al., 2010; Zhang et al., 2011). The pharmacokinetics (PK) behaviors of water-soluble drugs after inhalation of the powder form versus the liquid form have been reported to be similar in human subjects (Clark et al., 2008; Newhouse et al., 2003; Sakagami, 2004; Tolman and Williams, 2010). It indicated that dissolution kinetics may not be the rate-determining step for lung pharmacokinetics and pharmacodynamics following inhalation of water-soluble drugs. For poorly water-soluble drugs (e.g. budesonide, fluticasone and mometasone), the deposited dose may exceed the aqueous solubility due to the limited volume of pulmonary lining fluid (i.e., 10-30 mL in healthy human) (Patton et al., 2010). Consequently, the absorption rate is impacted by the dissolution controlled kinetics in the lung. Enhanced lung absorption using different formulation strategies, which are capable of improving the solubility of poorly water soluble drugs have been proposed recently (Dugas et al., 2013; Sinswat et al., 2008; Yang et al., 2008a; Yang et al., 2010).

Following dissolution, the absorption rate of the drug depends on the hydrophicility of the molecules. For small hydrophilic molecules, the absorption is relatively fast with a half-life of about one hour; for small hydrophobic molecules, the absorption is extremely fast, and the half-life is usually on the order of 1-2 minutes (Patton et al., 2004); the case is more complex for large molecules. Small peptides and proteins can be absorbed quickly but they are also metabolized at the same time. Large proteins are more resistant to metabolism compared to small peptides and proteins, but the absorption is slower and the bioavailability is more variable (Patton et al., 2004). There are several mechanisms that facilitate absorption from the lung into the blood, lymph or cells. Passive diffusion is an important one. It has been reported that hydrophilic compounds tend to be absorbed via paracellular diffusion and intercellular junction pores while the absorption of hydrophobic compounds occurs through transcellular diffusion (Effros and Mason, 1983). Drug transporters also play an important role in pulmonary absorption. The drug carrier transporters may mediate drug uptake into cells and transfer across the cell membrane, especially for drugs with low passive permeability (Olsson et al., 2011). In addition, membrane vesicles and caveolae that are present in alveolar type I cells have been shown to be involved in drug transport across the alveolar epithelium (Crandall and Matthay, 2001; Gumbleton, 2001).

If the aerosol particles are not immediately dissolved in the pulmonary lining fluid, they might be able to transport across the airway and alveolar epithelial cells as intact particles. In the upper airways where the mucus layer acts as a physical barrier, the pore size available for particle transport is approximately 500 nm. Additionally the high

viscosity of mucus can trap the particles and subject them to mucociliary clearance (Dawson et al., 2003; Sanders et al., 2000). In the alveolar region, the thin layer of lining fluid and alveolar type I cells provides very little resistance to particle transport; hence particle transport across the epithelial layer is mostly enhanced in this region (Patton et al., 2010). The mechanism of particle transport across the epithelial cells is transcytosis, which can be mediated by protein-binding (Schmid et al., 2009) or receptor-mediated caveolae (available for particles in the size range 50-100 nm) (Crandall and Matthay, 2001).

Drug absorption depends on the site of aerosol deposition, and the deposition pattern is greatly altered by lung diseases; consequently drug absorption is influenced by pulmonary disease as well. For obstructed airway diseases (e.g. asthma, COPD etc.), absorption of inhaled drugs is expected to be rendered due to the enhanced deposition in the diseased upper airways and potentially reduced surface area. Recently, the pharmacokinetic profile of a new long acting β_2 agonist (PF-00610355) used for once daily treatment of COPD has been studied to characterize systemic exposure related to drug adverse effects. The results are summarized from 264 subjects enrolled in 8 studies, including healthy volunteers, asthmatic and COPD patients(Diderichsen et al., 2013). As shown in Fig.1.5, the mean maximum concentration (C_{max}) is reduced by 52% and 31% for asthma and COPD patients, respectively, compared to healthy volunteers following the first inhalation dose. The decreased systemic drug concentration for patients with asthma and COPD can be attributed to the reduced aerosol deposition in the alveoli, where systemic absorption is maximized (Fig.1.5). Another clinical study among healthy

and asthmatic patients was carried out to evaluate the insulin pharmacokinetics and pharmacodynamics following a single inhalation of AERx insulin system (Henry et al., 2003). Inhaled insulin for healthy subjects displayed a significantly higher AUC and C_{max} compared to asthmatic patients, indicating that less insulin was absorbed in asthmatic patients. A consistently reduced blood glucose level for healthy subjects was observed compare to asthmatic patients. In addition, the asthmatic patients exhibited greater intrasubject variation than the healthy subjects, because the non-uniform diseased lesions between asthmatic subjects resulted in more variable deposition.

Similar reduction in systemic bioavailability was also observed in inhaled combination therapy of budesonide/formoterol and salmeterol/fluticasone for COPD patients versus healthy subjects (Dalby et al., 2009). One of the inhaled corticosteroids, fluticasone, has been shown to exhibit reduced systemic exposure in both asthmatic and COPD patients compared to health subjects (Falcoz et al., 2000; Singh et al., 2003). The mucus thickening of cystic fibrosis and chronic bronchitis may impede air-blood transfer of drug molecules or particles; thereby decreases systemic absorption and bioavailability of inhaled medicines (Geller et al., 2011; Lenney et al., 2011; Pilcer et al., 2008). Decreased systemic absorption of inhaled medicines in patients with obstructive lung diseases is beneficial for locally acting drugs; because it can achieve high drug exposure at the diseased sites and has the potential to lower adverse effects related to drug concentration in the systemic circulation. Therefore, the pharmacokinetics, safety-risk assessment and dose regimen determination should be conducted on patients with the relevant diseases in addition to healthy volunteers.

Other lung diseases may also have an impact on systemic absorption of inhaled pharmaceuticals. Emphysema, characterized by destruction of alveolar walls and consequent enlargement of air-spaces, will cause loss of functional surface area in the alveoli, and further results in decreased systemic drug absorption (West, 2012). Pulmonary fibrosis is a disease that is characterized by excess fibrous connective tissues in the lungs. As the severity increases, the diseased lesions become more heterogeneous. The reduction in vascular density and the increase in sclerotic conditions of the lung parenchyma will lead to a decrease of air-blood drug transfer; hence lower the systemic exposure of inhaled medicines (Patton et al., 2010). Pulmonary embolus is a lung disease that affects the blood vessels. The blood flow to one or more pulmonary arteries is obstructed by a thrombus, leading to decreased drug absorption into the systemic circulation. Pulmonary arterial hypertension (PAH) is another pulmonary vascular disease. In PAH, the pulmonary arteries constrict abnormally, leading to high pressures in the pulmonary vasculature and right ventricular dysfunction. Inhaled vasodilators (e.g. iloprost) have been shown to be an effective treatment for PAH. (Baker and Hockman, 2005; Mulligan and Beghetti, 2012). Due to the constriction, high pressure within the pulmonary arteries and reduced cardiac output, the systemic exposure of inhaled medications will be reduced for PAH patients compared to healthy subjects.

Inhalation therapies for lung cancer have been developed in animal models (Latimer et al., 2009) and human clinical trials (Wittgen et al., 2007). The rationale is attempting to achieve higher drug concentration at the disease sites and reduce systemic side effects. However, the impact of pulmonary tumors on drug absorption is not fully understood.

Lung tumors, for both sidewall and carinal tumors, will lead to obstructed or blockage of airways. Consequently, tumors will receive higher drug exposure when treated locally by inhaling anti-cancer agents. On the other hand, the systemic toxicity related to drug concentration will be reduced due to lower alveolar deposition. Therefore, treating tumors via the pulmonary route is a sound approach for lung cancer therapy.

Chronic airway inflammation is typically associated with epithelial dysfunction, injury and enhanced epithelium permeability due to loss of barrier integrity (Bayram et al., 2002; Knight and Holgate, 2003). In models of allergic airway inflammation, it has been shown that epithelial barrier function and tight junction proteins are dysregulated (Cloutier et al., 2004; Evans et al., 2002). Various inflammatory mediators are responsible for this dysfunction (Bruewer et al., 2003; Coyne et al., 2002; Han et al., 2003). Furthermore, the enhancement of epithelial permeability will accelerate paracellular transport of hydrophilic molecules. Permeability Edema (PE), is a major complication of severe pneumonia, acute respiratory distress syndrome and acute lung injury. PE will cause epithelial and endothelial barriers impairment and hyper permeability, which can further enhance the paracellular transport of hydrophilic molecules (Olsson et al., 2011).

Caveolae mediated transcytosis across the epithelium is another important drug absorption mechanism in the lung that in response to lung pathophysiological factors. Transcytosis starts with the pitch off of caveolae from plasma membrane on either front of the cell; forms discrete vesicle by membrane fusion and moves to the opposite front of endothelial cells in the fluid phase bypass the lysosomes; then fuses with plasma

membrane and discharges the cargo content to the perivascular space (Predescu et al., 2007). Caveolins are unique proteins in the caveolae. They are in charge of modulating cellular signaling and vesicular transport by generating a scaffolding domain that sequesters receptors, ion channels, second messenger producing enzymes and effector kinases to the caveolae (Tiruppathi et al., 2008). There are numerous caveolae and high levels of caveolins expressed in the lung; therefore they are significantly involved in the airway epithelium, smooth muscle, fibroblasts, inflammatory cells and the pulmonary vasculature. It has been suggested that the caveolae-mediated transcytosis is greatly impacted by changes in cellular signaling associated with asthma, COPD, lung cancer, pulmonary fibrosis and pulmonary vascular diseases (Gosens et al., 2008).

1.6 Pulmonary clearance influenced by lung diseases

1.6.1 Mucociliary clearance and impact of lung diseases

In the conducting airways (Fig.1.1, generation 0 to 16), mucociliary clearance (MCC) is the dominant defensive mechanism (Geiser and Kreyling, 2010). Mucus is secreted by mucous glands in the bronchial walls and by goblet cells in the bronchial epithelium (Martonen et al., 2013). The production rate of mucus is about 10-20 ml/day for a healthy human; in a patient with chronic bronchitis up to 10 times this volume may be produced per day (Toremalm, 1960). Beneath the mucus layer, there are millions of cilia with their tips reaching into the mucus and the coordinated beating of the cilia facilitates the moving of mucus towards the larynx/pharynx. Insoluble particles trapped in the mucus will be transported along with the mucus to the upper airway and swallowed (Fig.1.6)

(Antunes and Cohen, 2007). The velocity of mucus moving upwards varies at different regions of the airway, and it is reported to be as slow as 1 mm/min in small peripheral airways and up to 20 mm/min in the trachea (Olsson et al., 2011; Yeates et al., 1981).

Insoluble particles deposited in the airways having a geometric size larger than 6 µm are preferably cleared by MCC (Stahlhofen and Scheuch, 1990). Smaller particles deposited in the upper airways tend to penetrate the mucus layer, and are taken up by epithelial cells; thereby escaping from MCC (Kreyling et al., 2006). Once trapped in the mucus layer, the clearance rate of aerosol particles by MCC is independent of size, shape, charge and surface properties. Additionally the vertical penetration rate of trapped particles toward the epithelium is negligible compared to their horizontal MCC transportation rate (Kirch et al., 2012). The MCC rate is relatively fast, and it has been reported that insoluble particles are generally cleared from the conducting airways by MCC within 24 hours (Zhang et al., 2011).

MCC of insoluble particles has been fully investigated in vivo with the rapid development of modern technologies, e.g. bronchoscope, radiography or external imaging of radiolabelled aerosol particles. These technologies are widely used to determine the rate of MCC in healthy subjects and patients with lung diseases. The rate of MCC is affected by different lung diseases. Betaman et al. have conducted a study to measure the tracheobronchial MCC on patients with mild and stable asthma (Bateman et al., 1983). A group of 25 patients with mild stable asthma and a control group of 25 healthy subjects (matched for sex and age, non-smokers) inhaled 5 µm monodispersed polystyrene aerosol particles radiolabelled with technetium-99m (^{99m}Tc). All treatments

were withdrawn 24 hours before the test. The effect of initial particle deposition and distribution was taken into account as well. Some amount of aerosol particles are deposited in the alveolar region, which are capable of escaping the MCC. Therefore, the alveolar deposition was subtracted from the whole lung retention curve to generate the true tracheobronchial MCC rate for asthmatic patients and healthy subjects. Despite the short transport path due to the obstructed airway in asthmatic patients, the tracheobronchial MCC rate was significantly slower for patients with asthma than healthy subjects. This impairment of mucociliary clearance for asthmatic patients has been previously reported (Daviskas et al., 2005; Del Donno et al., 2000; Foster et al., 1982; Pavia, 1984; Pavia et al., 1985). The impairment is attributed to a combination effect of inflammation mediators, change of function and structure of cilia, and mucus hypersecretion during stable or exacerbations of asthma (Del Donno et al., 2000).

Mucociliary clearance is also reduced in patients with COPD, especially those with more predominant chronic bronchitis (Camner et al., 1973; Koblizek et al., 2011; Rogers, 2005). Patients with COPD usually have chronic sputum production approximately up to 100 mL per day (Snider et al., 1994) and the excess mucus produced by COPD patients is much more viscous than that of healthy subjects (Aikawa et al., 1989; Bhaskar et al., 1986; Lopez-Vidriero and Reid, 1978; Rogers, 2000). These factors are often associated with recurrent chest infection (Prescott et al., 1995). COPD patients also have an abnormal airway mucin composition. Mucins are long, thread-like high molecular weight glycoproteins which possess the viscosity of mucus. Mucins produced by COPD patients are less acidic than normal and have altered levels of glycosylation which may influence

mucus viscosity (Davies et al., 1996; Thornton et al., 1996). Reduced mucociliary clearance for COPD patients can lead to accumulation of pathogens in the lung and result in further infections (Sethi, 2000). Bacterial damage to the airway tissue causes further loss of ciliated cells and increased levels of mucus, which exacerbates the mucociliary dysfunction (Rogers, 2005).

It has been suggested that in addition to their bronchodilator effect, long-acting β-agonists (LABAs) are more capable of restoring the mucociliary dysfunction in asthma and COPD patients compared to short-acting β-agonists (SABAs).(Aalbers et al., 2002; Bennett, 2002; Devalia et al., 1992; Lindberg et al., 1995; Mahler et al., 1999; Melloni and Germouty, 1992; Pavia et al., 1987; Sackner, 1978; Yeates et al., 1986). Salmeterol and formoterol are two commonly used LABAs for treatment of asthma and COPD. Chambers et al. reported that salmeterol successfully enhanced the MCC by 60% compared with placebo in healthy volunteers (Chambers et al., 1999). Salmeterol also demonstrated an increase in tracheobronchial clearance relative to placebo in patients with asthma. In another study conducted by Melloni et al., MCC was also significantly improved by inhaled formoterol compared to placebo in patients with chronic bronchitis (Melloni and Germouty, 1992). β-agonists are capable of increasing the intracellular cyclic adenosine monophosphate (cAMP) levels leading to acceleration of cilia beating frequency (Devalia et al., 1992; Tamaoki et al., 1989). Moreover, β-agonists can enhance the airway Cl^- secretion through the activation of the cystic fibrosis transmembrane regulator (CFTR), and results in mucus hydration (Salathe, 2002). The less viscous hydrated mucus is more easily transported by cilia. β-agonists also increase airway mucin

production and augment ion transport through epithelial; adddtionaly they can improve water efflux and promote mucus secretion (Phipps et al., 1982; Wanner, 1985). The overall effect is improving mucociliary clearance. Inhaled corticosteroids alone with their anti-inflammatory effect do not seem to have a direct effect on mucociliary clearance (Duchateau et al., 1986); however, combination therapy with inhaled a LABA and a corticosteroid was shown to treat the multicomponent nature of COPD and asthma (Rogers, 2005).

Cystic fibrosis (CF) is a genetic disease that results in excess mucus production (Accurso, 2006). The genetic defect is in the cystic fibrosis transmembrane conductance regulator gene product. A cyclic AMP mediated membrane glycoprotein that forms a chloride channel but also intimately regulates the open probability of the sodium channel, ENaC, which is in charge of ion flux at epithelial surfaces (Wine, 1999). According to these functions, the pathophysiology of cystic fibrosis can be explained with two hypotheses: the excessive absorption of sodium ions resulting in impeded mucus movement (Boucher et al., 1986; Matsui et al., 1998), and defective chloride secretion leading to dehydration of secretions (Frizzell et al., 1986; Knowles et al., 1983). Studies have shown that patients with CF have reduced whole lung and regional clearance compared to healthy subjects (Armengot et al., 1997; Regnis et al., 1994; Robinson et al., 2000). For instance, in one of the studies conducted by Regnis et al., MCC was significantly impaired in patients with CF and there was a strong correlation between mucociliary clearance and the severity of disease (higher level of impairment was observed for higher degree of severe disease) (Regnis et al., 1994).

Several other pulmonary diseases affect the mucociliary clearance in the respiratory tract. MCC is reduced by an acute respiratory infection, such as pneumonia (Jarstrand et al., 1974) and influenza (Camner et al., 1973). Chronic respiratory infections like bronchiectasis cause the impairment of mucociliary clearance (Daviskas et al., 1999; Daviskas et al., 2001). Chronic rhinosinusitis, which is an inflammation of the paranasal sinuses will cause patients to suffer from ineffective sinonasal mucociliary clearance (Antunes and Cohen, 2007). Pulmonary edema has also been reported to decrease mucociliary clearance to a lower level (Foster and Wagner, 2001).

Cough is another important clearance mechanism in the upper airways when mucociliary clearance is impaired. Cough clearance was capable of eliminating up to 60% of the particles deposited in the central airways for patients with chronic bronchitis, compared to only 8% in healthy subjects (Puchelle et al., 1980).

1.6.2 Alveolar macrophage uptake

Macrophage uptake mainly occurs in the alveolar region. Insoluble or slowly dissolving particles that are able to penetrate to the alveolar region will be cleared by macrophage phagocytosis. Phagocytosis is described as occurring in four steps: 1) particles bind to the macrophage membrane by recognition of molecules on particle surface or via electrostatic forces; 2) transfer signal to activate receptors; 3) functionalize actin; and then 4) engulf particles into vesicular membrane and create phagosome based on the shape of the ingested particles (Geiser, 2010). Particle uptake by alveolar macrophages is dependent of geometric size. The optimum size for macrophage

phagocytosis is 1.5 to 3 μm (Oberdörster, 1988). Particles with size < 1 μm or >5 μm were found to have reduced macrophage uptake (Edwards et al., 1998; Edwards et al., 1997; Tabata and Ikada, 1988). Macrophage phagocytosis is also affected by particle shape and surface chemistry (Champion and Mitragotri, 2006; Evora et al., 1998). Based on these properties, numerous of approaches have been developed to increase the lung retention of inhaled medicines. These approaches include manipulating the particle size (Bailey and Berkland, 2009; Edwards et al., 1997; El-Sherbiny et al., 2010; Tsapis et al., 2002), shape (Crowder et al., 2002; Larhrib et al., 2003) and surface chemistry (Fu et al., 2002; Gill et al., 2011; Lee et al., 2009) to reduce macrophage clearance.

The uptake of particles by alveolar macrophages will be complete within 6 to 12 hours after deposition (Zhang et al., 2011). Usually 50-75% of the particles are uptake by 2-3 hours, more than 90% by 12 hours and almost 100% by 24 hours (Geiser, 2010). Once engulfed by the alveolar macrophages, particle carrying macrophages can be removed from the alveolar region by transportation upwards to the mucociliary escalator (Schmid et al., 2009); particles can also be disintegrated (e.g. by enzymes in lysosomes) or accumulated in the lymphatic system that drains both airways and alveoli, and accumulates in the lymph nodes (Geiser and Kreyling, 2010; Videira et al., 2002). Once particles are engulfed by macrophages, the clearance of these particle containing macrophages from the lung is relative slow, and usually takes days to months in humans (Oberdörster, 2007).

Macrophage phagocytosis can be affected by pulmonary diseases. Lay et al. assessed the phagocytic activity of airway macrophages for patients with mild allergic asthma

compared to healthy subjects. They monitored the radioactivity associated with cellular and supernatant in the sputum 2 hours after inhalation of radiolabelled aerosol (Lay et al., 2009). Significant enhancement of macrophage phagocytosis for asthmatic patients was observed compared to healthy individuals. The increased particle uptake was not strictly a function of macrophage numbers and percentages, but has a strong correlation with the severity of asthma (Alexis et al., 2001; Lay et al., 2009). The authors attributed this enhancement to a higher state of activation of airway phagocytes (including both macrophages and neutrophils) mediated by scavenger receptors such as MARCO15 or CD206 (macrophage mannose receptor). Moreover, changes of the airway surface liquid components (such as airway mucin, surfactant proteins, phospholipids, adenosine, and airway hydration) for asthmatic patients may also have an impact on macrophage phagocytic activity (Lay et al., 2009).

It has been suggested that the alveolar macrophages (AMs) may act differently than airway macrophages in response to asthma. For patients with mild to moderate asthma with good symptom control, no differences of AMs phagocytic activity were observed compared to healthy subjects (Alexis et al., 2001; Huynh et al., 2005). However, AMs phagocytosis is functionally impaired for patients with severe asthma (Apiou-Sbirlea et al., 2010; Fitzpatrick et al., 2008; Huynh et al., 2005). The impairment of phagocytosis can be attributed to the increased activation of AMs from asthmatic patients. Asthmatic patients have higher production level of superoxide anion, pro-inflammatory cytokines, and regulators of inflammatory gene expression (e.g. histone acetyltransferase) than healthy subjects. Antigen stimulation and decreased production of anti-inflammatory

cytokines (e.g. IL-10) can further augment this impact. Therefore, the overall effects lead to the impairment of asthmatic AMs and increased apoptosis (Fitzpatrick et al., 2008). Similar findings have been reported for patients with COPD (Accurso, 2006; Berenson et al., 2006; Culpitt et al., 2003; Hodge et al., 2003; Russell et al., 2002; Taylor et al., 2010) and cystic fibrosis (Brennan et al., 2009; Vandivier et al., 2002) . AMs phagocytic activity is greatly reduced for patients with these diseases compared to healthy subjects. Although different diseases may have different mechanisms responsible for AMs impairment, it has been demonstrated that the underlying inflammation might play an important role here (Fitzpatrick et al., 2008).

1.6.3 Clearance modeling

A variety of computational models of pulmonary clearance have been reported (Gerrity et al., 1983; Sanchis et al., 1972). Early models developed by Hofmann et al.(Hofmann et al., 1989) have simulated different clearance rate associated with different generations of the tracheobronchial airways (based on experimental data). Martonen et al. further upgraded the model of lung clearance as a function of spatial location within airway branching sites. Different clearance rates were simulated based on tubular airway segments, bifurcation zones, and carinal ridges (Martonen and Hofmann, 1991). Lung clearance will impact not only the retention time, but also the local distribution of inhaled particles. Therefore, it's essential to incorporate the clearance models into the deposition models to accurately predict the fate of inhaled pharmaceuticals or inhalation toxicology.

1.7 Clinical Aspects

We are optimistic about delivering medicines through the pulmonary route. Inhaled medicines tend to accumulate in the diseased areas of the lungs, while attaining reduced systemic exposure to protect sensitive organs from toxic drugs (Patton et al., 2010). However, dramatic changes may occur to the diseased lungs, which can impede the drugs from reaching and interacting with the target. For diseases in the upper airways, this might be insignificant, but the compromised pulmonary function/inflammation/ hyper-secreted mucus may limit the ability to deliver high doses reproducibly and efficiently; for deep lung targeting approaches, drug delivery may be hindered by changes such as airway narrowing, mucus thickening, fibrosis and poor blood circulation (Forbes et al., 2011). Therefore, risks still exist clinically for inhaled medicines in failing to deliver the therapeutics to their site of action.

Inhalation therapies are very commonly used to relieve the symptoms of chronic lung diseases, such as COPD, CF and asthma. In the treatment of severe asthma (status asthmaticus), numerous studies have demonstrated that inhaled beta-agonists are not only more effective but also have significantly less side effects compared to intravenous beta-agonists (Lalloo et al., 2013; Travers et al., 2012). Additionally, after lung transplantation, many transplant centers utilize inhaled antifungal therapy as prophylaxis against pulmonary fungal infections. Inhaled therapy has been shown to be effective without the numerous drug interactions seen with systemic antifungal therapy (Koo et al., 2012; Kuiper and Ruijgrok, 2009). In fact, inhaled medicines for treatment of lung infections or

interstitial lung diseases are rationale (Patton et al., 2010). In some cases, drugs reaching the diseased lesions of the lungs by systemic delivery are limited due to the blood-air barrier created by the diseases. While systemic delivery will be necessary to treat some forms of pulmonary diseases, inhaled medications either alone or in combination with systemic therapy have the potential to modify lung diseases by targeting therapy to the site of the underlying disease.

One essential aspect when designing pharmaceutical aerosols to treat pulmonary disease is the dosimetry. Accurate dosimetry plays an important role in determining the efficacy and safety of inhaled medicines. To estimate the deposited dose, the FDA uses deposition fraction (DF) based on early publications for preclinical and clinical studies (Snipes et al., 1989; Wolff and Dorato, 1993). The DF that the FDA applies are as follows: 10% for rats, 25% for dogs and 100% for humans (Forbes et al., 2011). Although the default DFs are widely used for inhalation product development, it's believed that the default DFs underestimate the deposition for animals and overestimate the deposition for humans (Forbes et al., 2011). Moreover, DFs are significantly affected by lung diseases factors. In silico modeling of aerosol deposition and clearance associated with lung diseases is potentially of great use in determining the dose regimen of inhaled medicines and designing inhalation therapy protocols. This type of modeling has the potential to reduce expensive pilot studies required in bringing new therapies to market.

1.8 Concluding Remarks

The fate of inhaled medicines in the lungs plays an important role in determining the pharmacokinetics and pharmacodynamics of any inhaled drug. Several mechanisms are involved, including deposition, dissolution, absorption and clearance. These mechanisms occur nearly simultaneously, which makes it more difficult to study each of them individually. Lung diseases may alter the anatomic structure of the respiratory tract, the ventilatory conditions and the breathing pattern of patients. They can further affect the fate of inhaled pharmaceuticals. The biopharmaceutics of aerosol drugs in the lung is very complex with many processes involved. Table 7 summarized the impact of different lung diseases on each of these processes. When considering the impact of lung diseases on the fate of inhaled medicines, all these effects mentioned above may occur spontaneously in accordance with different lung diseases associated with different clinical manifestations. There is still a large underdeveloped area of research regarding how inhaled drugs will act in various diseased lung states. The advances on inhaled medicines and formulation designs will be hindered if we don't address such questions. Nevertheless, it's generally believed that treatment of most lung diseases with inhaled medicines still offers therapeutic and compliance benefits compared to delivery of drugs orally or intravenously.

1.9 References

[1] J.S. Patton, P.R. Byron, Inhaling medicines: delivering drugs to the body through the lungs, Nat Rev Drug Discov, 6 (2007) 67-74.

[2] GOLD, Global Strategy for the Diagnosis, Management and Prevention of COPD. [Global Initiative for Chronic Obstructive Lung Disease (GOLD) web site]. Available at: http://www.goldcopd.org/. (2012).

[3] F. Ungaro, I. d'Angelo, A. Miro, M.I. La Rotonda, F. Quaglia, Engineered PLGA nano- and micro-carriers for pulmonary delivery: challenges and promises, J Pharm Pharmacol, 64 (2012) 1217-1235.

[4] GINA, Global Strategy for Asthma Management and Prevention. [Global Initiative for Asthma (GINA) web site]. Available at: http://www.ginasthma.org/. (2012).

[5] J. Zhang, L. Wu, H.K. Chan, W. Watanabe, Formation, characterization, and fate of inhaled drug nanoparticles, Adv Drug Deliv Rev, 63 (2011) 441-455.

[6] W. Yang, J.I. Peters, R.O. Williams, 3rd, Inhaled nanoparticles--a current review, Int J Pharm, 356 (2008) 239-247.

[7] J. Todoroff, R. Vanbever, Fate of nanomedicines in the lungs, Current Opinion in Colloid & Interface Science, 16 (2011) 246-254.

[8] B. Olsson, E. Bondesson, L. Borgstrom, Pulmonary Drug Metabolism, Clearance, and Absorption, in: H.D.C. Smyth, A.J. Hickey (Eds.) Controlled Pulmonary Drug Delivery, Springer, New York, NY, 2011.

[9] R.W. Niven, Toward managing chronic rejection after lung transplant: the fate and effects of inhaled cyclosporine in a complex environment, Adv Drug Deliv Rev, 63 (2011) 88-109.

[10] B. Forbes, B. Asgharian, L.A. Dailey, D. Ferguson, P. Gerde, M. Gumbleton, L. Gustavsson, C. Hardy, D. Hassall, R. Jones, R. Lock, J. Maas, T. McGovern, G.R. Pitcairn, G. Somers, R.K. Wolff, Challenges in inhaled product development and opportunities for open innovation, Adv Drug Deliv Rev, 63 (2011) 69-87.

[11] J.S. Patton, J.D. Brain, L.A. Davies, J. Fiegel, M. Gumbleton, K.J. Kim, M. Sakagami, R. Vanbever, C. Ehrhardt, The particle has landed--characterizing the fate of inhaled pharmaceuticals, Journal of aerosol medicine and pulmonary drug delivery, 23 Suppl 2 (2010) S71-87.

[12] E.R. Weibel, Morphometry of the human lung, Academic Press, New York,, 1963.

[13] J.B. West, Nomal Physiology: Exercise, in: Pulmonary physiology and pathophysiology : an integrated, case-based approach, Wolters Kluwer Health/Lippincott Williams & Wilkins, Philadelphia, 2007, pp. vii, 150 p.

[14] M. Geiser, Update on macrophage clearance of inhaled micro- and nanoparticles, Journal of aerosol medicine and pulmonary drug delivery, 23 (2010) 207-217.

[15] S. El-Chemaly, G. Pacheco-Rodriguez, Y. Ikeda, D. Malide, J. Moss, Lymphatics in idiopathic pulmonary fibrosis: new insights into an old disease, Lymphatic research and biology, 7 (2009) 197-203.

[16] J.B. West, Pulmonary pathophysiology : the essentials, 8th ed., Wolters Kluwer/Lippincott Williams & Wilkins Health, Philadelphia, 2012.

[17] P.G. Rogueda, D. Traini, The nanoscale in pulmonary delivery. Part 1: deposition, fate, toxicology and effects, Expert Opin Drug Deliv, 4 (2007) 595-606.

[18] P.R. Byron, Prediction of drug residence times in regions of the human respiratory tract following aerosol inhalation, J Pharm Sci, 75 (1986) 433-438.

[19] M. Crampton, R. Kinnersley, J. Ayres, Sub-micrometer particle production by pressurized metered dose inhalers, J Aerosol Med, 17 (2004) 33-42.

[20] J. Heyder, J. Gebhart, G. Rudolf, C.F. Schiller, W. Stahlhofen, Deposition of particles in the human respiratory-tract in the size range 0.005-15 μm., Journal of Aerosol Science, 17 (1986) 811-825.

[21] G. Scheuch, J. Heyder, Dynamic Shape Factor of Nonspherical Aerosol Particles in the Diffusion Regime., Aerosol Science and Technology, 12 (1990) 270-277.

[22] D.A. Edwards, J. Hanes, G. Caponetti, J. Hrkach, A. Ben-Jebria, M.L. Eskew, J. Mintzes, D. Deaver, N. Lotan, R. Langer, Large porous particles for pulmonary drug delivery, Science, 276 (1997) 1868-1871.

[23] J.F. Tomashefski Jr., C.R. Abrmowsky, B.B. Dahms, The pathology of cystic fibrosis., in: P.B. Davis (Ed.) Cystic fibrosis, M. Dekker, New York, 1993, pp. 435-489.

[24] S.P. Duddu, S.A. Sisk, Y.H. Walter, T.E. Tarara, K.R. Trimble, A.R. Clark, M.A. Eldon, R.C. Elton, M. Pickford, P.H. Hirst, S.P. Newman, J.G. Weers, Improved lung delivery from a passive dry powder inhaler using an Engineered PulmoSphere powder, Pharm Res, 19 (2002) 689-695.

[25] C. Plumley, E.M. Gorman, N. El-Gendy, C.R. Bybee, E.J. Munson, C. Berkland, Nifedipine nanoparticle agglomeration as a dry powder aerosol formulation strategy, Int J Pharm, 369 (2009) 136-143.

[26] P.C. Richardson, A.H. Boss, Technosphere insulin technology, Diabetes Technol Ther, 9 Suppl 1 (2007) S65-72.

[27] R. Vanbever, J.D. Mintzes, J. Wang, J. Nice, D. Chen, R. Batycky, R. Langer, D.A. Edwards, Formulation and physical characterization of large porous particles for inhalation, Pharm Res, 16 (1999) 1735-1742.

[28] A.B. Watts, Y.B. Wang, K.P. Johnston, R.O. Williams, 3rd, Respirable low-density microparticles formed in situ from aerosolized brittle matrices, Pharm Res, 30 (2013) 813-825.

[29] T.M. Crowder, J.A. Rosati, J.D. Schroeter, A.J. Hickey, T.B. Martonen, Fundamental effects of particle morphology on lung delivery: predictions of Stokes' law and the particular relevance to dry powder inhaler formulation and development, Pharm Res, 19 (2002) 239-245.

[30] P.R. Byron, J.S. Patton, Drug delivery via the respiratory tract, J Aerosol Med, 7 (1994) 49-75.

[31] T.D. Sweeney, J.D. Brain, T. A.F., J.J. Godleski, Deposition of particles in hamsters with pulmonary fibrosis., Am Rev Respir Dis, 128 (1983) 138-143.

[32] J.D. Brain, T.D. Sweeney, A.F. Tryka, W.A. Skornik, J.J. Godleski, Effects of pulmonary fibrosis on aerosol deposition in hamsters., J Aerosol Sci., 15 (1984) 217-218.

[33] T.D. Sweeney, J.D. Brain, S.A. Leavitt, J.J. Godleski, Emphysema alters the deposition pattern of inhaled particles in hamsters, Am J Pathol, 128 (1987) 19-28.

[34] T.D. Sweeney, W.A. Skornik, J.D. Brain, V. Hatch, J.J. Godleski, Chronic bronchitis alters the pattern of aerosol deposition in the lung, Am J Respir Crit Care Med, 151 (1995) 482-488.

[35] C.S. Kim, T.C. Kang, Comparative measurement of lung deposition of inhaled fine particles in normal subjects and patients with obstructive airway disease, Am J Respir Crit Care Med, 155 (1997) 899-905.

[36] J.S. Brown, K.L. Zeman, W.D. Bennett, Ultrafine particle deposition and clearance in the healthy and obstructed lung, Am J Respir Crit Care Med, 166 (2002) 1240-1247.

[37] P.J. Anderson, J.D. Blanchard, J.D. Brain, H.A. Feldman, J.J. McNamara, J. Heyder, Effect of cystic fibrosis on inhaled aerosol boluses, Am Rev Respir Dis, 140 (1989) 1317-1324.

[38] P.J. Anderson, J.D. Wilson, F.C. Hiller, Respiratory tract deposition of ultrafine particles in subjects with obstructive or restrictive lung disease, Chest, 97 (1990) 1115-1120.

[39] R.G. Love, D.C. Muir, Aerosol deposition and airway obstruction, Am Rev Respir Dis, 114 (1976) 891-897.

[40] R. Siekmeier, C.H.F. Schiller-Scotland, J. Gebhart, H. Kronenberger, Pharmacon-induced airway obstruction in healthy subjects: Dose dependent changes of inspired aerosol boluses., J. Aerosol Sci., 21 (1990) S423.

[41] P.J. Anderson, L.P. Gann, R.C. Walls, K.B. Tennal, F.C. Hiller, Utility of aerosol bolus behavior as a diagnostic index of asthma during bronchoprovocation., Am. J. Respir. Crit. Care Med., 149 (1994) A1047.

[42] H. Itoh, Y. Ishii, H. Maeda, G. Todo, K. Torizuka, G.C. Smaldone, Clinical observations of aerosol deposition in patients with airways obstruction, Chest, 80 (1981) 837-840.

[43] J.S. Brown, K.L. Zeman, W.D. Bennett, Regional deposition of coarse particles and ventilation distribution in healthy subjects and patients with cystic fibrosis, J Aerosol Med, 14 (2001) 443-454.

[44] T.B. Martonen, J.A. Rosati, K.K. Isaacs, Modeling Deposition of Inhaled Particles, in: L.S. Ruzer, N.H. Harley (Eds.) Aerosols handbook measurement, dosimetry, and health effects, CRC Press,, Boca Raton, 2013.

[45] T.B. Martonen, Analytical model of hygroscopic particle behavior in human airways, Bull Math Biol, 44 (1982) 425-442.

[46] T.B. Martonen, D. Hwang, I. Katz, Y. Yang, X. Guan, Cystic fibrosis: treatment with a supercomputer drug delivery model., Advances in Engineering Software, 28 (1997) 359-364.

[47] T. Martonen, J. Fleming, J. Schroeter, J. Conway, D. Hwang, In silico modeling of asthma, Adv Drug Deliv Rev, 55 (2003) 829-849.

[48] J. Conway, J. Fleming, M. Bennett, T. Havelock, The co-imaging of gamma camera measurements of aerosol deposition and respiratory anatomy, Journal of aerosol medicine and pulmonary drug delivery, 26 (2013) 123-130.

[49] J. Fleming, J. Conway, C. Majoral, L. Tossici-Bolt, I. Katz, G. Caillibotte, D. Perchet, M. Pichelin, B. Muellinger, T. Martonen, P. Kroneberg, G. Apiou-Sbirlea, The use of combined single photon emission computed tomography and X-ray computed tomography to assess the fate of inhaled aerosol, Journal of aerosol medicine and pulmonary drug delivery, 24 (2011) 49-60.

[50] R.A. Segal, T.B. Martonen, C.S. Kim, M. Shearer, Computer simulations of particle deposition in the lungs of chronic obstructive pulmonary disease patients, Inhalation toxicology, 14 (2002) 705-720.

[51] G. Sbirlea-Apiou, M. Lemaire, I. Katz, J. Conway, J. Fleming, T. Martonen, Simulation of the regional manifestation of asthma, J Pharm Sci, 93 (2004) 1205-1216.

[52] T. Martonen, I. Katz, W. Cress, Aerosol deposition as a function of airway disease: cystic fibrosis, Pharm Res, 12 (1995) 96-102.

[53] T.B. Martonen, X. Guan, Effects of tumors on inhaled pharmacologic drugs: II. Particle motion, Cell biochemistry and biophysics, 35 (2001) 245-253.

[54] T.B. Martonen, X. Guan, Effects of tumors on inhaled pharmacologic drugs: I. Flow patterns, Cell biochemistry and biophysics, 35 (2001) 233-243.

[55] A. Farkas, I. Balásházy, Simulation of the effect of local obstructions and blockage on airflow and aerosol deposition in central human airways., Aerosol Science, 38 (2007) 865-884.

[56] C.S. Kim, S.C. Hu, Total respiratory tract deposition of fine micrometer-sized particles in healthy adults: empirical equations for sex and breathing pattern, Journal of applied physiology, 101 (2006) 401-412.

[57] P. Brand, I. Friemel, T. Meyer, H. Schulz, J. Heyder, K. Haubetainger, Total deposition of therapeutic particles during spontaneous and controlled inhalations, J Pharm Sci, 89 (2000) 724-731.

[58] A. Ari, R.D. Restrepo, C. American Association for Respiratory, Aerosol delivery device selection for spontaneously breathing patients: 2012, Respir Care, 57 (2012) 613-626.

[59] Y. Zhang, K. Gilbertson, W.H. Finlay, In vivo-in vitro comparison of deposition in three mouth-throat models with Qvar and Turbuhaler inhalers, J Aerosol Med, 20 (2007) 227-235.

[60] U. EPA., Total Risk Integrated Methodology (TRIM) Air Pollutants Exposure Model Documentation (TRIM.Expo/APEX, Version 4.3). in, Office of Air Quality Planning and Standards, Research Triangle Park, NC., 2008a, pp. http://www.epa.gov/ttn/fera/human_apex.html.

[61] J.M. Burke, M.J. Zufall, H. Ozkaynak, A population exposure model for particulate matter: case study results for PM(2.5) in Philadelphia, PA, Journal of exposure analysis and environmental epidemiology, 11 (2001) 470-489.

[62] U.S. EPA., Exposure Model for Individuals., in, pp. http://www.epa.gov/heasd/products/emi/emi.html.

[63] A. Clark, M.C. Kuo, S. Newman, P. Hirst, G. Pitcairn, M. Pickford, A comparison of the pulmonary bioavailability of powder and liquid aerosol formulations of salmon calcitonin, Pharm Res, 25 (2008) 1583-1590.

[64] M.T. Newhouse, P.H. Hirst, S.P. Duddu, Y.H. Walter, T.E. Tarara, A.R. Clark, J.G. Weers, Inhalation of a dry powder tobramycin PulmoSphere formulation in healthy volunteers, Chest, 124 (2003) 360-366.

[65] M. Sakagami, Insulin disposition in the lung following oral inhalation in humans : a meta-analysis of its pharmacokinetics, Clin Pharmacokinet, 43 (2004) 539-552.

[66] J.A. Tolman, R.O. Williams, 3rd, Advances in the pulmonary delivery of poorly water-soluble drugs: influence of solubilization on pharmacokinetic properties, Drug Dev Ind Pharm, 36 (2010) 1-30.

[67] H.L. Dugas, J.I. Peters, R.O. Williams, 3rd, Nebulization of mycophenolate mofetil inhalation suspension in rats: comparison with oral and pulmonary administration of Cellcept(R), Int J Pharm, 441 (2013) 19-29.

[68] P. Sinswat, K.A. Overhoff, J.T. McConville, K.P. Johnston, R.O. Williams, 3rd, Nebulization of nanoparticulate amorphous or crystalline tacrolimus--single-dose pharmacokinetics study in mice, Eur J Pharm Biopharm, 69 (2008) 1057-1066.

[69] J.Z. Yang, A.L. Young, P.C. Chiang, A. Thurston, D.K. Pretzer, Fluticasone and budesonide nanosuspensions for pulmonary delivery: preparation, characterization, and pharmacokinetic studies, J Pharm Sci, 97 (2008) 4869-4878.

[70] W. Yang, K.P. Johnston, R.O. Williams, 3rd, Comparison of bioavailability of amorphous versus crystalline itraconazole nanoparticles via pulmonary administration in rats, Eur J Pharm Biopharm, 75 (2010) 33-41.

[71] J.S. Patton, C.S. Fishburn, J.G. Weers, The Lungs as a Portal of Entry for Systemic Drug Delivery, Proc Am Thorac Soc, 1 (2004) 338-344.

[72] R.M. Effros, G.R. Mason, Measurements of pulmonary epithelial permeability in vivo, Am Rev Respir Dis, 127 (1983) S59-65.

[73] E.D. Crandall, M.A. Matthay, Alveolar epithelial transport. Basic science to clinical medicine, Am J Respir Crit Care Med, 163 (2001) 1021-1029.

[74] M. Gumbleton, Caveolae as potential macromolecule trafficking compartments within alveolar epithelium, Adv Drug Deliv Rev, 49 (2001) 281-300.

[75] M. Dawson, D. Wirtz, J. Hanes, Enhanced viscoelasticity of human cystic fibrotic sputum correlates with increasing microheterogeneity in particle transport, J Biol Chem, 278 (2003) 50393-50401.

[76] N.N. Sanders, S.C. De Smedt, E. Van Rompaey, P. Simoens, F. De Baets, J. Demeester, Cystic fibrosis sputum: a barrier to the transport of nanospheres, Am J Respir Crit Care Med, 162 (2000) 1905-1911.

[77] O. Schmid, W. Moller, M. Semmler-Behnke, G.A. Ferron, E. Karg, J. Lipka, H. Schulz, W.G. Kreyling, T. Stoeger, Dosimetry and toxicology of inhaled ultrafine particles, Biomarkers : biochemical indicators of exposure, response, and susceptibility to chemicals, 14 Suppl 1 (2009) 67-73.

[78] P.M. Diderichsen, E. Cox, S.W. Martin, A. Cleton, J. Ribbing, Characterizing systemic exposure of inhaled drugs: application to the long-acting beta2-agonist PF-00610355, Clin Pharmacokinet, 52 (2013) 443-452.

[79] R.R. Henry, S.R. Mudaliar, W.C. Howland, 3rd, N. Chu, D. Kim, B. An, R.R. Reinhardt, Inhaled insulin using the AERx Insulin Diabetes Management System in healthy and asthmatic subjects, Diabetes Care, 26 (2003) 764-769.

[80] C. Dalby, T. Polanowski, T. Larsson, L. Borgstrom, S. Edsbacker, T.W. Harrison, The bioavailability and airway clearance of the steroid component of budesonide/formoterol and salmeterol/fluticasone after inhaled administration in patients with COPD and healthy subjects: a randomized controlled trial, Respir Res, 10 (2009) 104.

[81] C. Falcoz, R. Oliver, J.E. McDowall, P. Ventresca, A. Bye, P.T. Daley-Yates, Bioavailability of orally administered micronised fluticasone propionate, Clin Pharmacokinet, 39 Suppl 1 (2000) 9-15.

[82] S.D. Singh, C. Whale, N. Houghton, P. Daley-Yates, S.M. Kirby, A.A. Woodcock, Pharmacokinetics and systemic effects of inhaled fluticasone propionate in chronic obstructive pulmonary disease, Br J Clin Pharmacol, 55 (2003) 375-381.

[83] D.E. Geller, P.A. Flume, D.C. Griffith, E. Morgan, D. White, J.S. Loutit, M.N. Dudley, Pharmacokinetics and safety of MP-376 (levofloxacin inhalation solution) in cystic fibrosis subjects, Antimicrob Agents Chemother, 55 (2011) 2636-2640.

[84] W. Lenney, F. Edenborough, P. Kho, J.M. Kovarik, Lung deposition of inhaled tobramycin with eFlow rapid/LC Plus jet nebuliser in healthy and cystic fibrosis subjects, J Cyst Fibros, 10 (2011) 9-14.

[85] G. Pilcer, J. Goole, B. Van Gansbeke, D. Blocklet, C. Knoop, F. Vanderbist, K. Amighi, Pharmacoscintigraphic and pharmacokinetic evaluation of tobramycin DPI formulations in cystic fibrosis patients, Eur J Pharm Biopharm, 68 (2008) 413-421.

[86] S.E. Baker, R.H. Hockman, Inhaled iloprost in pulmonary arterial hypertension, Ann Pharmacother, 39 (2005) 1265-1274.

[87] C. Mulligan, M. Beghetti, Inhaled iloprost for the control of acute pulmonary hypertension in children: a systematic review, Pediatr Crit Care Med, 13 (2012) 472-480.

[88] P. Latimer, M. Menchaca, R.M. Snyder, W. Yu, B.E. Gilbert, B.G. Sanders, K. Kline, Aerosol delivery of liposomal formulated paclitaxel and vitamin E analog reduces murine mammary tumor burden and metastases, Exp Biol Med (Maywood), 234 (2009) 1244-1252.

[89] B.P. Wittgen, P.W. Kunst, K. van der Born, A.W. van Wijk, W. Perkins, F.G. Pilkiewicz, R. Perez-Soler, S. Nicholson, G.J. Peters, P.E. Postmus, Phase I study of aerosolized SLIT cisplatin in the treatment of patients with carcinoma of the lung, Clin Cancer Res, 13 (2007) 2414-2421.

[90] H. Bayram, C. Rusznak, O.A. Khair, R.J. Sapsford, M.M. Abdelaziz, Effect of ozone and nitrogen dioxide on the permeability of bronchial epithelial cell cultures of non-asthmatic and asthmatic subjects, Clinical and experimental allergy : journal of the British Society for Allergy and Clinical Immunology, 32 (2002) 1285-1292.

[91] D.A. Knight, S.T. Holgate, The airway epithelium: structural and functional properties in health and disease, Respirology, 8 (2003) 432-446.

[92] M.M. Cloutier, L. Guernsey, C.A. Wu, R.S. Thrall, Electrophysiological properties of the airway: epithelium in the murine, ovalbumin model of allergic airway disease, Am J Pathol, 164 (2004) 1849-1856.

[93] S.M. Evans, D.I. Blyth, T. Wong, S. Sanjar, M.R. West, Decreased distribution of lung epithelial junction proteins after intratracheal antigen or lipopolysaccharide challenge: correlation with neutrophil influx and levels of BALF sE-cadherin, Am J Respir Cell Mol Biol, 27 (2002) 446-454.

[94] M. Bruewer, A. Luegering, T. Kucharzik, C.A. Parkos, J.L. Madara, A.M. Hopkins, A. Nusrat, Proinflammatory cytokines disrupt epithelial barrier function by apoptosis-independent mechanisms, J Immunol, 171 (2003) 6164-6172.

[95] C.B. Coyne, M.K. Vanhook, T.M. Gambling, J.L. Carson, R.C. Boucher, L.G. Johnson, Regulation of airway tight junctions by proinflammatory cytokines, Molecular biology of the cell, 13 (2002) 3218-3234.

[96] X. Han, M.P. Fink, R.L. Delude, Proinflammatory cytokines cause NO*-dependent and -independent changes in expression and localization of tight junction proteins in intestinal epithelial cells, Shock, 19 (2003) 229-237.

[97] S.A. Predescu, D.N. Predescu, A.B. Malik, Molecular determinants of endothelial transcytosis and their role in endothelial permeability, Am J Physiol Lung Cell Mol Physiol, 293 (2007) L823-842.

[98] C. Tiruppathi, J. Shimizu, K. Miyawaki-Shimizu, S.M. Vogel, A.M. Bair, R.D. Minshall, D. Predescu, A.B. Malik, Role of NF-kappaB-dependent caveolin-1 expression in the mechanism of increased endothelial permeability induced by lipopolysaccharide, J Biol Chem, 283 (2008) 4210-4218.

[99] R. Gosens, M. Mutawe, S. Martin, S. Basu, S.T. Bos, T. Tran, A.J. Halayko, Caveolae and caveolins in the respiratory system, Curr Mol Med, 8 (2008) 741-753.

[100] M. Geiser, W.G. Kreyling, Deposition and biokinetics of inhaled nanoparticles, Part Fibre Toxicol, 7 (2010) 2.

[101] N.G. Toremalm, The daily amoung of tracheo-bronchial secretions in man. A method for continuous tracheal aspiration in laryngectomized and tracheotomized patients, Acta oto-laryngologica. Supplementum, 158 (1960) 43-53.

[102] M.B. Antunes, N.A. Cohen, Mucociliary clearance--a critical upper airway host defense mechanism and methods of assessment, Current opinion in allergy and clinical immunology, 7 (2007) 5-10.

[103] D.B. Yeates, T.R. Gerrity, C.S. Garrard, Particle deposition and clearance in the bronchial tree, Ann Biomed Eng, 9 (1981) 577-592.

[104] W. Stahlhofen, G. Scheuch, [Measuring human mucociliary clearance], Pneumologie, 44 Suppl 1 (1990) 422-423.

[105] W.G. Kreyling, M. Semmler-Behnke, W. Moller, Ultrafine particle-lung interactions: does size matter?, J Aerosol Med, 19 (2006) 74-83.

[106] J. Kirch, M. Guenther, N. Doshi, U.F. Schaefer, M. Schneider, S. Mitragotri, C.M. Lehr, Mucociliary clearance of micro- and nanoparticles is independent of size, shape and charge--an ex vivo and in silico approach, J Control Release, 159 (2012) 128-134.

[107] J.R. Bateman, D. Pavia, N.F. Sheahan, J.E. Agnew, S.W. Clarke, Impaired tracheobronchial clearance in patients with mild stable asthma, Thorax, 38 (1983) 463-467.

[108] W.M. Foster, E.G. Langenback, E.H. Bergofsky, Lung mucociliary function in man: interdependence of bronchial and tracheal mucus transport velocities with lung clearance in bronchial asthma and healthy subjects, Ann Occup Hyg, 26 (1982) 227-244.

[109] D. Pavia, Lung mucociliary clearance, in: S.W. Clarke, D. Pavia (Eds.) Aerosols and the lung : clinical and experimental aspects, Butterworths, London ; Boston, 1984, pp. 275.

[110] E. Daviskas, S.D. Anderson, J. Shaw, S. Eberl, J.P. Seale, I.A. Yang, I.H. Young, Mucociliary clearance in patients with chronic asthma: effects of beta agonists, Respirology, 10 (2005) 426-435.

[111] M. Del Donno, D. Bittesnich, A. Chetta, D. Olivieri, M.T. Lopez-Vidriero, The effect of inflammation on mucociliary clearance in asthma: an overview, Chest, 118 (2000) 1142-1149.

[112] D. Pavia, J.R. Bateman, N.F. Sheahan, J.E. Agnew, S.W. Clarke, Tracheobronchial mucociliary clearance in asthma: impairment during remission, Thorax, 40 (1985) 171-175.

[113] P. Camner, B. Mossberg, K. Philipson, Tracheobronchial clearance and chronic obstructive lung disease, Scandinavian journal of respiratory diseases, 54 (1973) 272-281.

[114] V. Koblizek, M. Tomsova, E. Cermakova, P. Papousek, S. Pracharova, R.A. Mandalia, J. Ceral, J. Novosad, L. Fila, V. Sedlak, J. Ruta, V. Bartos, F. Salajka, M. Hrnciarik, Impairment of nasal mucociliary clearance in former smokers with stable chronic obstructive pulmonary disease relates to the presence of a chronic bronchitis phenotype, Rhinology, 49 (2011) 397-406.

[115] D.F. Rogers, Mucociliary dysfunction in COPD: effect of current pharmacotherapeutic options, Pulmonary pharmacology & therapeutics, 18 (2005) 1-8.

[116] G.L. Snider, L.J. Faling, S.I. Rennard, Chronic bronchitis and emphysema, in: J.F. Murray, J.A. Nadel (Eds.) Textbook of respiratory medicine, Saunders, Philadelphia, 1994, pp. 1331-1397.

[117] T. Aikawa, S. Shimura, H. Sasaki, T. Takishima, H. Yaegashi, T. Takahashi, Morphometric analysis of intraluminal mucus in airways in chronic obstructive pulmonary disease, Am Rev Respir Dis, 140 (1989) 477-482.

[118] K.R. Bhaskar, D.D. O'Sullivan, H. Opaskar-Hincman, L.M. Reid, S.J. Coles, Density gradient analysis of secretions produced in vitro by human and canine airway mucosa: identification of lipids and proteoglycans in such secretions, Exp Lung Res, 10 (1986) 401-422.

[119] M.T. Lopez-Vidriero, L. Reid, Chemical markers of mucous and serum glycoproteins and their relation to viscosity in mucoid and purulent sputum from various hypersecretory diseases, Am Rev Respir Dis, 117 (1978) 465-477.

[120] D.F. Rogers, Mucus pathophysiology in COPD: differences to asthma, and pharmacotherapy, Monaldi Arch Chest Dis, 55 (2000) 324-332.

[121] E. Prescott, P. Lange, J. Vestbo, Chronic mucus hypersecretion in COPD and death from pulmonary infection, Eur Respir J, 8 (1995) 1333-1338.

[122] J.R. Davies, H.W. Hovenberg, C.J. Linden, R. Howard, P.S. Richardson, J.K. Sheehan, I. Carlstedt, Mucins in airway secretions from healthy and chronic bronchitic subjects, Biochem J, 313 (Pt 2) (1996) 431-439.

[123] D.J. Thornton, I. Carlstedt, M. Howard, P.L. Devine, M.R. Price, J.K. Sheehan, Respiratory mucins: identification of core proteins and glycoforms, Biochem J, 316 (Pt 3) (1996) 967-975.

[124] S. Sethi, Bacterial infection and the pathogenesis of COPD, Chest, 117 (2000) 286S-291S.

[125] J.L. Devalia, R.J. Sapsford, C. Rusznak, M.J. Toumbis, R.J. Davies, The effects of salmeterol and salbutamol on ciliary beat frequency of cultured human bronchial epithelial cells, in vitro, Pulmonary pharmacology, 5 (1992) 257-263.

[126] S. Lindberg, R. Khan, T. Runer, The effects of formoterol, a long-acting beta 2-adrenoceptor agonist, on mucociliary activity, Eur J Pharmacol, 285 (1995) 275-280.

[127] B. Melloni, J. Germouty, [The influence of a new beta agonist: formoterol on mucociliary function], Revue des maladies respiratoires, 9 (1992) 503-507.

[128] D. Pavia, J.E. Agnew, P.P. Sutton, M.T. Lopez-Vidriero, M.M. Clay, M. Killip, S.W. Clarke, Effect of terbutaline administered from metered dose inhaler (2 mg) and subcutaneously (0.25 mg) on tracheobronchial clearance in mild asthma, British journal of diseases of the chest, 81 (1987) 361-370.

[129] M.A. Sackner, Effect of respiratory drugs on mucociliary clearance, Chest, 73 (1978) 958-966.

[130] D.B. Yeates, D.M. Spektor, B.R. Pitt, Effect of orally administered orciprenaline on tracheobronchial mucociliary clearance, European journal of respiratory diseases, 69 (1986) 100-108.

[131] W.D. Bennett, Effect of beta-adrenergic agonists on mucociliary clearance, J Allergy Clin Immunol, 110 (2002) S291-297.

[132] D.A. Mahler, J.F. Donohue, R.A. Barbee, M.D. Goldman, N.J. Gross, M.E. Wisniewski, S.W. Yancey, B.A. Zakes, K.A. Rickard, W.H. Anderson, Efficacy of salmeterol xinafoate in the treatment of COPD, Chest, 115 (1999) 957-965.

[133] R. Aalbers, J. Ayres, V. Backer, M. Decramer, P.A. Lier, P. Magyar, J. Malolepszy, R. Ruffin, G.W. Sybrecht, Formoterol in patients with chronic obstructive pulmonary disease: a randomized, controlled, 3-month trial, Eur Respir J, 19 (2002) 936-943.

[134] C.E. Chambers, B. Corrigan, M.T. Newhouse, Salmeterol speeds mucociliary transport in healthy subjects., Am J Respir Crit Care Med, 159 (1999) A636.

[135] J. Tamaoki, M. Kondo, T. Takizawa, Effect of cAMP on ciliary function in rabbit tracheal epithelial cells, Journal of applied physiology, 66 (1989) 1035-1039.

[136] M. Salathe, Effects of beta-agonists on airway epithelial cells, J Allergy Clin Immunol, 110 (2002) S275-281.

[137] R.J. Phipps, I.P. Williams, P.S. Richardson, J. Pell, R.J. Pack, N. Wright, Sympathomimetic drugs stimulate the output of secretory glycoproteins from human bronchi in vitro, Clin Sci (Lond), 63 (1982) 23-28.

[138] A. Wanner, Effects of methylxanthines on airway mucociliary function, Am J Med, 79 (1985) 16-21.

[139] G.S. Duchateau, J. Zuidema, F.W. Merkus, The in vitro and in vivo effect of a new non-halogenated corticosteroid - budesonide - aerosol on human ciliary epithelial function, Allergy, 41 (1986) 260-265.

[140] F.J. Accurso, Update in cystic fibrosis 2005, Am J Respir Crit Care Med, 173 (2006) 944-947.

[141] J.J. Wine, The genesis of cystic fibrosis lung disease, J Clin Invest, 103 (1999) 309-312.

[142] H. Matsui, B.R. Grubb, R. Tarran, S.H. Randell, J.T. Gatzy, C.W. Davis, R.C. Boucher, Evidence for periciliary liquid layer depletion, not abnormal ion composition, in the pathogenesis of cystic fibrosis airways disease, Cell, 95 (1998) 1005-1015.

[143] R.C. Boucher, M.J. Stutts, M.R. Knowles, L. Cantley, J.T. Gatzy, Na+ transport in cystic fibrosis respiratory epithelia. Abnormal basal rate and response to adenylate cyclase activation, J Clin Invest, 78 (1986) 1245-1252.

[144] R.A. Frizzell, G. Rechkemmer, R.L. Shoemaker, Altered regulation of airway epithelial cell chloride channels in cystic fibrosis, Science, 233 (1986) 558-560.

[145] M. Knowles, J. Gatzy, R. Boucher, Relative ion permeability of normal and cystic fibrosis nasal epithelium, J Clin Invest, 71 (1983) 1410-1417.

[146] M. Robinson, S. Eberl, C. Tomlinson, E. Daviskas, J.A. Regnis, D.L. Bailey, P.J. Torzillo, M. Menache, P.T. Bye, Regional mucociliary clearance in patients with cystic fibrosis, J Aerosol Med, 13 (2000) 73-86.

[147] J.A. Regnis, M. Robinson, D.L. Bailey, P. Cook, P. Hooper, H.K. Chan, I. Gonda, G. Bautovich, P.T. Bye, Mucociliary clearance in patients with cystic fibrosis and in normal subjects, Am J Respir Crit Care Med, 150 (1994) 66-71.

[148] M. Armengot, A. Escribano, C. Carda, C. Sanchez, C. Romero, J. Basterra, Nasal mucociliary transport and ciliary ultrastructure in cystic fibrosis. A comparative study with healthy volunteers, Int J Pediatr Otorhinolaryngol, 40 (1997) 27-34.

[149] C. Jarstrand, P. Camner, K. Philipson, Mycoplasma pneumoniae and tracheobronchial clearance, Am Rev Respir Dis, 110 (1974) 415-419.

[150] E. Daviskas, S.D. Anderson, S. Eberl, H.K. Chan, G. Bautovich, Inhalation of dry powder mannitol improves clearance of mucus in patients with bronchiectasis, Am J Respir Crit Care Med, 159 (1999) 1843-1848.

[151] E. Daviskas, S.D. Anderson, S. Eberl, H.K. Chan, I.H. Young, The 24-h effect of mannitol on the clearance of mucus in patients with bronchiectasis, Chest, 119 (2001) 414-421.

[152] W.M. Foster, E.M. Wagner, Bronchial edema alters (99m)Tc-DTPA clearance from the airway surface in sheep, J Appl Physiol, 91 (2001) 2567-2573.

[153] E. Puchelle, J.M. Zahm, F. Girard, A. Bertrand, J.M. Polu, F. Aug, P. Sadoul, Mucociliary transport in vivo and in vitro. Relations to sputum properties in chronic bronchitis, European journal of respiratory diseases, 61 (1980) 254-264.

[154] G. Oberdörster, Lung clearance of inhaled insoluble and soluble particles, J Aerosol Med, 1 (1988) 289.

[155] D.A. Edwards, A. Ben-Jebria, R. Langer, Recent advances in pulmonary drug delivery using large, porous inhaled particles, J Appl Physiol, 85 (1998) 379-385.

[156] Y. Tabata, Y. Ikada, Effect of the size and surface charge of polymer microspheres on their phagocytosis by macrophage, Biomaterials, 9 (1988) 356-362.

[157] J.A. Champion, S. Mitragotri, Role of target geometry in phagocytosis, Proc Natl Acad Sci U S A, 103 (2006) 4930-4934.

[158] C. Evora, I. Soriano, R.A. Rogers, K.N. Shakesheff, J. Hanes, R. Langer, Relating the phagocytosis of microparticles by alveolar macrophages to surface chemistry: the effect of 1,2-dipalmitoylphosphatidylcholine, J Control Release, 51 (1998) 143-152.

[159] N. Tsapis, D. Bennett, B. Jackson, D.A. Weitz, D.A. Edwards, Trojan particles: large porous carriers of nanoparticles for drug delivery, Proc Natl Acad Sci U S A, 99 (2002) 12001-12005.

[160] M.M. Bailey, C.J. Berkland, Nanoparticle formulations in pulmonary drug delivery, Medicinal research reviews, 29 (2009) 196-212.

[161] I.M. El-Sherbiny, S. McGill, H.D. Smyth, Swellable microparticles as carriers for sustained pulmonary drug delivery, J Pharm Sci, 99 (2010) 2343-2356.

[162] H. Larhrib, G.P. Martin, C. Marriott, D. Prime, The influence of carrier and drug morphology on drug delivery from dry powder formulations, Int J Pharm, 257 (2003) 283-296.

[163] K.C. Lee, S.Y. Chae, T.H. Kim, S. Lee, E.S. Lee, Y.S. Youn, Intrapulmonary potential of polyethylene glycol-modified glucagon-like peptide-1s as a type 2 anti-diabetic agent, Regul Pept, 152 (2009) 101-107.

[164] K.K. Gill, S. Nazzal, A. Kaddoumi, Paclitaxel loaded PEG(5000)-DSPE micelles as pulmonary delivery platform: formulation characterization, tissue distribution, plasma pharmacokinetics, and toxicological evaluation, Eur J Pharm Biopharm, 79 (2011) 276-284.

[165] J. Fu, J. Fiegel, E. Krauland, J. Hanes, New polymeric carriers for controlled drug delivery following inhalation or injection, Biomaterials, 23 (2002) 4425-4433.

[166] M.A. Videira, M.F. Botelho, A.C. Santos, L.F. Gouveia, J.J. de Lima, A.J. Almeida, Lymphatic uptake of pulmonary delivered radiolabelled solid lipid nanoparticles, Journal of drug targeting, 10 (2002) 607-613.

[167] G. Oberdörster, Biokinetics and effects of nanoparticles, in: P.P. Simeonova, N. Opopol, M.I. Luster (Eds.) Nanotechnology--toxicological issues and environmental safety, Springer, Dordrecht, Netheralnds, 2007, pp. 15-51.

[168] J.C. Lay, N.E. Alexis, K.L. Zeman, D.B. Peden, W.D. Bennett, In vivo uptake of inhaled particles by airway phagocytes is enhanced in patients with mild asthma compared with normal volunteers, Thorax, 64 (2009) 313-320.

[169] N.E. Alexis, J. Soukup, S. Nierkens, S. Becker, Association between airway hyperreactivity and bronchial macrophage dysfunction in individuals with mild asthma, Am J Physiol Lung Cell Mol Physiol, 280 (2001) L369-375.

[170] M.L. Huynh, K.C. Malcolm, C. Kotaru, J.A. Tilstra, J.Y. Westcott, V.A. Fadok, S.E. Wenzel, Defective apoptotic cell phagocytosis attenuates prostaglandin E2 and 15-hydroxyeicosatetraenoic acid in severe asthma alveolar macrophages, Am J Respir Crit Care Med, 172 (2005) 972-979.

[171] G. Apiou-Sbirlea, I.M. Katz, T.B. Martonen, The effects of simulated airway diseases and affected flow distributions on aerosol deposition, Respir Care, 55 (2010) 707-718.

[172] A.M. Fitzpatrick, F. Holguin, W.G. Teague, L.A. Brown, Alveolar macrophage phagocytosis is impaired in children with poorly controlled asthma, J Allergy Clin Immunol, 121 (2008) 1372-1378, 1378 e1371-1373.

[173] C.S. Berenson, M.A. Garlipp, L.J. Grove, J. Maloney, S. Sethi, Impaired phagocytosis of nontypeable Haemophilus influenzae by human alveolar macrophages in chronic obstructive pulmonary disease, J Infect Dis, 194 (2006) 1375-1384.

[174] S.V. Culpitt, D.F. Rogers, P. Shah, C. De Matos, R.E. Russell, L.E. Donnelly, P.J. Barnes, Impaired inhibition by dexamethasone of cytokine release by alveolar macrophages from patients with chronic obstructive pulmonary disease, Am J Respir Crit Care Med, 167 (2003) 24-31.

[175] S. Hodge, G. Hodge, R. Scicchitano, P.N. Reynolds, M. Holmes, Alveolar macrophages from subjects with chronic obstructive pulmonary disease are deficient in their ability to phagocytose apoptotic airway epithelial cells, Immunol Cell Biol, 81 (2003) 289-296.

[176] R.E. Russell, S.V. Culpitt, C. DeMatos, L. Donnelly, M. Smith, J. Wiggins, P.J. Barnes, Release and activity of matrix metalloproteinase-9 and tissue inhibitor of metalloproteinase-1 by alveolar macrophages from patients with chronic obstructive pulmonary disease, Am J Respir Cell Mol Biol, 26 (2002) 602-609.

[177] A.E. Taylor, T.K. Finney-Hayward, J.K. Quint, C.M. Thomas, S.J. Tudhope, J.A. Wedzicha, P.J. Barnes, L.E. Donnelly, Defective macrophage phagocytosis of bacteria in COPD, Eur Respir J, 35 (2010) 1039-1047.

[178] S. Brennan, P.D. Sly, C.L. Gangell, N. Sturges, K. Winfield, M. Wikstrom, S. Gard, J.W. Upham, C.F. Arest, Alveolar macrophages and CC chemokines are increased in children with cystic fibrosis, Eur Respir J, 34 (2009) 655-661.

[179] R.W. Vandivier, V.A. Fadok, P.R. Hoffmann, D.L. Bratton, C. Penvari, K.K. Brown, J.D. Brain, F.J. Accurso, P.M. Henson, Elastase-mediated phosphatidylserine receptor cleavage impairs apoptotic cell clearance in cystic fibrosis and bronchiectasis, J Clin Invest, 109 (2002) 661-670.

[180] T.R. Gerrity, C.S. Garrard, D.B. Yeates, A mathematical model of particle retention in the air-spaces of human lungs, Br J Ind Med, 40 (1983) 121-130.

[181] J. Sanchis, M. Dolovich, R. Chalmers, M. Newhouse, Quantitation of regional aerosol clearance in the normal human lung, J Appl Physiol, 33 (1972) 757-762.

[182] W. Hofmann, M.G. Ménache, T.B. Martonen, Age-dependent lung dosimetry of radon progeny, in: J.D. Crapo, E.D. Smolko, F.J. Miller, J.A. Graham, A.W. Hayes (Eds.) Extrapolation of Dosimetric Relationships for Inhaled Particles and Gases, Academic Press, San Diego, 1989.

[183] T.B. Martonen, W. Hofmann, Dosimetry of localised accumulations of cigarette smoke and radon progeny at bifurcations, Radiat Prot Dosim, 38 (1991) 81.

[184] A.H. Travers, A.P. Jones, C.A. Camargo, Jr., S.J. Milan, B.H. Rowe, Intravenous beta(2)-agonists versus intravenous aminophylline for acute asthma, Cochrane Database Syst Rev, 12 (2012) CD010256.

[185] U.G. Lalloo, G.M. Ainslie, M.S. Abdool-Gaffar, A.A. Awotedu, C. Feldman, M. Greenblatt, E.M. Irusen, R. Mash, S.S. Naidoo, J. O'Brien, W. Otto, G.A. Richards, M.L. Wong, S. South African Thoracic, Guideline for the management of acute asthma in adults: 2013 update, S Afr Med J, 103 (2013) 189-198.

[186] S. Koo, D.W. Kubiak, N.C. Issa, A. Dietzek, S. Boukedes, P.C. Camp, H.J. Goldberg, L.R. Baden, A.L. Fuhlbrigge, F.M. Marty, A targeted peritransplant antifungal strategy for the prevention of invasive fungal disease after lung transplantation: a sequential cohort analysis, Transplantation, 94 (2012) 281-286.

[187] L. Kuiper, E.J. Ruijgrok, A review on the clinical use of inhaled amphotericin B, Journal of aerosol medicine and pulmonary drug delivery, 22 (2009) 213-227.

[188] M.B. Snipes, R.O. McClellan, J.L. Mauderly, R.K. Wolff, Retention patterns for inhaled particles in the lung: comparisons between laboratory animals and humans for chronic exposures, Health Phys, 57 Suppl 1 (1989) 69-77; discussion 77-68.

[189] R.K. Wolff, M.A. Dorato, Toxicologic testing of inhaled pharmaceutical aerosols, Critical reviews in toxicology, 23 (1993) 343-369.

Chapter 2 : In Vitro and In Vivo Performance of Dry Powder Inhalation Formulations: Comparison of Particles Prepared by Thin Film Freezing and Micronization

2.1 Abstract

Recently, inhaled immunosuppressive agents have attracted increasing attention for maintenance therapy following lung transplantation. The rationale for this delivery approach includes a more targeted and localized delivery to the diseased site with reduced systemic exposure, potentially leading to decreased adverse side effects. In this study, the in vitro and in vivo performance of an amorphous formulation prepared by thin film freezing (TFF) and a crystalline micronized formulation produced by milling was compared for Tacrolimus (TAC). Despite the relatively large geometric size, the TFF processed formulation was capable of achieving deep lung delivery due to its low density, highly porous and brittle characteristics. When emitted from a Miat® monodose inhaler, TFF processed TAC formulations exhibited a fine particle fraction (FPF) of 83.3% and a mass median aerodynamic diameter (MMAD) of 2.26 μm. Single dose 24-h pharmacokinetic studies in rats demonstrated that the TAC formulation prepared by TFF exhibited higher pulmonary bioavailability with a prolonged retention time in the lung, possibly due to decreased clearance (e.g., macrophage phagocytosis), compared to the micronized TAC formulation. Additionally, TFF formulation generated a lower systemic

TAC concentration with smaller variability than the micronized formulation following inhalation, potentially leading to reduced side effects related to the drug in systemic circulation.

2.2 Introduction

Since 1954, when the first long-term organ transplant was successfully performed, tremendous progress has been made in the field of surgical techniques and transplant medications. The importance of medicines that inhibit the immune system and prevent rejection of a transplanted organ is now better realized. Currently, lung transplantation is the least successful in terms of post-transplant survival rate among all the common solid organ transplants with survival rates of 88% at 3 months, 79% at 1 year, 64% at 3 years, 53% at 5 years and 31% at 10 years [1]. The low survival rate is due to such conditions as bronchiolitis obliterans syndrome (BOS) associated with acute and chronic allograft rejection [1, 2]. Over the last two decades, immunosuppressive agents have gained more attention in treating rejection after organ and tissue transplantation. Present immunosuppressive therapy consists of a combination of a three orally administered drug regimen, a calcineurin inhibitor (Cyclosporine A or Tacrolimus), an antimetabolite (Mycophenolate mofetil or Azathioprine), and a corticosteroid [3].

Cyclosporine A (CsA) and Tacrolimus (TAC) are the two most commonly used calcineurin inhibitors for maintenance therapy after organ transplantation [4]. CsA was commercialized in 1983 by Novartis under the brand name Sandimmune® for systemic or oral treatment of acute and chronic transplant rejection. TAC, a more potent

immunosuppressive drug than CsA [5], can be administered twice daily for maintenance therapy (Prograf®, Astellas). Most recently, an extended release oral formulation of TAC was reported (Astagraf XL®, Astellas) and is taken once daily. It has been reported that TAC improves both short-term graft success and long-term patient survival rates with lower systemic toxicity compared to CsA [6-9]. In light of this, TAC is used more frequently than CsA [10]. However, the use of TAC is limited by its erratic oral bioavailability (varies from 4%-93%) and a variety of adverse side effects associated with elevated systemic concentrations over prolonged periods of therapy, such as nephrotoxicity, neurotoxicity, hypertension, diabetes mellitus, and increased risk of opportunistic infection [4].

Another approach to improve clinical outcomes of immunosuppressive agents in lung transplant patients is to administer the drugs via pulmonary inhalation. The rationale for this approach is more targeted and localized delivery with lower systemic exposure related to adverse side effects. Numerous studies reported inhaled CsA formulations to prevent rejection after lung transplantation [11-16]. One formulation, Cyclosporine Inhalation Solution (CIS) in propylene glycol (300 mg/4.8 mL, administered three times a week) has been investigated and demonstrated positive results [17]. Although CIS exhibited no statistical improvements in acute graft rejection compared to inhaled placebo, prevention of chronic rejection and patient survival rates were significantly improved [17]. This therapy was denied approval by the FDA due to uncertainties with the carrier vehicle and a lack of clinical efficacy [18]. Since TAC is more potent than CsA and formulated as a dry powder in the present study, it is possible that inhaled TAC

will achieve better clinical outcomes compared to inhaled CsA. Recently, alternative delivery systems containing TAC have been reported for inhalation applications to treat lung diseases, including a metered dose inhaler [19-21], nebulized solution in 70% ethanol [22, 23], nebulized nanoparticle dispersions [4, 24, 25], nano-liposomal dry powder inhalation [26] and respirable low-density brittle matrix particles [27]. Similar or slightly enhanced effects (suppression of airway inflammation or prevention of chronic and acute rejection after lung transplantation) and greatly reduced systemic exposure related to potentially decreased side effects were observed for inhaled TAC compared to oral or intramuscular injected TAC. Therefore, inhaled TAC is a feasible approach for maintenance therapy after lung transplantation.

Pulmonary drug delivery by Dry Powder Inhalers (DPIs) has been well established as a valuable and efficient method for local and systemic treatment of diseases. Almost all the marketed DPIs are carried-based formulations, which have high dose variability and low delivery efficiency (%FPF ranging from 10%-35%) [27]. Recently, engineered particles capable of more efficient pulmonary delivery have gained increasing attention. Large, porous, low-density particles were first introduced by Edwards et al., which are able to achieve deep lung delivery despite their relatively large geometric size (up to 20 μm) [28]. Since then a variety of technologies have been developed to enhance the pulmonary deposition efficiency of DPIs, including AIR® [29], PulmoSphere® [30, 31], Technosphere® [32], NanoCluster® [33] and brittle matrix particles prepared by Thin Film Freezing (TFF) [27]. Additionally, it has been reported that engineered particles with geometric diameter larger than 10 μm or smaller than 100 nm can escape from

macrophage phagocytosis, leading to prolonged lung retention time [34]. Moreover, the tailored physicochemical properties of engineered particles (e.g. amorphous, enhanced surface area, high porosity etc.) have demonstrated improved drug dissolution rate in the lung lining fluid [4, 35]. Therefore, TFF process was selected in this study to prepare the TAC formulation suitable for dry powder inhalation which was compared with traditional micronized particles.

Lactose is the only excipient approved by the U.S. Food and Drug Administration (FDA), which can be used in DPIs at a high amount (up to 25 mg). Nearly all the carrier-based DPI products on the market used lactose as carrier [27]. Mannitol (MAN) is also approved by the FDA as an excipient for inhalation, but limited to a very low content (0.051%). However, MAN can be inhaled up to doses of 365mg (Aridol®, Pharmaxis Ltd.) to assess bronchial hyperresponsivesness in patients. It has been reported by Watts et al. that respirable brittle matrix particles prepared by TFF were susceptible to moisture induced matrix collapse and hygroscopicity when lactose was used as excipient; in contrast, the aerosolization properties of TFF processed powders with MAN were not influenced by high humidity [27]. Therefore, MAN was chosen in this study due to its superior formulation stability.

The objective of this study is to compare the in vitro and in vivo performance of dry powder inhalation formulations of TAC made by TFF to that made by micronization. We hypothesize that pulmonary delivery of the TFF processed formulation would yield higher deposition and more prolonged drug retention in the lung, compared to the micronized formulation, due to its aerodynamic properties and differences in clearance.

Additionally the TFF processed formulation will generate lower systemic concentration with smaller variability compared to micronized formulation, which could possibly lead to decreased side effects. To our knowledge, the pharmacokinetic properties of TAC following dry powder inhalation of amorphous TFF processed formulation versus crystalline micronized formulation have not been previously reported.

2.3 Materials and methods

2.3.1 Materials

The following materials were purchased: Tacrolimus monohydrate (Haroui Pharma-Chem Inc.,Irvine, CA); Ascomycin (ASCO, LC Laboratories, Woburn, MA); Mannitol, HPLC grade acetonitrile and methanol (Fisher Scientific, Pittsburgh, PA); Polysorbate 80 (Spectrum, Gardena, CA); Ethanol (Decon Labs, King of Prussia, PA); 0.9% sodium chloride for injection and heparin sodium 10,000 units/mL (TW Medical, Lago Vista, TX).

2.3.2 Preparation of micronized TACMAN and TFF TACMAN

Micronized TAC powders were prepared by wet ball milling followed by size reduction utilizing jet milling. Two grams of bulk TAC powders (mean particle size 84.7 µm with 100% < 127.8 µm, as received from supplier) were dispersed in 25 mL of purified water in a ceramic jar with Zirconia grinding media (1/2 inch radius end cylinder) (US Stoneware, East Palestine, OH). The TAC dispersion was milled on a ball mill at 100 rpm under room temperature for 24 hours , and the resulting slurry was combined with several successive washings of the ceramic jar and milling media using purified water.

The obtained TAC particle dispersion was pre-cooled in a -80°C freezer and lyophilized in a VirTis Advantage bench top tray lyophilizer (The VirTis Company, Inc., Gardiner, NY, USA). Further size reduction was achieved by feeding the obtained TAC dry powder into an air-jet mill (Aljet mill, Fluid Energy, Plumsteadville, PA, USA) with a feed pressure of 80 psi and a grinding pressure of 65 psi. Samples were collected and analyzed from the collecting chamber. Micronized MAN was produced by jet milling the bulk materials 4-5 times until the particle size reached the respirable range (1-5 μm). The particle size before and after milling was monitored using a Sympatec Helos laser diffraction instrument (Sympatec GmbH, Germany) equipped with a R3 lens. Briefly, the powder was dispersed in a non-solvent system (water for TAC, acetone for MAN) by 5 seconds of sonication. The detector was activated at a minimum optical concentration of between 4% and 5%. Once the desirable size of the TAC and MAN particles were obtained, a physical mixture of micronized TAC and micronized MAN (1:1 by weight, micronized TACMAN) was acquired by blending the two powders using a tubular mixer.

TFF TACMAN was prepared by Thin Film Freezing (TFF) technology. A detailed description of the TFF process was previously reported by Engstrom et al. [36]. Briefly, MAN was dissolved in purified water and TAC was dissolved in acetonitrile (ACN), respectively. A co-solvent mixture of ACN and water (60:40 v/v) containing TAC and MAN (1:1 w/w) was obtained by adequate mixing of the two solutions. The total solid concentration of the co-solvent was 0.75% (w/v). The co-solvent solution was rapidly frozen on a on a cryogenically cooled rotating stainless steel surface (−50 ± 3°C). The resulting thin film was removed from the surface by a scraper and maintained in the

frozen state in liquid nitrogen. Solvents were sublimated by lyophilization over 48 hours at pressures less than 200mTorr while the shelf temperature was gradually ramped from −40°C to 25°C. Prior to sample removal from the lyophilizer, dry nitrogen was purged into the chamber to equilibrate to atmospheric pressure and the final product was stored in a vacuum desiccator at room temperature.

2.3.3 Differential Scanning Calorimetry (DSC)

Thermal properties of micronized TACMAN, TFF TACMAN and each of their components were determined by a modulated temperature DSC (TA Instruments Model 2920, New Castle, DE) equipped with a refrigerated cooling system. Dry nitrogen gas was purged through the DSC cell at a flow rate of 40 mL/min. Then 5–10 mg of samples were weighed into aluminum crimped pans (Kit 0219-0041, Perkin–Elmer Instruments, Norwalk, CT) and heated at a ramp rate of 10°C/min from 30 to 250 °C with a modulation temperature amplitude of 1°C/60 s. Data were analyzed using TA Universal Analysis 2000 software (TA Instruments, New Castle, DE).

2.3.4 Powder X-ray Diffraction (XRD)

The crystallinity of the same set of samples was evaluated by wide angle XRD (A Philips 1710 X-ray diffractometer, Cu Ka1 radiation, $\lambda = 1.54059$ Å, 40 kV, 40 mA). Samples were analyzed ranging from 5° to 40° at a 2θ step size of 0.05° and a dwell time of 2 seconds.

2.3.5 Attenuated Total Reflectance-Fourier Transform Infrared Spectroscopy (ATR-FTIR)

Infrared spectra were obtained using a Bruker Equinox55 FTIR spectrophotometer (Karlsruhe, Germany) equipped with a deuterated triglycine sulfate detector and an attached attenuated total reflectance unit (Thermo Scientific, Hudson, NH). The same pressure was applied to all samples against the diamond crystal of the ATR cell by a pressure applicator with a torque knob monitor. Measurements were carried out with a scanning range of 800 to 4000 cm^{-1}, resolution of 4 cm^{-1} and 16 scans per sample. Before each measurement background was scanned and subtracted, and all measurements were conducted at least three times to ensure the reproducibility.

2.3.6 Scanning Electron Microscopy (SEM)

SEM was employed to evaluate the morphology of both micronized and TFF particles. Prior to imaging, samples were mounted under vacuum onto aluminum stages with double-side carbon tape and coated using sputter coater (Electron Microscopy Sciences, USA) with platinum/palladium targeted for 12 nm thickness. Sample images were captured using a Leo 1530 scanning electron microscopy operating at an accelerating voltage of 10 kV.

2.3.7 Brunauer–Emmett–Teller (BET) specific surface area analysis

Specific surface area was determined by a Monosorb MS-21 surface area analyzer. The Monosorb utilizes a modified BET equation for extremely rapid, single-point determinations of surface area ($P/P_0 = 0.294$). Samples were degassed at 30 °C by

nitrogen purging (20 psi) for at least 2 hours prior to measurement, and 30% Nitrogen in helium was used as the adsorbate gas.

2.3.8 Geometric particle size measurement

Geometric particle size of micronized TACMAN and TFF TACMAN aerosolized from a Miat monodose inhaler® (Miat, Milan, Italy) was measured by low angle light scattering technique using a Malvern Spraytec® (Malvern, UK) equipped with an inhalation cell and an induction port. The inhaler was loaded with a size 3 hypromellose (HPMC) capsule (Capsugel, Peapack, NJ) containing 3 mg of formulation and fitted to the mouth of the induction port by a silicone adapter. A pre-determined flow rate of 90 L/min to achieve a 4 kPa pressure drop across the device was used for all measurements [37]. Data were collected over 4 seconds upon actuation when laser transmission dropped below 98%. Values reported are the average of at least three measurements.

2.3.9 In vitro aerosol performance

The aerodynamic properties of TFF TACMAN were investigated by a Next Generation Impactor (NGI) (MSP Corp., Shoreview, MN). A similar set up with the geometric particle size measurement was used. The Miat monodose inhaler® loaded with size 3 HPMC capsules containing 3 mg of formulation was secured to the induction port by a silicone adapter. Aerosols were generated over 2.7 seconds at a flow rate of 90 L/min to achieve an inhalation volume of 4 L. Prior to actuation, surfaces of collection stages were coated with 1% polysorbate 80 in enthanol (v/v) and allowed to completely dry, as recommended by the European Pharmaceutical Aerosol Group (EPAG) [38]. The

cut-off size for each stage was calculated to be 6.48, 3.61, 2.30, 1.37, 0.76, 0.43 and 0.26 µm from stages 1 to 7 and micro-orifice collector (MOC), respectively [39]. Following actuation, the deposited powders in the capsule, inhaler, adaptor, induction port, stages 1 to 7 and MOC were collected by rinsing each area with 10 mL of methanol:water (90:10, v/v), which is the mobile phase for TAC quantification [40]. Briefly, TAC content was analyzed using a Dionex high performance liquid chromatography (HPLC) system equipped with a reversed phase C18 column (150 mm × 4.6 mm, 5 µm, 300 Å) with a Universal security guard column (Phenomenex, Torrance, CA). The mobile phase consisted of 90/10 (v/v) methanol/water and the injection volume was 20 µL. TAC was eluted over 6 minutes at a flow rate of 0.8 mL/min and a detection wavelength of 210 nm.

The emitted dose (ED) was calculated as the percentage of drug emitted from the inhaler with respect to the total loaded dose into the capsule. The mass median aerodynamic diameter (MMAD), geometric standard deviation (GSD) and fine particle fraction (FPF) were calculated according to the USP 32-NF 27 General Chapter 601 [41]. A plot of cumulative percentage of mass less than stated aerodynamic diameter versus aerodynamic diameter (cut-off size for each stage) was built and fit to a 4 parameters logistic curve using Sigmaplot (Systat Software Inc., San Jose, CA). MMAD and GSD were calculated based on the drug deposition from stage 1 to 7 and MOC. FPF was determined as the percentage of aerosolized particles with a MMAD less than 5 µm with respect to the emitted dose.

2.3.10 In vivo pulmonary dosing in rats

In vivo pharmacokinetic study was conducted using Sprague–Dawley rats (Charles River Laboratories, Inc., Wilmington, MA) in compliance with the Institutional Animal Care and Use Committee (IACUC) guidelines at The University of Texas at Austin. The rats (male and female: weighing from 250-300 g with an average weight of 270 g) were housed in a 12-h light/dark cycle with access to food and water *ad libitum*. Rats were subjected to one week of acclimation time to the housing environment and another week of restraint training in the nose-only dosing chamber. Powder aerosols were generated by a rotating brush generator (Palas RBG 1000, Palas GmbH, Karlsruhe, Germany). A detailed set up of the dosing apparatus was illustrated in Fig.2.1. Sixteen rats were dosed for each formulation group (12 non pre-catheterized rats for lung sample collection and 4 pre-catheterized rats for blood sample collection). Prior to dosing, the exposure time for micronized TACMAN and TFF TACMAN were calculated to ensure that same TAC concentrations in the chamber were achieved. After exposure to the aerosolized powders, blood samples were withdrawn from a jugular vein catheter at 0.25, 1, 2, 4, 8 ,12 and 24 hours and stored in a BD Vacutainer® blood collection tube at -80°C until analyzed. Equivalent volume of saline was replaced after each withdrawing. Three rats from each group were sacrificed at each time point (0.5, 1, 2, 8, and 24 hours) and lung samples were obtained. Prior to lung sample collection, a modified bronchoalveolar lavage (BAL) procedure was performed [26]. Briefly, the trachea was exposed by blunt dissection of the sternohyoideus muscle and a small incision was made to insert the lavage needle

outfitted with a 5 mL BD syringe. Approximately 3 mL of sterile phosphate buffered saline (PBS) was slowly injected to fill the lungs and the BAL fluid was withdrawn by gentle aspiration. This procedure was conducted twice so the total yield of BAL was between 4-5 mL. Then the lung was excised and stored in a -80°C freezer prior to analysis.

2.3.11 Quantification of TAC concentration in the lung and blood

TAC concentration in the lung and blood was quantified by liquid chromatography mass spectrometry (LC/MS/MS). The LC/MS/MS system consisted of a Shimadzu SCL-10A Controller, LC-10AD pump with a FCV-10AL mixing chamber, SIL-10AD autosampler, and an AB Sciex API 3200 tandem mass spectrometer with turbo ion spray. The analytical column (Grace Alltima C18, 4.6 x 150 mm, 5 µm, Alltech, Deerfield, IL) was maintained at 60^{o}C during the chromatographic runs using a Shimadzu CTO-10A column oven. Mobile phase A contained 10 mM ammonium formate and 0.1% formic acid dissolved in HPLC grade methanol. Mobil phase B contained 10 mM ammonium formate and 0.1% formic acid dissolved in 90% HPLC grade methanol. The flow rate was maintained at 0.5 ml/min and TAC was eluted with a step gradient. The column was equilibrated with 100% mobile phase B. At 6.1 minutes after injection, the system was switched to 100% mobile phase A. Finally, at 15.1 min; the system was switched back to 100% mobile phase B in preparation for the next injection. The TAC transition was detected at 931.6 Da (precursor ion) and the daughter ion was detected at 864.5 Da. Ascomycin (ASCO, internal standard) was detected at 809.574 Da and the daughter ion

was 756.34 Da. The ratio of the peak area of TAC to that of the internal standard (response ratio) for each unknown sample was compared against a linear regression of calibrator response ratios to quantify TAC.

For extraction of TAC from whole blood sample, 100 µL of calibrator and unknown whole blood samples were mixed with 10 µL of 0.5 µg/mL ASCO (internal standard), 300 µL of a solution containing 0.1% formic acid and 10 mM ammonium formate dissolved in 95% HPLC grade methanol. The samples were vortexed vigorously for 2 min, and centrifuged at 15,000 *g* for 5 min. Supernatants were transferred to 1.5 ml microfilterfuge tubes and centrifuged at 15,000 *g* for 1 minute, then 40 µL of the final extracts were injected into the LC/MS/MS system. The concentration of TAC was expressed as ng/mL in the whole blood.

TAC was extracted from rat lung tissue according to the following protocol. Briefly, 100 mg of calibrator, control, and unknown tissue samples were mixed by sonication (three 5 seconds bursts) with 10 µL of 0.5 µg/mL ASCO (internal standard) and 300 µL of a solution containing 0.1% formic acid and 10 mM ammonium formate dissolved in 95% HPLC grade methanol. After sonication, the samples were vortexed vigorously for 2 min, and then centrifuged at 15,000 *g* for 5 min. Supernatants were transferred to 1.5 mL microfilterfuge tubes and centrifuged at 15,000 *g* for 1 minute and then 40 µL of the final extracts were injected into the LC/MS/MS. The concentration of TAC was expressed as ng/g in the lung tissue.

2.3.12 Pharmacokinetic and statistical analysis

Plots of the concentration of TAC in the lung tissue and whole blood versus time were used to compare the pharmacokinetic behaviors of micronized TACMAN and TFF TACMAN. The TAC concentration at the first time point (0.5 h) was considered as the initial dose. The TAC concentrations in the lung were normalized with respect to the TAC concentration at the first time point (0.5 h) and expressed as the percentage of initial concentration measured in the lung. A two-compartmental model was selected to calculate the pharmacokinetic parameters of TAC in the rat lung with the assistance of WinNonlin Professional Version 2.1 (Pharsight Corporation, Mountain View, CA). The area under the concentration versus time curve (AUC_{0-24h}) was calculated by the linear trapezoidal rule using average TAC concentrations in lung. Student's t tests were conducted to determine the significance between the two dosing groups. For all tests, statistical significance was defined by $p \leq 0.05$.

2.4 Results and discussion

2.4.1 Crystallinity

DSC was used to evaluate the thermal properties of micronized TACMAN, TFF TACMAN and their individual components (Fig.2.2). Micronized TAC displayed a melting peak at 127.16 °C and an enthalpy of fusion of 32.11 J/g; micronized MAN exhibited a melting peak at 171.17 °C and an enthalpy of fusion of 292.8 J/g, indicating that both components are crystalline after micronization. Both of the melting peaks of TAC and MAN were present in micronized TACMAN (1:1). For 1 gram of micronized

TACMAN (1:1), there were 0.497 gram of TAC and 0.503 gram of MAN, so the enthalpy of fusion for TAC endothermic peak based on the mass of TAC in micronized TACMAN (1:1) equals to 16.16/0.497 J/g, namely 32.52 J/g, which was very similar to the experimentally determined enthalpy of fusion of micronized TAC alone. Hence, nearly 100% of the TAC in micronized TACMAN (1:1) was crystalline [42]. Similarly the enthalpy of fusion for MAN endothermic peak based on the mass of MAN in micronized TACMAN (1:1) equals 149.8/0.503 = 297.8 J/g, which correlated to the enthalpy of fusion in micronized MAN alone, indicating 100% of the MAN in micronized TACMAN (1:1) was crystalline as well. TFF TAC only (no excipients, 100% potency) displayed a single glass transition temperature (T_g) of TAC at 75.42 °C. TFF MAN only exhibited an endothermic melting peak of MAN with an enthalpy of fusion (280.2 J/g) very close to the enthalpy of fusion of micronized MAN alone (292.8 J/g), meaning that the MAN in TFF MAN only was nearly 100% crystalline. In the TFF TACMAN (1:1) DSC profile, there was a single T_g (76.28 °C) corresponding to the T_g of TAC (75.42 °C) and no melting peak of TAC was detected, indicating the TAC in TFF TACMAN was amorphous; there was also an endothermic melting peak at 167.75 °C corresponding to the melting of MAN (169.09 °C) with an enthalpy of fusion of 138.2 J/g. Based on the potency (50.7%) of MAN in TFF TACMAN (1:1), the enthalpy of fusion for MAN endothermic peak based on the mass of MAN in TFF TACMAN (1:1) is equal to 138.2/50.7% = 272.6 J/g, similar to the melting of MAN alone, therefore, the MAN in TFF TACMAN (1:1) was 100% crystalline. In summary, TAC and MAN exhibited amorphous and crystalline properties, respectively, in TFF TACMAN (1:1).

In the XRD diffraction pattern (Fig.2.3), TAC exhibited intense characteristic crystalline peaks at 8.55, 12.75, 13.85, 14.25, 15.4, and 19.85 2-theta degrees in the micronized TAC, distinguished from the crystalline peaks of MAN at 14.7, 16.85, 18.85, 20.5, 21.15, 24.65, and 36.1 2-theta degrees in micronized MAN. Micronized TACMAN (1:1) had both the characteristic peaks of TAC and MAN, indicating that both TAC and MAN were crystalline in micronized TACMAN (1:1). All of the characteristic peaks of TAC disappeared in TFF TAC only, indicating a highly amorphous morphology of TAC molecules [43]. In the TFF MAN only XRD profile, some of the characteristic peaks of MAN disappeared and the intensity of some peaks have been greatly reduced. It has been reported that the reduction of XRD peak intensity and broad halo peaks may be attributed to the reduction of particle size or change in crystalline microstructure [44]. As seen in the SEM images (Fig.2.5), TFF produced formulations exhibited a highly porous structure. Although it was not a complete particle size reduction due to aggregation if discrete particles are considered, the large pores between particles may cause molecules to lose their long-range crystalline order but still not be amorphous [44]. Therefore, the MAN in TFF MAN only exhibited crystalline properties. TFF TACMAN (1:1) displayed no characteristic crystalline peaks of TAC, but some broaden and intensity-reduced peaks of MAN corresponding to the peaks in TFF MAN only. Hence, the TAC in TFF TACMAN (1:1) was amorphous and MAN was crystalline.

According to the DSC and XRD results, the crystalline state of TAC and MAN can be predicted during the entire manufacturing process. Initially, TAC was dissolved in acetonitrile (ACN) and MAN was dissolved in water. TAC molecules and MAN

molecules were homogenously dispersed in the co-solvent composed of ACN and water due to the high miscibility of ACN and water. During the TFF process, TAC and MAN are capable of transitioning into a glassy amorphous state because the extremely rapid cooling rate (estimated to be 10^6 K/s) can prevent the nucleation and growth of crystals [43]. Then during the lyophilization process, TAC remained amorphous due to its high T_g (75.42 °C); MAN started to crystallize at its T_g (13 °C, measured from quench-cooled melt [45]). It has been reported that with a second component added into the MAN solution, the relative concentration threshold above which MAN will crystallize during the lyophilization process is about 30% (w/w), and this ratio is largely independent of the nature of the second solute [45]. In our case, TAC was considered as the second solute and the weight ratio of MAN in the formulation is about 50% (w/w), therefore, MAN was still crystalline after being freeze-dried. The seeding of crystalline MAN did not have an impact on TAC molecules because there is no interaction between TAC and MAN molecules according to the ATR-FTIR results (data shown in Fig.2.4; explanation follows below). Consequently the final product, TFF TACMAN (1:1), consists of both amorphous TAC domains and crystalline MAN domains.

2.4.2 Molecular interactions investigated by ATR-FTIR

ATR-FTIR was conducted in order to investigate the molecular interactions between TAC and MAN (Fig.2.4). The micronized TAC spectrum exhibits absorption bands of C=C stretch at 1638 cm^{-1}, and resonating amidic C=O and ketonic C=O stretching vibrations at 1740, 1728 and 1693 cm^{-1}, which can be distinguished from the spectrum of

micronized MAN with a broad OH stretch peak only [46]. In the micronized TACMAN (1:1) spectrum, all these bands were observed with the same absorbance, indicating that there were no interactions between TAC and MAN molecules that existed in this physical mixture of micronized TACMAN. However, in the spectrum of TFF TAC only, the band of C=C stretch shifted from 1638 cm^{-1} to 1650 cm^{-1}, and the bands of resonating amidic C=O and ketonic C=O stretching vibrations shifted from 1740, 1728 and 1693 to 1746, 1716 and 1684 $cm^{-1,}$ respectively. It has been reported that the absorbance of FTIR peaks are very sensitive to the crystal-packing configuration of different forms [47]. Accordingly the shiftiness of TAC absorption peaks in TFF TAC only was attributed to the state change from crystalline to amorphous. The same absorption peaks were observed in TFF TACMAN (1:1) compared with TFF TAC only, indicating there was no interaction between TAC and MAN molecules in TFF TACMAN. In summary, there is no evidence from the spectra of any hydrogen-bond interactions between tacrolimus and mannitol in either the micronized formulation or TFF formulation.

2.4.3 Morphology, geometric particle size and aerodynamic properties

Micronization was employed to physically reduce the particle size and maintain their original crystalline structure. Dry milling in a fluid energy mill (e.g., air-jet mill) is a typically used micronization technique. Despite the high energy input for jet milling, the process is extremely rapid and the materials are subjected to limited thermal stress [48]. However, the major issue with jet milling is the relatively low yield and loss of valuable materials during the repeated feeding and discharging compared to other milling

techniques [49]. Low energy wet ball milling is another widely used micronization technique. Theoretically, the yield from a wet ball milling process can reach up to 100%, but this micronization process requires a long time (hours to days) due to the low energy input [48]. Therefore, a combination of wet ball milling and jet milling was employed in the present study to achieve a high yield of micron-size drug particles and shorten the processing time.

For pulmonary drug delivery, the optimum particle size is 1-5 μm [50]. In the present study, the mean particle size of TAC was reduced from 84.7 μm (bulk unprocessed TAC as received from supplier) to 8.6 μm (ranging from 1.5-22.8 μm) by wet ball milling for 24 hours. No further size reduction was observed for longer milling times (up to one week) because the milling efficiency not only depends on the processing time, but it is also controlled by other parameters, such as the hardness of the material, nature of the milling medium and the wetting of the solids [35]. Following non-solvent removal by lyophilization, the size of the TAC particles was further reduced by feeding the dry TAC powders processed from wet ball milling to a jet mill. After one run on the jet mill, the mean particle size of TAC particles decreased from 8.6 μm (D10=1.5 μm, D90=22.8 μm) to 3.4 μm (D10=1.1 μm, D90=7.4 μm). Mannitol was micronized only by jet milling. After 3-4 runs on the jet mill, the particle size distribution of MAN was reduced to approximately the same size as the micronized TAC (D10=1.1 μm, D50=3.2 μm, D90=7.0 μm). The potency of TAC in micronized TACMAN (1:1) was 49.7%, indicating that adequate mixing was achieved and the mixture of micronized TAC and MAN is homogenous.

From the SEM images shown in Fig.2.5a, micronized TACMAN (1:1) is composed of fractured, irregular shaped particles with a wide size range and a large portion of particle agglomerates due to their cohesive behavior from electrostatic charge generated during the milling process [51]. On the other hand, TFF TACMAN (1:1) exhibited a highly porous structure composed of aggregated particle networking, in which discrete particles are barely distinguishable, as displayed in Fig.2.5b. The specific surface area of micronized TACMAN and TFF TACMAN was 2.87 and 32.45 m^2/g (Table 2.1), respectively, corresponding to an effective particle diameter of 2.09 and 0.18 μm (assuming monodispersed unit density spherical particles).

From a formulation perspective, the efficacy of drugs administered by pulmonary delivery is largely determined by the aerodynamic diameter of the aerosol particles [50]. In general, the optimum aerodynamic diameter for achieving deep lung deposition is 1-3 μm [52]. The aerodynamic properties of TFF TACMAN were described in terms of the ED, MMAD, GSD, and FPF of the emitted dose, as illustrated in Fig.2.6. TFF TACMAN was capable of emitting 94.2% of the loaded dose from the device, because of the low density and highly porous structure of TFF particles, the turbulent airflow readily entered into the large pores to shear the aggregated particles apart and emit them from the device. The FPF and MMAD of TFF TACMAN were 83.3% and 2.26 μm, respectively, indicating that the shear and impaction forces generated by the air flow and the device were able to break the TFF brittle matrix particles into respirable low-density microparticles [27]. In addition, ED×FPF represents the percentage of total emitted dose that can achieve deep lung delivery; in this study, up to 78.5% of the TFF TACMAN can

be delivered to the lung using Miat® Monodose inhaler. GSD gives an indication of aerosol particle size distribution; TFF TACMAN had a relatively small aerodynamic size distribution with a GSD of 2.08 µm. From the results obtained, we can conclude that TFF TACMAN is suitable for deep lung delivery when incorporated into a commercially available DPI.

Besides aerodynamic diameter, geometric particle size also plays an important role in determining the fate of aerosol particles in the lung. It is well known that the two main clearance mechanisms active in the lung are mucociliary clearance (MCC) in the central and small airways and macrophage phagocytosis in the alveolar region [53]. Particles with a geometric size larger than 6 µm are usually cleared by MCC in the ciliated region of the lung [54] and particles with diameters between 1-5 µm are preferably engulfed by alveolar macrophages in the alveoli [34]. The geometric size distribution of emitted aerosol particles was measured by dynamic light scattering following aerosol generation from the Miat® monodose inhaler. Micronized TACMAN exhibited a polydispersed size distribution with D10, D50 and D90 (diameter at which the cumulative sample volume was less than 10%, 50% and 90%) values of 0.93, 1.92 and 4.82 µm, respectively. On the other hand, aerosolized TFF TACMAN had a significantly larger geometric size (shown in Table 2.1, D10=4.39 µm, D50=17.84 µm, D90=64.49 µm). The aerodynamic diameter is calculated by the following equation:

$$D_{ae} = D_{eq}\sqrt{\rho_p/\rho_0 X}$$

where D_{eq} is the geometric diameter of the particle, ρ_p is the particle density and X is the dynamic shape factor derived from a sphere. Hence, the aerodynamic diameter is not only dependent on geometric size, but also controllable by the particle density and shape. In the case of TFF TACMAN, assuming the shape of aerosolized particles is spherical, the calculated particle density is 0.016 g/cm^3. Therefore, micronized TACMAN is likely to be cleared by macrophage phagocytosis when they reach the alveolar region due to their geometric size (1.92 μm); by contrast TFF TACMAN particles have the potential to escape from macrophage uptake while achieving deep lung delivery due to their relatively large geometric size (17.84 μm) and small aerodynamic diameter (2.26 μm).

2.4.4 Pharmacokinetic analysis of micronized TACMAN verses TFF TACMAN

The in vivo performance of inhaled micronized TACMAN and TFF TACMAN was investigated in a rat model. Rats were exposed via nose-only administration to aerosolized powders generated by a rotating brush generator (RBG). The delivered dose is calculated according to the equation below:

$$DD = C \times RMV \times D$$

where DD is the delivered dose (mg), C is the concentration of substance in air (mg/L), RMV is respiratory minute volume (i.e., the volume of air inhaled in one minute, L/min), and D is the exposure duration (min). The RMV for rats is calculated according to the formula: RMV (L/min) = 0.608 × BW (kg) $^{0.852}$ where BW represents the body weight of the tested subjects [55]. Of the delivered dose, only a small percentage will actually deposit in the lungs. The deposition fraction of the delivered dose in rats

typically ranges between 10% and 5% of the delivered dose and has been shown to be dependent on particle size distribution [56].

Following exposure of the aerosolized powder, a 24-hour pharmacokinetic profile was determined in lung tissue and blood for micronized TACMAN and TFF TACMAN. For comparison purposes, TAC concentrations in the lung were normalized with respect to the concentration at the first time point (0.5 h) and expressed as a percentage of initial doses (%) and determined as a function of time (Fig.2.7). The TAC concentrations in the lung at 0.5 hour were 265.8 ng/g for TFF TACMAN and 122.6 ng/g for micronized TACMAN. A 2-compartment model (Fig.2.9) was used to calculate the PK parameters in the lung for micronized TACMAN and TFF TACMAN and the results are shown in Table 2.2. In the model, the rate constant K10 describes the lung clearance rate, which represents a combination effect of mucociliary clearance, macrophage phagocytosis and metabolism. K12 and K21 are exchange rates of drug between the lung and the blood compartments. As seen in Table 2.2, K10 of micronized TACMAN (2.64 h^{-1}) is approximately 4.7 times greater than that of TFF TACMAN (0.56 h^{-1}), indicating that the lung clearance rate is much faster for micronized particles compared to aerosolized TFF particles. Micronized TACMAN exhibited faster clearance rate because most of the particles tend to be engulfed by macrophages due to the phagocytic favorable geometric size (mean 1.92 μm); in contrast, TFF TACMAN had a relatively large geometric particle size (mean 17.84 μm). Based on estimations from macrophage uptake studies, it could be predicted that more than 90% of the TFF particles are capable of escaping clearance from macrophage phagocytosis [57]. It is also possible that TFF particles undergo rapid

dissolution, leaving little to be cleared by macrophages compared to the more kinetically stable crystalline particles [4, 24]. The lung clearance trends observed from the two formulations differ significantly from 2 h to 8 h. This difference is supported by prior macrophage clearance studies where 50-75% of the micron-sized particles are cleared by macrophages by 2-3 h and 90% or more by 10 h [58]. The systemic absorption rate of TAC from the lung epithelium (K12) is slightly higher for TFF TACMAN (2.16 h^{-1}) compared to micronized TACMAN (1.70 h^{-1}). According to Fick's first law, K12 is proportional to the membrane permeability, surface area over which the drug is deposited and the drug concentration in the lung lining fluids. While in humans deposition of particles less than 3 μm is thought to occur predominately in the deep lung. Kuehl et al. showed that in mice and rats particles with different mean sizes (0.5, 1, 3, 5 μm) deposited along the entire airway including oral/nasal, trachea/bronchi, and lungs [56]. In the present study, the aerodynamic size distribution of the aerosol generated by the RBG was very similar for TFF TACMAN and micronized TACMAN (with MMAD values measured at about 1.5 μm). Hence the regional deposition pattern should be comparable for the two formulations. Accordingly, the drug permeability due to regional deposition should be similar for both formulations. Drug permeability, however, may not be the same in both formulations due to the differences in physicochemical properties described earlier. It has been reported that amorphous TAC can reach up to 10-times supersaturated solubility compared to crystalline TAC [4]. These in vitro studies provided evidence that TFF TACMAN dissolved more rapidly and to a greater extent than the micronized blend in this study. Additionally, the faster dissolution rate of amorphous TFF TACMAN may

make it less susceptible to mucociliary clearance since drug is rapidly dissolved and able to permeate into airway tissues. All of the effects mentioned above could contribute to enhanced pulmonary bioavailability of TFF TACMAN. If we normalize the data by assuming that the same dose was delivered in both groups, the average $AUC_{0\text{-}24h}$ in the lung is 1707.47 ng*hr/g and 729.53 ng*hr/g for TFF TACMAN and micronized TACMAN, respectively. Once the TAC dissolves in the lung lining fluid, it is available for absorption and will either remain in pulmonary tissue or cross into the blood stream. As evident from several investigations of inhaled TAC in rodents, absorbed TAC molecules seem to preferably remain in lung tissue rather than going into systemic circulation [4, 19-23, 25]. The higher lung AUC of TFF TACMAN can be attributed to the faster dissolution rate, leading to more TAC molecules available for absorption into the lung tissue. The overall clearance rate (CL) is much slower for TFF TACMAN compared with micronized TACMAN (data presented in Table 2.1). The nearly 2.3-times greater AUC and slower clearance rate in the lung tissue for TFF TACMAN demonstrated that this formulation is favorable for localized lung delivery while a micronized formulation may be more susceptible to the lung's clearance mechanisms.

The systemic TAC concentration after exposure to the aerosolized powder of micronized TACMAN and TFF TACMAN is illustrated in Fig.2.8. Based on a larger K12 value, the systemic absorption rate of TAC through the lung epithelium is slightly faster for amorphous TFF particles compared to crystalline blend. However, a much higher and more variable blood concentration of TAC was observed for micronized TACMAN compared to TFF TACMAN, likely due to clearance and subsequently

gastrointestinal (GI) tract absorption. Once deposited, the slowly dissolving micronized crystalline particles undergo mucociliary clearance towards the mouth where they are eventually mixed with saliva and swallowed, then available for absorption via the GI tract into systemic circulation. The more variable blood concentration of TAC that was found for micronized TACMAN at 2h and 4h was due to its erratic oral bioavailability (varies from 4%-93%) [59]. Additionally, it is possible that the undissolved micronized particles are engulfed by macrophages, which can then be slowly transported along the alveolar surface to the mucociliary escalator or translocation to the intersitium and lymph nodes [53, 54]. As shown in Fig.2.8, besides the first peak concentrations around 1h, there was a significant second peak at either 4 or 8 hours for both experimental groups, which corresponded to the re-absorption of TAC from the GI tract. The calculation of K20 (TAC clearance rate from the blood) is based on the elimination phase in the plasma compartment. However, if TAC was still being absorbed at 8 hours, it's not feasible to determine K20 just based on the testing period (up to 24 hours) in this study. A slightly increasing trend of TAC concentration in the blood towards the end of the test (from 12h to 24h) was observed for the micronized group, possibly because the TAC-carrying macrophages slowly moved to the mucociliary escalator and were absorbed orally or TAC transported to the lymphatic system and eventually partitioned into circulation [60]. On the other hand, the blood concentration of TAC for TFF TACMAN group remained low (1-5 ng/mL) for the entire testing period (24h) due to reduced clearance and oral absorption. In summary, by delivering TAC as a more rapidly dissolving formulation,

TFF TACMAN is able to provide bioavailable TAC on the pulmonary epithelium and avoid the lung's clearance mechanisms, while minimizing systemic concentration.

2.5 Conclusion

Engineered particles containing tacrolimus and mannitol were successfully prepared by TFF. The amorphous TFF-processed formulation demonstrated excellent aerodynamic properties when incorporated into a commercially available DPI. Following a single dose dry powder inhalation study in a rat model, TFF-processed powders achieved a significantly higher pulmonary bioavailability with longer lung retention time compared to micronized powders, likely due to their ability to avoid pulmonary clearance mechanisms (mucociliary clearance and macrophage uptake). Additionally lower systemic exposure with small intersubject variability was observed for the TFF-processed formulation, which could potentially reduce adverse side effects. In this study, production of inhaled tacrolimus by TFF has demonstrated the capability to localize therapeutic drug levels to the lungs more effectively than an inhaled micronized blend and minimize systemic level.

2.6 References

[1] R.D. Yusen, J.D. Christie, L.B. Edwards, A.Y. Kucheryavaya, C. Benden, A.I. Dipchand, F. Dobbels, R. Kirk, L.H. Lund, A.O. Rahmel, J. Stehlik, H. International Society for, T. Lung, The registry of the international society for heart and lung transplantation: thirtieth adult lung and heart-lung transplant report-2013; focus theme: age, J Heart Lung Transplant, 32 (2013) 965-978.

[2] A. Boehler, M. Estenne, Obliterative bronchiolitis after lung transplantation., Curr Opin Pulm Med, 6 (2000) 133-139.

[3] C. Knoop, A. Haverich, S. Fischer, Immunosuppressive therapy after human lung transplantation, Eur Respir J, 23 (2004) 159-171.

[4] A.B. Watts, J.I. Peters, R.L. Talbert, K.P. O'Donnell, J.J. Coalson, R.O. Williams, 3rd, Preclinical evaluation of tacrolimus colloidal dispersion for inhalation, Eur J Pharm Biopharm, 77 (2011) 207-215.

[5] T. Kino, H. Hatanaka, S. Miyata, N. Inamura, M. Nishiyama, T. Yajima, T. Goto, M. Okuhara, M. Kohsaka, H. Aoki, et al., FK-506, a novel immunosuppressant isolated from a Streptomyces. II. Immunosuppressive effect of FK-506 in vitro, J Antibiot (Tokyo), 40 (1987) 1256-1265.

[6] S. Hariharan, V.R. Peddi, R. Munda, A.M. Demmy, T.J. Schroeder, J.W. Alexander, M.R. First, Long-term renal and pancreas function with tacrolimus rescue therapy following kidney/pancreas transplantation, Transplant Proc, 29 (1997) 652-653.

[7] R.J. Keenan, H. Konishi, A. Kawai, I.L. Paradis, D.R. Nunley, A.T. Iacono, R.L. Hardesty, R.J. Weyant, B.P. Griffith, Clinical trial of tacrolimus versus cyclosporine in lung transplantation, Ann Thorac Surg, 60 (1995) 580-584; discussion 584-585.

[8] J.G. O'Grady, A. Burroughs, P. Hardy, D. Elbourne, A. Truesdale, Uk, G. Republic of Ireland Liver Transplant Study, Tacrolimus versus microemulsified ciclosporin in liver transplantation: the TMC randomised controlled trial, Lancet, 360 (2002) 1119-1125.

[9] C. Knoop, P. Thiry, F. Saint-Marcoux, A. Rousseau, P. Marquet, M. Estenne, Tacrolimus pharmacokinetics and dose monitoring after lung transplantation for cystic fibrosis and other conditions, Am J Transplant, 5 (2005) 1477-1482.

[10] K. Wagner, S.A. Webber, G. Kurland, G.J. Boyle, S.A. Miller, L. Cipriani, B.P. Griffith, F.J. Fricker, New-onset diabetes mellitus in pediatric thoracic organ recipients receiving tacrolimus-based immunosuppression, J Heart Lung Transplant, 16 (1997) 275-282.

[11] T.E. Corcoran, Inhaled delivery of aerosolized cyclosporine, Adv Drug Deliv Rev, 58 (2006) 1119-1127.

[12] S. Groves, M. Galazka, B. Johnson, T. Corcoran, A. Verceles, E. Britt, N. Todd, B. Griffith, G.C. Smaldone, A. Iacono, Inhaled cyclosporine and pulmonary function in lung transplant recipients, Journal of aerosol medicine and pulmonary drug delivery, 23 (2010) 31-39.

[13] S. Onoue, H. Sato, Y. Kawabata, T. Mizumoto, N. Hashimoto, S. Yamada, In vitro and in vivo characterization on amorphous solid dispersion of cyclosporine A for inhalation therapy, J Control Release, 138 (2009) 16-23.

[14] S. Onoue, H. Sato, K. Ogawa, Y. Kojo, Y. Aoki, Y. Kawabata, K. Wada, T. Mizumoto, S. Yamada, Inhalable dry-emulsion formulation of cyclosporine A with improved anti-inflammatory effects in experimental asthma/COPD-model rats, Eur J Pharm Biopharm, 80 (2012) 54-60.

[15] T. Wang, S. Noonberg, R. Steigerwalt, M. Lynch, R.A. Kovelesky, C.A. Rodriguez, K. Sprugel, N. Turner, Preclinical safety evaluation of inhaled cyclosporine in propylene glycol, J Aerosol Med, 20 (2007) 417-428.

[16] J. Behr, G. Zimmermann, R. Baumgartner, H. Leuchte, C. Neurohr, P. Brand, C. Herpich, K. Sommerer, J. Seitz, G. Menges, S. Tillmanns, M. Keller, G. Munich Lung Transplant, Lung deposition of a liposomal cyclosporine A inhalation solution in patients after lung transplantation, Journal of aerosol medicine and pulmonary drug delivery, 22 (2009) 121-130.

[17] A.T. Iacono, B.A. Johnson, W.F. Grgurich, J.G. Youssef, T.E. Corcoran, D.A. Seiler, J.H. Dauber, G.C. Smaldone, A. Zeevi, S.A. Yousem, J.J. Fung, G.J. Burckart, K.R. McCurry, B.P. Griffith, A randomized trial of inhaled cyclosporine in lung-transplant recipients, N Engl J Med, 354 (2006) 141-150.

[18] http://www.fda.gov/ohrms/dockets/ac/05/briefing/2005-4135B1_02_A-FDA-Pulminiq.pdf.

[19] N. Ide, T. Nagayasu, K. Matsumoto, T. Tagawa, K. Tanaka, T. Taguchi, Y. Sumida, M. Nakashima, Efficacy and safety of inhaled tacrolimus in rat lung transplantation, J Thorac Cardiovasc Surg, 133 (2007) 548-553.

[20] A. Ingu, K. Komatsu, S. Ichimiya, N. Sato, Y. Hirayama, M. Morikawa, T. Abe, Effects of inhaled FK 506 on the suppression of acute rejection after lung transplantation: use of a rat orthotopic lung transplantation model, J Heart Lung Transplant, 24 (2005) 538-543.

[21] Y. Morishita, Y. Hirayama, K. Miyayasu, K. Tabata, A. Kawamura, Y. Ohkubo, S. Mutoh, FK506 aerosol locally inhibits antigen-induced airway inflammation in Guinea pigs, International archives of allergy and immunology, 136 (2005) 372-378.

[22] T. Deuse, F. Blankenberg, M. Haddad, H. Reichenspurner, N. Phillips, R.C. Robbins, S. Schrepfer, Mechanisms behind local immunosuppression using inhaled tacrolimus in preclinical models of lung transplantation, Am J Respir Cell Mol Biol, 43 (2010) 403-412.

[23] S. Schrepfer, T. Deuse, H. Reichenspurner, J. Hoffmann, M. Haddad, J. Fink, M.P. Fischbein, R.C. Robbins, M.P. Pelletier, Effect of inhaled tacrolimus on cellular and humoral rejection to prevent posttransplant obliterative airway disease, Am J Transplant, 7 (2007) 1733-1742.

[24] P. Sinswat, K.A. Overhoff, J.T. McConville, K.P. Johnston, R.O. Williams, 3rd, Nebulization of nanoparticulate amorphous or crystalline tacrolimus--single-dose pharmacokinetics study in mice, Eur J Pharm Biopharm, 69 (2008) 1057-1066.

[25] A.B. Watts, A.M. Cline, A.R. Saad, S.B. Johnson, J.I. Peters, R.O. Williams, 3rd, Characterization and pharmacokinetic analysis of tacrolimus dispersion for nebulization in a lung transplanted rodent model, Int J Pharm, 384 (2010) 46-52.

[26] M. Chougule, B. Padhi, A. Misra, Nano-liposomal dry powder inhaler of tacrolimus: preparation, characterization, and pulmonary pharmacokinetics, International journal of nanomedicine, 2 (2007) 675-688.

[27] A.B. Watts, Y.B. Wang, K.P. Johnston, R.O. Williams, 3rd, Respirable low-density microparticles formed in situ from aerosolized brittle matrices, Pharm Res, 30 (2013) 813-825.

[28] D.A. Edwards, J. Hanes, G. Caponetti, J. Hrkach, A. Ben-Jebria, M.L. Eskew, J. Mintzes, D. Deaver, N. Lotan, R. Langer, Large porous particles for pulmonary drug delivery, Science, 276 (1997) 1868-1871.

[29] R. Vanbever, J.D. Mintzes, J. Wang, J. Nice, D. Chen, R. Batycky, R. Langer, D.A. Edwards, Formulation and physical characterization of large porous particles for inhalation, Pharm Res, 16 (1999) 1735-1742.

[30] L.A. Dellamary, T.E. Tarara, D.J. Smith, C.H. Woelk, A. Adractas, M.L. Costello, H. Gill, J.G. Weers, Hollow porous particles in metered dose inhalers, Pharm Res, 17 (2000) 168-174.

[31] S.P. Duddu, S.A. Sisk, Y.H. Walter, T.E. Tarara, K.R. Trimble, A.R. Clark, M.A. Eldon, R.C. Elton, M. Pickford, P.H. Hirst, S.P. Newman, J.G. Weers, Improved lung delivery from a passive dry powder inhaler using an Engineered PulmoSphere powder, Pharm Res, 19 (2002) 689-695.

[32] P.C. Richardson, A.H. Boss, Technosphere insulin technology, Diabetes Technol Ther, 9 Suppl 1 (2007) S65-72.

[33] C. Plumley, E.M. Gorman, N. El-Gendy, C.R. Bybee, E.J. Munson, C. Berkland, Nifedipine nanoparticle agglomeration as a dry powder aerosol formulation strategy, Int J Pharm, 369 (2009) 136-143.

[34] M. Geiser, Update on macrophage clearance of inhaled micro- and nanoparticles, Journal of aerosol medicine and pulmonary drug delivery, 23 (2010) 207-217.

[35] W. Yang, K.P. Johnston, R.O. Williams, 3rd, Comparison of bioavailability of amorphous versus crystalline itraconazole nanoparticles via pulmonary administration in rats, Eur J Pharm Biopharm, 75 (2010) 33-41.

[36] J.D. Engstrom, E.S. Lai, B.S. Ludher, B. Chen, T.E. Milner, R.O. Williams, 3rd, G.B. Kitto, K.P. Johnston, Formation of stable submicron protein particles by thin film freezing, Pharm Res, 25 (2008) 1334-1346.

[37] D.J. Ball, P.H. Hirst, S.P. Newman, B. Sonet, B. Streel, F. Vanderbist, Deposition and pharmacokinetics of budesonide from the Miat Monodose inhaler, a simple dry powder device, Int J Pharm, 245 (2002) 123-132.

[38] J.P. Mitchell, Practices of coating collection surfaces of cascade impactors: a survey of members of the european pharmaceutical aerosol group (EPAG). Drug Deliv Lung, 14 (2003) 75-78.

[39] V.A. Marple, B.A. Olson, K. Santhanakrishnan, J.P. Mitchell, S.C. Murray, B.L. Hudson-Curtis, Next generation pharmaceutical impactor (a new impactor for pharmaceutical inhaler testing). Part II: Archival calibration, J Aerosol Med, 16 (2003) 301-324.

[40] M.A. Moyano, L.D. Simionato, M.T. Pizzorno, A.I. Segall, Validation of a liquid chromatographic method for determination of tacrolimus in pharmaceutical dosage forms, J AOAC Int, 89 (2006) 1547-1551.

[41] USP 32-NF 27 General Chapter 601: Aerosols, Nasal sprays, Metered-dose inhalers, and Dry powder inhalers., 218-239.

[42] A. Gombás, P. Szabó-Révész, M. Kata, R.J. G., I. Erõs, QUANTITATIVE DETERMINATION OF CRYSTALLINITY OF a-LACTOSE MONOHYDRATE BY DSC, Journal of Thermal Analysis and Calorimetry, 68 (2002) 503-510.

[43] L.R. Hilden, K.R. Morris, Physics of amorphous solids, J Pharm Sci, 93 (2004) 3-12.

[44] Z. Deng, S. Xu, S. Li, Understanding a relaxation behavior in a nanoparticle suspension for drug delivery applications, Int J Pharm, 351 (2008) 236-243.

[45] A.I. Kim, M.J. Akers, S.L. Nail, The physical state of mannitol after freeze-drying: effects of mannitol concentration, freezing rate, and a noncrystallizing cosolute, J Pharm Sci, 87 (1998) 931-935.

[46] A.S. Zidan, Z. Rahman, V. Sayeed, A. Raw, L. Yu, M.A. Khan, Crystallinity evaluation of tacrolimus solid dispersions by chemometric analysis, Int J Pharm, 423 (2012) 341-350.

[47] M. Zhao, S.A. Barker, P.S. Belton, C. McGregor, D.Q. Craig, Development of fully amorphous dispersions of a low T(g) drug via co-spray drying with hydrophilic polymers, Eur J Pharm Biopharm, 82 (2012) 572-579.

[48] N. Rasenack, B.W. Muller, Micron-size drug particles: common and novel micronization techniques, Pharm Dev Technol, 9 (2004) 1-13.

[49] I.Y. Saleem, H.D. Smyth, Micronization of a soft material: air-jet and micro-ball milling, AAPS PharmSciTech, 11 (2010) 1642-1649.

[50] P.G. Rogueda, D. Traini, The nanoscale in pulmonary delivery. Part 1: deposition, fate, toxicology and effects, Expert Opin Drug Deliv, 4 (2007) 595-606.

[51] M.M. de Villiers, Influence of cohesive properties of micronized drug powders on particle size analysis, J Pharm Biomed Anal, 13 (1995) 191-198.

[52] P.R. Byron, Prediction of drug residence times in regions of the human respiratory tract following aerosol inhalation, J Pharm Sci, 75 (1986) 433-438.

[53] J. Zhang, L. Wu, H.K. Chan, W. Watanabe, Formation, characterization, and fate of inhaled drug nanoparticles, Adv Drug Deliv Rev, 63 (2011) 441-455.

[54] B. Olsson, E. Bondesson, L. Borgstrom, Pulmonary Drug Metabolism, Clearance, and Absorption, in: H.D.C. Smyth, A.J. Hickey (Eds.) Controlled Pulmonary Drug Delivery, Springer, New York, NY, 2011.

[55] D.J. Alexander, C.J. Collins, D.W. Coombs, I.S. Gilkison, C.J. Hardy, G. Healey, G. Karantabias, N. Johnson, A. Karlsson, J.D. Kilgour, P. McDonald, Association of Inhalation Toxicologists (AIT) working party recommendation for standard delivered dose calculation and expression in non-clinical aerosol inhalation toxicology studies with pharmaceuticals, Inhalation toxicology, 20 (2008) 1179-1189.

[56] P.J. Kuehl, T.L. Anderson, G. Candelaria, B. Gershman, K. Harlin, J.Y. Hesterman, T. Holmes, J. Hoppin, C. Lackas, J.P. Norenberg, H. Yu, J.D. McDonald, Regional particle size dependent deposition of inhaled aerosols in rats and mice, Inhalation toxicology, 24 (2012) 27-35.

[57] D.A. Edwards, A. Ben-Jebria, R. Langer, Recent advances in pulmonary drug delivery using large, porous inhaled particles, Journal of applied physiology, 85 (1998) 379-385.

[58] B.E. Lehnert, P.E. Morrow, Association of 59iron oxide with alveolar macrophages during alveolar clearance, Exp Lung Res, 9 (1985) 1-16.

[59] R. Venkataramanan, L.M. Shaw, L. Sarkozi, R. Mullins, J. Pirsch, G. MacFarlane, D. Scheller, D. Ersfeld, M. Frick, W.E. Fitzsimmons, M. Virji, A. Jain, K.L. Brayman, A. Shaked, Clinical utility of monitoring tacrolimus blood concentrations in liver transplant patients, J Clin Pharmacol, 41 (2001) 542-551.

[60] S.B. Shin, H.Y. Cho, D.D. Kim, H.G. Choi, Y.B. Lee, Preparation and evaluation of tacrolimus-loaded nanoparticles for lymphatic delivery, Eur J Pharm Biopharm, 74 (2010) 164-171.

Chapter 3 : Effect of Processing Parameters on the Physicochemical and Aerodynamic Properties of Respirable Brittle Matrix Powders Produced by Thin Film Freezing

3.1 Abstract

Thin film freezing (TFF) was employed to produce brittle matrix powders, capable of forming into respirable low-density particles upon aerosolization. The objective of this study is to investigate the impact of processing parameters in the TFF process on the physicochemical and aerodynamic properties of the resulting formulations. TFF formulation produced at the higher freezing rate (cryogenic surface temperature: -140°C) showed greater specific surface area, higher porosity and lower density, compared to the TFF formulation prepared at the intermediate freezing rate (cryogenic surface temperature: -50 °C) and slow freezing rate (slow freezing on the shelf of -40°C). All of these enhanced properties induced by faster freezing rate further contributed to an increased fine particle fraction (FPF) of the obtained formulations. Moreover, an increasing trend of FPF was observed for these TFF powders when the initial solid concentration was reduced, probably due to the enhanced brittleness. The variation of the freezing rate and initial solid loading in the TFF process enabled the production of formulations with tailored physicochemical properties and brittleness, leading to improved aerodynamic performance.

3.2 Introduction

Recently, engineered particles capable of more efficient pulmonary delivery have gained increasing attention [1, 2]. Particle engineering technologies such as milling, spray drying, spray-freeze drying, supercritical fluid processing, and controlled precipitation have been widely used to produce dry powders suitable for inhalation [3-7]. Large porous low-density particles were first introduced by Edwards et al., which are able to achieve deep lung delivery despite their relatively large geometric size (up to 20 μm) while prolonged the pulmonary retention time due to their ability of escaping the lung's natural clearance mechanisms [8]. Since then a variety of technologies have been proposed to enhance the pulmonary deposition efficiency of DPIs, including AIR® [9], PulmoSphere® [10, 11], Technosphere® [12], and NanoCluster® [13]. In addition to the enhanced delivery efficiency, there are several other advantages for engineered particles in pulmonary drug delivery. For instance, it has been reported that particles with geometric diameter larger than 10 μm or smaller than 100 nm can escape from macrophage phagocytosis, leading to prolonged lung retention time, which enables substantial time for dissolution and absorption [14, 15]. Moreover, the tailored physicochemical properties of engineered particles (e.g. amorphous, enhanced surface area, high porosity etc.) have demonstrated improved drug dissolution rate in the lung lining fluid and potentially improved aerodynamic properties [16, 17]. A innovative particle engineering process, thin film freezing (TFF) has been shown to produce brittle matrix powders, which can be sheared into respirable low-density microparticles upon

aerosolization from a passive dry powder inhaler [18].Therefore, TFF process was selected in this study to investigate formulations suitable for dry powder inhalation.

In the TFF process, frozen thin films are formed rapidly by applying a solution containing the API(s) and excipients directly onto a cryogenic substrate surface. Then the frozen thin films are removed from the surface and maintained in the frozen state until solvent is removed by lyophilization [19]. This rapid freezing process is capable of preventing the crystallization and aggregation of the dissolved solute, resulting in low-density brittle matrix structure [18]. Mannitol (MAN) is a commonly used excipient in developing lyophilized pharmaceutical products [20]. One of the reasons for the widespread use of MAN as a bulking agent in the lyophilizaiton process is due to its tendency to crystallize from frozen aqueous solutions, leading to a physically stable freeze-dried product [20]. Moreover, the high melting temperature of the mannitol/ice eutectic mixture (around -1.5 °C) makes it possible to achieve primary drying at a relatively high temperature, therefore improves process efficiency [21]. Another potential application of MAN is acting as a lyoprotectant for biopharmaceuticals in the freeze-dried process [22, 23]. Watts et al. found that respirable brittle matrix particles prepared by TFF were susceptible to moisture induced matrix collapse and very hygroscopic, leading to altered aerodynamic performance when amorphous content (e.g. lactose and raffinose) was present; in contrast, the aerosolization properties of crystalline TFF processed powders with MAN were not influenced by high humidity [18]. Therefore, MAN was chosen in this study due to its superior formulation stability and robustness to moisture. Due to its lack of absorption in the ultraviolet-visible (UV-Vis) spectral region,

it's difficult to quantify MAN using high-pressure liquid chromatography (HPLC) with a UV/Vis detector. Hence a commonly used dye compound Rhodamine B (RHO, peak absorption at 525nm) was added in the composition (1% w/w), to facilitate the quantification of these TFF formulations.

It has been previously demonstrated by our research group that different solvent systems used in the TFF process (e.g. tert-butanol versus acetonitrile) generated thin films with different thickness and diameter, which impacted the freezing rate, and consequently affected the morphology of the resulting TFF formulations [19]. Engstrom et al. used the same solvent system (i.e. water) but differed the temperature of the cryogenic substrate in the TFF process. Thin films with different geometry and cooling rate was observed, resulting in different surface morphology of the TFF powders [24]. Theoretical modeling of the cooling time was correlated to the infrared imaging results [19, 24]. However, the physicochemical and aerodynamic properties of these TFF powders prepared at different freezing rates have not been fully investigated. Therefore, in the preset study, formulations were prepared at three different freezing rates (TFF with cryogenic substrate temperature at -140°C, -50°C and freezing directly on the shelf of the lyophilizer for slow freezing) and their impact on the physicochemical and aerodynamic properties was evaluated. Moreover, the influence of different initial solid concentrations on the aerosolization properties of the TFF powders was investigated.

The objectives of this study are to prepare MAN formulations that are suitable for dry powder inhalation using thin film freezing technology (TFF) and evaluate how process parameters (e.g. freezing rate and initial solid loading) impact the morphology

and aerodynamic properties of the obtaining formulations. We hypothesize that: (1) formulations prepared at different freezing rate will exhibit different physicochemical properties, leading to variable aerodynamic performances; (2) the initial solid concentrations will affect the density and brittleness of the TFF processed powders, further impact the aerosolization properties of the resulting formulations.

3.3 Materials and Methods

3.3.1 Materials

The following materials were purchased: Rhodamine B, Mannitol, HPLC grade acetonitrile and methanol (Fisher Scientific, Pittsburgh, PA); Polysorbate 80 (Spectrum, Gardena, CA); Ethanol (Decon Labs, King of Prussia, PA).

3.3.2 Formulation Preparation

Thin Film Freezing (TFF) technique was employed in this study to prepare the formulations. A detailed description of the TFF process was demonstrated by Engstrom et al. [24]. Briefly, RHO and MAN was dissolved in purified water at different solid concentrations (0.5%, 1%, 5% and 10%, w/v). Same initial solid loading (1%, w/v) was used to compare different freezing rates. A solution of RHO and MAN (1:99, w/w) was rapidly frozen on a on a cryogenically cooled rotating stainless steel surface (−50°C or -140°C). The resulting thin films were removed from the surface by a scraper and maintained in the frozen state in liquid nitrogen. For the slow freezing RHOMAN, solution of RHO and MAN was slowly frozen in scintillation vials on the shelf (SFS, -40°C). Following the freezing processes, solvents were sublimated by lyophilization over

48 hours at pressures less than 200mTorr while the shelf temperature was gradually ramped from −40°C to 25°C. Prior to sample removal from the lyophilizer, dry nitrogen was purged into the chamber to equilibrate to atmospheric pressure and the final product was stored in a vacuum desiccator at room temperature.

3.3.3 Differential Scanning Calorimetry (DSC)

Thermal properties of the bulk powders and each of their components were determined by a modulated temperature DSC (TA Instruments Model 2920, New Castle, DE) equipped with a refrigerated cooling system. Dry nitrogen gas was purged through the DSC cell at a flow rate of 40 mL/min. 5–10 mg of samples were weighed into aluminum crimped pans (Kit 0219-0041, Perkin–Elmer Instruments, Norwalk, CT) and heated at a ramp rate of 10°C/min from 30 to 250 °C with a modulation temperature amplitude of 1°C/60 s. Data were analyzed using TA Universal Analysis 2000 software (TA Instruments, New Castle, DE).

3.3.4 Powder X-ray Diffraction (XRD)

The crystallinity of the same set of samples was evaluated by wide angle XRD (A Philips 1710 X-ray diffractometer, Cu Ka1 radiation, λ = 1.54059 Å, 40 kV, 40 mA). Samples were analyzed ranging from 5° to 40° at a 2θ step size of 0.05° and a dwell time of 2 s.

3.3.5 Powder Bulk Density and Porosity

Bulk density of powders was determined according to a modified method from USP <616>. Briefly, bulk powders were gently poured into a 5 mL graduated cylinder. The mass and volume were recorded to calculate the bulk density of the powders.

The porosity of the bulk powders was measured by mercury porosimetry (Micromeritics, Norcross, GA). The sample was evacuated 5 minutes and the mercury filling pressure was set to be 1.73 Pa. The standard equilibration time used in the experiments was 10 seconds. The results were calculated by multiple linear regression analysis.

3.3.6 Brunauer–Emmett–Teller (BET) specific surface area analysis

Specific surface area was determined by a Monosorb MS-21 surface area analyzer. The Monosorb utilizes a modified BET equation for extremely rapid, single-point determinations of surface area ($P/P_0 = 0.294$). Samples were degassed at 30 °C by nitrogen purging (20 psi) for at least 2 hours prior to measurement. 30% Nitrogen in helium was used as the adsorbate gas.

3.3.7 Aerodynamic Performance

The aerodynamic properties of different formulations were investigated by a Next Generation Impactor (NGI) (MSP Corp., Shoreview, MN). Miat monodose inhaler® loaded with size 3 HPMC capsules containing approximately 3 mg of formulation was secured to the induction port by a silicone adapter. A pre-determined flow rate of 90 L/min to achieve a 4 kPa pressure drop across the device was used for all measurements.

Aerosols were generated over 2.7 s at a flow rate of 90 L/min to achieve an inhalation volume of 4 L. Prior to actuation, surfaces of the collection stages were coated with 1% polysorbate 80 in enthanol (v/v) and allowed to completly dry, which is recommended by the European Pharmaceutical Aerosol Group (EPAG) [25]. The cut-off size for each stage was calculated to be 6.48, 3.61, 2.30, 1.37, 0.76, 0.43 and 0.26 µm from stages 1 to 7 and micro-orifice collector (MOC), respectively [26]. Following actuation, the deposited powders in the capsule, inhaler, adaptor, induction port, stages 1 to 7 and MOC was collected by rinsing with 10 mL of acetonitrile (ACN):water (70:30, v/v), which is the mobile phase for RHO quantification [27]. Briefly, RHO content was analyzed using a Dionex high performance liquid chromatography (HPLC) system equipped with a reversed phase C18 column (150 mm × 4.6 mm, 5 µm, 300 Å) with a Universal security guard column (Phenomenex, Torrance, CA). The mobile phase consisted of 70/30 (v/v) ACN/water and the injection volume was 20 µL. RHO eluted at approximately 5 minutes with a flow rate of 1.0 mL/min and a detection wavelength of 525 nm.

Total Emitted dose (TED) was calculated as the percentage of drug emitted from the inhaler with respect to the total loaded dose into the capsule. Mass median aerodynamic diameter (MMAD), geometric standard deviation (GSD) and fine particle fraction (FPF) were calculated according to the USP 32-NF 27 General Chapter 601 [28]. Plot of cumulative percentage of mass less than stated aerodynamic diameter versus aerodynamic diameter (cut-off size for each stage) was built and fit to a 4 parameters logistic curve using Sigmaplot (Systat Software Inc, San Jose, CA). MMAD and GSD were calculated based on the drug deposition from stage 1 to 7 and MOC. FPF was

determined as the percentage of aerosolized particles with a MMAD less than 5 µm with respect to the delivered dose.

3.3.8 Geometric Particle Size Measurement

Geometric size of aerosolized particles from a Miat monodose inhaler® (Miat, Milan, Italy) was measured by low angle light scattering technique using a Malvern Spraytec® (Malvern, UK) equipped with an inhalation cell and an induction port. Inhaler was loaded with a size 3 hypromellose (HPMC) capsule (Capsugel, Peapack, NJ) containing 3 mg of formulation and fitted to the mouth of the induction port by a silicone adapter. Aerosols were generated over 2.7 s at a flow rate of 90 L/min to achieve an inhalation volume of 4 L. Data was collected over 3 s upon actuation when laser transmission dropped below 98%. Values reported are the average of at least three measurements.

3.3.9 Mechanical Testing

The mechanical properties of the bulk powders were evaluated using a Texture Analyzer (TA.XT.plus, Stable Micro Systems, Godalming, United Kingdom) equipped with a 5 kg load cell. A cylindrical stainless steel probe with a diameter of 7 mm was used in the study and test was conducted at a speed of 1 mm/s and a maximal immersion into the bulk powders of 10 mm. Compression mode was applied in the test. The cylindrical probe compresses the bulk powders by proceeding at constant speed and the force needed for the immersion was recorded. The resulting immersion force represents the force requires for breakage of the bulk powders. At the end of the immersion, the

probe returned to its original height. Measurements were performed in triplicate and averaged.

3.4 Results and Discussion

3.4.1 Formulations prepared by different freezing processes

The phenomena of droplet spreading and freezing upon impinging with a cryogenic solid substrate in the TFF process have been previously studied [19, 24]. The diameter of the frozen cylindrical disks were measured across two directions and averaged for 10 droplets. The measured average diameters for both TFF formulations prepared at different freezing temperatures (-50°C and -140°C) were 12 mm. The thickness of the frozen cylindrical disks was then calculated to be 176.8 μm by assuming that a droplet impacting on the cryogenic substrate will deform into a cylindrical disk with the same volume as the original droplet. It was previously demonstrated with infrared imaging of cooling thin films that the water droplets' spreading occurred within the first 10 milliseconds upon impact with the cryogenic surface, which is much shorter than the freezing time (hundred to thousand milliseconds) [24]. The cooling rate of the thin films can be predicted with a simplified analytical heat transfer model, which was validated with experimental IR data [19].

A one-dimensional heat transfer for a finite slab with an insulating boundary condition on the top and a constant temperature boundary condition on the bottom above is described by the following equation:

$$T(x,t) = T_{cryo} + \frac{2}{L}\sum_{n=0}^{\infty} e^{-\alpha(2n+1)^2\pi^2 t/4L^2} \times \cos\frac{(2n+1)\pi x}{2L}\left\{\frac{2L(-1)^{n+1}T_{cryo}}{(2n+1)\pi} + \int_0^L T_i \frac{\cos(2n+1)\pi x'}{2L}dx'\right\}$$

where x is the distance from the top of the spread droplet, T(x,t) is the temperature in the film reaching distance x and at time t, T_{cryo} is the temperature of the cryogenic substrate in contact with the bottom thin film surface, and L is the film thickness [29]. Then the cooling time (ms) was calculated by determining the time t, it takes for the top surface of the thin film at x=0 with thickness L to reach a given temperature T (freezing point of water, 273.15K). The cooling rate (K/s) was determined by dividing the temperature change at the top surface of the thin film (from room temperature to freezing point of water) by the cooling time. As shown in Table 3.1, the calculated cooling time for TFF process at -140°C and -50°C were 106ms (cooling rate 2.36×10^2 K/s) and 148ms (cooling rate 1.69×10^2 K/s), respectively. For the sample frozen directly on the tray of the lyophilizer, the observed cooling time was more than 10^6ms with a very slow cooling rate ($<2.5\times10^{-5}$ K/s).

Table 3.1 presents the physicochemical properties of powders prepared at different freezing rates. The degree of supercooling, the freezing rate, and the time required for complete solidification directly affected the ice crystal formation and growth during the freezing process, eventually impact the morphology and porosity of the final dried product after sublimation of ice [30, 31]. As illustrated in Fig.3.1, at high cooling rate

(left figure), the very thin water channels between the frozen ice crystals reduce the chance of aggregation and growth of MAN crystals. for an intermediate cooling rate (middle figure), MAN particle growth is intermediately prevented by the slightly thicker water domains left between the ice crystals; for extremely low freezing rate (right figure), fewer ice crystal domains were created compared to the rapid cooling process, leaving very thick channel of water domain, thus higher chance for crystalline growth of MAN particles [24]. Therefore, less aggregated MAN crystal particles resulted from TFF (-140°C) exhibited higher porosity (6.8%) than TFF formulation prepared at -50°C (4.2%). Due to the enhancement of porosity by increasing the cooling rate, TFF RHOMAN (-140°C) exhibited SSA of 77.4 m^2/g, approximately 2-times greater than TFF RHOMAN (-50°C) with SSA of 38.6 m^2/g. Moreover, increases of porosity lead to enlargement of the gap between matrix particles, further resulted in a lower bulk density for TFF RHOMAN (-140°C; 10.38 mg/cm^3) compared to TFF RHOMAN (-50°C; 12.31 mg/cm^3). For the slow freezing on the shelf formulation, due to the increased chance for MAN particles to aggregate, porosity was undetectable, the surface area is extremely low (0.8 m^2/g) and the bulk density (26.84 mg/cm^3) was higher than TFF formulations.

The crystallinity of these powders was analyzed by DSC and XRD. In the DSC profiles shown in Fig.3.2, bulk RHO melts and discomposes simultaneously around 210°C; bulk MAN has a melting point around 170°C with an enthalpy of fusion about 280 J/g; physical mixture of RHOMAN (1:99, w/w) displayed a single melting point around 170 °C with enthalpy of fusion similar to bulk MAN. All the three formulations prepared by different freezing processes exhibited a single melting point of MAN with

enthalpy of fusion similar to bulk MAN, indicating that MAN is completely crystalline in the formulations. Since the potency of RHO is only 1% (w/w), DSC was unable to detect its thermal properties in the physical mixture and three other formulations [32]. XRD demonstrated that RHO after processed by TFF was completely amorphous (Fig.3.3). Crystallinity still existed in MAN after processed by TFF with characteristic peaks at 9.05, 14.7, 16.85, 18.85, 20.5, 21.15, 24.65, and 36.1 2-theta degrees. These peaks were also found in all the other three formulations prepared by different freezing process and the peak intensity (which is a reflection of crystallinity) increased with the increases of freezing rate, TFF -140°C >TFF -50°C >slow freezing on the shelf of -40°C (SFS).

The aerodynamic properties of the powders are shown in Fig.3.4. The TED of the three formulations was comparable (around 85%), indicating that for all formulations aerosolized particles upon shearing and impaction were small enough to exit the capsule and enter into the impactor. The FPFs of TFF RHOMAN (-140°C), TFF RHOMAN (-50°C) and SFS RHOMAN (-40°C) were calculated to be 72.2%, 59.6% and 23.3%, respectively. Correlated to the FPF, TFF RHOMAN (-140°C) exhibited the smallest MMAD (2.47 μm) and GSD (2.59 μm); TFF RHOMAN (-50°C) had an intermediate MMAD of 3.29 μm and GSD of 3.11 μm; SFS RHOMAN (-40°C) displayed the largest MMAD (6.34 μm) and GSD (4.89 μm). All the results above demonstrated that faster freezing rate generated powders with better aerodynamic performance (higher FPF, lower MMAD and GSD). As illustrated in Fig.3.1, higher freezing rate results in an increased porosity, further lead to a thinner matrix structure of the obtained formulation. Therefore, when the same shear and impaction forces was generated from the air flow and DPI

device, more brittle fracture occurs when a thinner matrix structure is present in the formulation. These theories correlated with the results (Fig.3.4) that TFF RHOMAN (-140°C) exhibited better aerodynamic performance (highest FPF, smallest MMAD and GSD) than TFF RHOMAN (-50°C). On the other hand, the lower porosity and surface area of SFS RHOMAN (-40°C) resulted in very low FPF, large MMAD and GSD.

The geometric size distribution of formulations prepared at different freezing rates is demonstrated in Fig.3.5. For TFF processed formulations, a wider size distribution was observed for TFF RHOMAN (-50°C) with D10, D50 and D90 (diameter at which the cumulative sample density was under 10%, 50% and 90%) values of 9.32, 39.84 and 184.26 µm compared to TFF RHOMAN (-140°C, D10: 5.74 µm, D50: 33.46 µm and 93.9 µm). SFS RHOMAN (-40°C) exhibited a double peak with D10, D50 and D90 values of 10.74, 49.85 and 339.64 µm, respectively. The mean geometric size of aerosolized particles decreased as the freezing rate increased (Table 3.2), confirming that formulations with higher porosity and thinner matrix structure were brittle fractured into geometrically smaller particles. As we know, the aerodynamic diameter is calculated by the following equation:

$$D_{ae} = D_{eq}\sqrt{\rho_p/\rho_0 X}$$

Where D_{eq} is the geometric diameter of the particle, ρ_p is the particle density and X is the dynamic shape factor derivate from sphere. Dynamic shape factor of 1.50, MMAD and D50 were used for calculation of particle density based on the equation above [18]. The calculated density shown in Table 3.2 was well correlated to the measured bulk

density for all three formulations, indicating that only brittle fracture occurred with no powder collapse or compressions during the aerosolization process.

In order to understand the underlying mechanism of why powders freezing at different rates have different aerodynamic performance, the mechanical force necessary for breakage of the matrix powders was determined using a Texture Analyzer by immersion a cylindrical probe into the bulk powders. No significant difference in terms of immersion force was observed for the three formulations prepared by different freezing processes (data not shown), indicating that there is no significant difference in term of mechanical properties between formulations prepared by different freezing processes. In summary, TFF formulations prepared at higher freezing rate lead to powders with superior aerodynamic properties, compared to TFF processed powders at intermediate cooling rate and slow freezing on the shelf products.

3.4.2 TFF powders prepared at different initial solid concentrations

To determine the influence of solids concentration during TFF production, several different solution concentrations were investigated, 0.5%, 1%, 5% and 10%. The same freezing process (TFF at -50°C) was employed for comparison purposes. As illustrated in Fig.3.6, similar thin water channels will be generated between the ice crystal domains. However, due to the different initial solid concentrations, the molecules' intensity is different at the same thin water channels. For TFF formulations prepared at higher initial solid loading (right figure), there are many more molecules mobilized in the water channels between the ice crystal domains, increase the chance for MAN crystals to grow

and aggregate until completely frozen; For TFF formulations prepared at lower initial concentration (left figure), fewer MAN molecules were mobilized between the ice crystal domain, leading to less aggregated MAN particles with higher porosity.

The aerodynamic performance of TFF RHOMAN prepared at different solid concentrations determined by NGI is shown in Fig.3.7. No difference was observed between 0.5% TFF RHOMAN and 1% TFF RHOMAN in terms of TED (around 85%), indicating that the shear and impaction forces generated by air flow and device were able to break the bulk matrix particles into aerosol particles that were small enough to exit the holes on the pierced capsule. When initial solid loading increased to 5% and 10%, the TED of the TFF formulations decreased to 52.9% and 30.9%, respectively, because there were certain amount of matrix particles can't be fractured into particles that were smaller enough to exit the capsule. A significantly decreasing trend of FPF for these TFF formulations was observed (Fig.3.7) when the initial solid concentrations increased, because higher solid concentration resulted in TFF powders with less porosity, thinner matrix structure and lower density, which is beneficial for the aerosolization properties. Correspondingly, MMAD and GSD increased when the initial solid concentration increased.

The geometric particle size distribution of aerosol particles for TFF RHOMAN prepared at different solid concentrations is shwon in Fig.3.8. The mean geometric particle size (D50) of aerosolized TFF particles decreased as the initial solid loading increased, probably because more brittle fracture occurred when thinner matrix structure was generated from lower initial solid concentration in the TFF process. The resulting

bulk density of the powders prepared at different concentrations is displayed in Table 3.3. The bulk density of TFF RHOMAN (0.5%) and TFF RHOMAN (1%) were slightly higher than the theoretical values. Since minor brittle fracture was induced during the collection process due to the high brittleness of the TFF formulations prepared at lower solid concentration, fractured matrix particles tend to collapse with each other and causing the measured bulk density to be higher than the theoretical value. However, for TFF formulations prepared at relatively high solid concentrations (5% and 10%, w/v), it's difficult to fracture the matrix particles due to their low brittleness, hence the measured bulk densities correlated well with the theoretical values. A linear relationship was found for the bulk density to the initial solid concentrations (Fig.3.9). Therefore, in the TFF process, initial solid concentration is an essential parameter that can be manipulated to control the bulk density of the resulting formulations, further optimize the aerodynamic performance of TFF processed brittle matrix powders.

Mechanical testing revealed marked differences of the immersion forces for bulk TFF powders prepared with different solid concentrations, as shown in Fig.3.10. In this experiment, a probe was moved at a set rate through a powder bed of each concentration of TFF formulation. The data was analyzed to report the resulting forces versus compaction of a given mass of powder. By comparing the resulting forces over a given mass for each powder formulation, we can determine which matrix resulted in more brittle fracture/deformation and which resisted fraction/deformation. Not surprisingly, 10% TFF powders resisted compaction more than formulations made at lower concentrations likely due to a stronger, less brittle, matrix structure. . The slopes for 0.5%, 1%, 5% and

10% TFF RHOMAN were 0.109, 0.254, 1.635 and 3.019 N/g, respectively (Fig.3.10). The value of these slopes increased with the increases of initial solid loading, indicating that TFF formulations prepared at higher solid concentration generated less fracturable powders, which may require higher energy to achieve brittle fracture during the aerosolization process. Since the TFF particles need to be fractured into respirable particles during the aerosolization process, we can conclude that brittleness and fragility of TFF matrix powders demonstrated by a smaller slope in the immersion-force curve is essential for a good aerodynamic performance. By lowering the initial solid concentrations in the TFF process, it is possible to improve the fracture abilities of TFF processed powders and accordingly the aerodynamic properties.

3.5 Conclusion

Engineered particles containing bulking agent mannitol and Rhodamine B as a marker were successfully prepared by TFF process. Despite their relatively large size (50-100 μm), these brittle matrix powders were highly respirable due to their low density and brittle nature. By varying the freezing process, different cooling time and freezing rate were achieved. Formulations prepared at higher freezing rate exhibited greater surface area, higher porosity and lower density, which further lead to better aerodynamic performance (higher FPF) for these brittle matrix powders. A linear relationship of the resulting bulk density to the initial solid concentrations was observed for TFF processed powders. Moreover, as decreasing the initial solid concentration, the FPF of TFF formulations demonstrated an increasing trend due to the lower density and enhanced

brittleness. Therefore, the aerodynamic properties of TFF produced formulations can be optimized by altering the freezing rate and initial solid concentrations of the TFF process.

3.6 References

[1] A.H. Chow, H.H. Tong, P. Chattopadhyay, B.Y. Shekunov, Particle engineering for pulmonary drug delivery, Pharm Res, 24 (2007) 411-437.

[2] J. Zhang, L. Wu, H.K. Chan, W. Watanabe, Formation, characterization, and fate of inhaled drug nanoparticles, Adv Drug Deliv Rev, 63 (2011) 441-455.

[3] N. Rasenack, B.W. Muller, Micron-size drug particles: common and novel micronization techniques, Pharm Dev Technol, 9 (2004) 1-13.

[4] I.Y. Saleem, H.D. Smyth, Micronization of a soft material: air-jet and micro-ball milling, AAPS PharmSciTech, 11 (2010) 1642-1649.

[5] S.P. Velaga, R. Berger, J. Carlfors, Supercritical fluids crystallization of budesonide and flunisolide, Pharm Res, 19 (2002) 1564-1571.

[6] L.C. Grisedale, M.J. Jamieson, P.S. Belton, S.A. Barker, D.Q. Craig, Characterization and quantification of amorphous material in milled and spray-dried salbutamol sulfate: a comparison of thermal, spectroscopic, and water vapor sorption approaches, J Pharm Sci, 100 (2011) 3114-3129.

[7] H. Chiou, L. Li, T. Hu, H.K. Chan, J.F. Chen, J. Yun, Production of salbutamol sulfate for inhalation by high-gravity controlled antisolvent precipitation, Int J Pharm, 331 (2007) 93-98.

[8] D.A. Edwards, J. Hanes, G. Caponetti, J. Hrkach, A. Ben-Jebria, M.L. Eskew, J. Mintzes, D. Deaver, N. Lotan, R. Langer, Large porous particles for pulmonary drug delivery, Science, 276 (1997) 1868-1871.

[9] R. Vanbever, J.D. Mintzes, J. Wang, J. Nice, D. Chen, R. Batycky, R. Langer, D.A. Edwards, Formulation and physical characterization of large porous particles for inhalation, Pharm Res, 16 (1999) 1735-1742.

[10] L.A. Dellamary, T.E. Tarara, D.J. Smith, C.H. Woelk, A. Adractas, M.L. Costello, H. Gill, J.G. Weers, Hollow porous particles in metered dose inhalers, Pharm Res, 17 (2000) 168-174.

[11] S.P. Duddu, S.A. Sisk, Y.H. Walter, T.E. Tarara, K.R. Trimble, A.R. Clark, M.A. Eldon, R.C. Elton, M. Pickford, P.H. Hirst, S.P. Newman, J.G. Weers, Improved lung

delivery from a passive dry powder inhaler using an Engineered PulmoSphere powder, Pharm Res, 19 (2002) 689-695.

[12] P.C. Richardson, A.H. Boss, Technosphere insulin technology, Diabetes Technol Ther, 9 Suppl 1 (2007) S65-72.

[13] C. Plumley, E.M. Gorman, N. El-Gendy, C.R. Bybee, E.J. Munson, C. Berkland, Nifedipine nanoparticle agglomeration as a dry powder aerosol formulation strategy, Int J Pharm, 369 (2009) 136-143.

[14] M. Geiser, Update on macrophage clearance of inhaled micro- and nanoparticles, Journal of aerosol medicine and pulmonary drug delivery, 23 (2010) 207-217.

[15] W. Yang, J.I. Peters, R.O. Williams, 3rd, Inhaled nanoparticles--a current review, Int J Pharm, 356 (2008) 239-247.

[16] A.B. Watts, J.I. Peters, R.L. Talbert, K.P. O'Donnell, J.J. Coalson, R.O. Williams, 3rd, Preclinical evaluation of tacrolimus colloidal dispersion for inhalation, Eur J Pharm Biopharm, 77 (2011) 207-215.

[17] W. Yang, K.P. Johnston, R.O. Williams, 3rd, Comparison of bioavailability of amorphous versus crystalline itraconazole nanoparticles via pulmonary administration in rats, Eur J Pharm Biopharm, 75 (2010) 33-41.

[18] A.B. Watts, Y.B. Wang, K.P. Johnston, R.O. Williams, 3rd, Respirable low-density microparticles formed in situ from aerosolized brittle matrices, Pharm Res, 30 (2013) 813-825.

[19] K.A. Overhoff, J.D. Engstrom, B. Chen, B.D. Scherzer, T.E. Milner, K.P. Johnston, R.O. Williams, 3rd, Novel ultra-rapid freezing particle engineering process for enhancement of dissolution rates of poorly water-soluble drugs, Eur J Pharm Biopharm, 65 (2007) 57-67.

[20] A.I. Kim, M.J. Akers, S.L. Nail, The physical state of mannitol after freeze-drying: effects of mannitol concentration, freezing rate, and a noncrystallizing cosolute, J Pharm Sci, 87 (1998) 931-935.

[21] C. Telang, L. Yu, R. Suryanarayanan, Effective inhibition of mannitol crystallization in frozen solutions by sodium chloride, Pharm Res, 20 (2003) 660-667.

[22] K. Izutsu, S. Kojima, Excipient crystallinity and its protein-structure-stabilizing effect during freeze-drying, J Pharm Pharmacol, 54 (2002) 1033-1039.

[23] K. Izutsu, S. Yoshioka, T. Terao, Effect of mannitol crystallinity on the stabilization of enzymes during freeze-drying, Chem Pharm Bull (Tokyo), 42 (1994) 5-8.

[24] J.D. Engstrom, E.S. Lai, B.S. Ludher, B. Chen, T.E. Milner, R.O. Williams, 3rd, G.B. Kitto, K.P. Johnston, Formation of stable submicron protein particles by thin film freezing, Pharm Res, 25 (2008) 1334-1346.

[25] J.P. Mitchell, Practices of coating collection surfaces of cascade impactors: a survey of members of the european pharmaceutical aerosol group (EPAG). Drug Deliv Lung, 14 (2003) 75-78.

[26] V.A. Marple, B.A. Olson, K. Santhanakrishnan, J.P. Mitchell, S.C. Murray, B.L. Hudson-Curtis, Next generation pharmaceutical impactor (a new impactor for pharmaceutical inhaler testing). Part II: Archival calibration, J Aerosol Med, 16 (2003) 301-324.

[27] S. Dixit, S.K. Khanna, M. Das, A simple method for simultaneous determination of basic dyes encountered in food preparations by reversed-phase HPLC, J AOAC Int, 94 (2011) 1874-1881.

[28] USP 32-NF 27 General Chapter 601: Aerosols, Nasal sprays, Metered-dose inhalers, and Dry powder inhalers., 218-239.

[29] H.S. Carslaw, J.C. Jaeger, Conduction of heat in solids, 2d ed., Clarendon Press, Oxford,, 1973.

[30] S. Claus, C. Weiler, J. Schiewe, W. Friess, Optimization of the fine particle fraction of a lyophilized lysozyme formulation for dry powder inhalation, Pharm Res, 30 (2013) 1698-1713.

[31] J.C. Kasper, W. Friess, The freezing step in lyophilization: physico-chemical fundamentals, freezing methods and consequences on process performance and quality attributes of biopharmaceuticals, Eur J Pharm Biopharm, 78 (2011) 248-263.

[32] S. Wies, A. Geyer, W. Eysel, The limit of detection in differential scanning calorimetry., J Therm Anal, 38 (1992) 277-287.

Tables

Table 1.1 Current inhaled pharmaceuticals for treatment of lung diseases (a) and systemic applications on the market or undergoing clinical studies.
(a)

Therapeutic usage	Drug	Drugs	Inhalation device	Current
COPD and asthma	Short-acting beta-2 agonist (SABAs)	Salbutamol (albuterol)	Nebulizer, pMDI,	Marketed
		Fenoterol	pMDI	Marketed outside
		Pirbuterol	Nebulizer, pMDI	Discontinued by
		Terbutaline	DPI	Marketed
		Levalbuterol	pMDI	Marketed
	Long-acting beta-2 agonist (LABAs)	Salmeterol	pMDI, DPI	Marketed
		Formeterol	pMDI, DPI	Marketed
		Arformoterol	Nebulizer	Marketed
		Indacaterol	DPI	Marketed
	Anticholinergic agents	Ipratropium bromide	Nebulizer, pMDI	Marketed
		Tiotropium bromide	pMDI, DPI	Marketed
		Aclidinium bromide	DPI	Marketed
		Oxitropium bromide	pMDI	Outside of US
		Glycopyrronium	DPI	Outside of US
	Inhaled corticosteroids (ICS)	Beclomethasone	Nebulizer, pMDI,	Marketed
		Budesonide	Nebulizer, DPI	Marketed
		Fluticasone propionate	pMDI, DPI	Marketed
		Mometasone furoate	pMDI, DPI	Marketed
		Ciclesonide	pMDI	Marketed
	Combination therapy	Fenoterol/Ipratropium	pMDI	Marketed
		salbuterol/Ipratropium	pMDI	Marketed
		Formeterol/Budesonide	pMDI, DPI	Marketed
		Formeterol/Mometason	DPI	Marketed
		Salmeterol/Fluticasone	pMDI, DPI	Marketed
		Glycopyrronium/formot	pMDI	Phase II
	Sugar alcohol	Mannitol	DPI	Marketed
	Antisense oligonucleotides	AIR-645	Nebulizer	Phase II
		PXSTPI-1100	Nebulizer	Preclinical
		ATL-1102	Nebulizer	Preclinical
	CpG	QAX-935 (IMO-2134)	Nebulizer	Phaes I
	siRNA	Excellair	Nebulizer	Phase II
Cystic fibrosis	Antibiotics	Tobramycin	Nebulizer, DPI	Marketed
		Aztreonam	Nebulizer	Marketed
		Colistimethate sodium	Nebulizer	Pilot trials
		Liposomal	Nebulizer	Phase II
		Liposomal amikacin	Nebulizer	Phase III
		Levofloxacin	Nebulizer	Phase III
		PUR118	DPI	Phase I

Table 1.1a continued

	Mucous	Dornase alfa	Nebulizer	Outside of US
		Lancovutide	Nebulizer	Phase II
	Restore Airway Surface Liquid	Hypertonic saline	Nebulizer	Marketed
		Mannitol	DPI	Phase III
	Antiproteases	$Alpha_1$-antitrypsin	Nebulizer	Phase II
	MRSA lung	Vancomycin	DPI	Phase II
Respiratory Distress	Pulmonary	Phospholipids/surfactan	Endo-tracheal tube	Marketed
Respiratory Syncytial	Antiviral	MDT-637	Novel inhaler	Phase II

There are more than 70 pipeline medicines in development for asthma and more than 50 pipeline medicines in development for COPD. For more information, please refer to Medicines in Development Asthma 2012 report and Medicines in Development COPD 2012 report presented by Pharmaceutical Research and Manufacturers of America (available on PhRMA's web site).

(b)

Therapeutic usage	Drug classifications	Drugs	Inhalation	Current development
Analgesia	Opioids	Fentanyl	Novel inhaler	Phase II
		Liposomal fentanyl	Nebulizer	Phase II
Migrane	Triptan	Sumatriptan	Intranasal	Phase III
Diabetes	Peptides	Insulin	DPI	Phase III
		Glucagon-like	DPI	Phase I
Nerve gas	Nerve agent antidote	Atropine	Novel inhaler	Phase I
Parkinson's	Psychoactive drug	Levodopa	DPI	Phase II
Schizophrenia	Antipsychotic medicati	Loxapine	DPI	Outside of US

DPI, dry powder inhaler; pMDI, pressurized Metered Dose Inhaler. Adapted with permission from Ungaro et al. *J Pharm Pharmacol* 64, 1217-1235 (2012). Other sources are from Global Initiative for Chronic Obstructive Lung Disease (GOLD) web site, Global Initiative for Asthma (GINA) web site and http://clinicaltrials.gov/

Table 1.2 Most commonly occurring lung diseases, their definitions, causes, symptoms and pathophysiology.

Common lung diseases	Definitions	Causes	Symptoms	Pathophysiology
Chronic obstructive pulmonary disease (COPD)	COPD is an ill-defined term that is often applied to patients who have emphysema, chronic bronchitis, or a mixture of the two.	Smoking air pollution	Shortness of breath, cough, cough up mucus	Chronic bronchitis: hypertrophy of mucous glands in large bronchi, inflammation in small airways, excessive mucus production. Emphysema: loss of alveolar walls, destruction of capillary bed, small airways narrowed and reduced in number.
Asthma	Asthma is characterized by increased responsiveness of the airways to various stimuli and is manifested by widespread narrowing of the airways that change in severity, either spontaneously or as a result	Allergy Smoking exercise	Coughing, Wheezing Shortness of breath Chest tightness, pain, or pressure	Hypertrophied smooth muscle and mucus glands, bronchoconstriction, edema of the bronchial wall, thick tenacious and slow-moving mucus
Cystic Fibrosis	Cystic fibrosis is an autosomal recessive genetic disorder that affects most critically the lungs, and also the pancreas, liver, and intestine. It is characterized by abnormal transport of chloride and sodium across an epithelium, leading to thick, viscous	Genetic	Salty-tasting skin, coughing, wheezing, Difficulty breathing, Big appetite but poor weight gain	thick and sticky mucus, excessive absorption of sodium ions, defective chloride secretion
Pneumonia	Inflammation of the lung parenchyma associated with alveolar filling by exudate.	Bacteria, Virus, Fungi, Parasites	Fever, cough, malaise, pleuritic pain	Alveoli crammed with cells, necrosis of tissue, lung abscess
Pulmonary edema	Abnormal accumulation of fluid in the extravascular spaces and tissues of the lung.	Heart failure, lung injury	shortness of breath, Chest discomfort or heaviness, Fatigue etc.	Engorgement of interstitial tissue, increased lymph flow and widen lymphatic, fluid-filled alveoli
Lung carcinoma	Lung carcinoma is a disease characterized by uncontrolled cell growth in tissues of the lung.	Smoking	Coughing, weight loss, shortness of breath.	Small cell lung cancers (SCLC) form central tumors and non-small cell lung cancers (NSCLC) form both central and peripheral tumors.
Pulmonary Embolus	Obstruction of blood flow to one or more arteries of the lung by a thrombus (other emboli – fat, air, and amniotic fluid) lodged in pulmonary vessels.	Blood clot in a vein on the leg or on the pelvis	Shortness of breath, low blood oxygen levels.	Venous thrombi formed, static of blood, alteration in the blood coagulation system, abnormal vessel wall
Pulmonary arterial hypertension (PAH)	PAH is a progressive disorder characterized by abnormally high blood pressure (hypertension) in the pulmonary artery, the blood vessel that carries blood from the heart	Cause unclear genetic	Shortness of breath, chest pain	Hypertrophy and thickening of artery wall, increased capillary permeability, reduced lymph drainage

All the definitions in this table are cited from West 2012. Pulmonary pathophysiology : the essentials, 8th ed. Wolters Kluwer/Lippincott Williams & Wilkins Health, Philadelphia.

Table 1.3 Advanced technologies for production of dry powder formulations designated for inhalation.

Technologies	Company	Preparation Process	Device	Respirable Fraction (%)	References
AIR®	Alkermes	Spray drying	Spinhaler®	up to 49%	Vanbever et al., 1999
PulmoSphere®	Novartis	Spray drying of double emulsion	Eclipse® DPI	up to 60%	Duddu et al., 2002
Technosphere®	MannKind	Acid-induced particle self-assembly	MedTone® DPI	up to 57%	Richardson and Boss, 2007
NanoCluster®	Savara	Salt flocculation	N/A	up to 84%	Plumley et al., 2009
Thin Film Freezing	Patented by Univ. of Texas at Austin	Rapid freezing	Handihaler®	up to 74%	Watts et al., 2013

Table 1.4 Particle deposition equations at different flow conditions for the three deposition mechanisms.

Flow conditions	Deposition mechanisms		
	Inertial impaction P(I)	Sedimentation P(S)	Diffusion P(D)
Laminar	$\frac{2}{\pi}[e(1-e^2)^{1/2} + \arcsin(e)]$	$\frac{2}{\pi}[f(1-f^2)^{1/2} + \arcsin(f)]$	$4(\frac{K}{\pi})^{1/2} - K$
Turbulent	$1 - \exp(\frac{-4e}{\pi})$	$1 - \exp(\frac{-8\tau Gt(I)\cos(\phi(I))}{\pi D(I)})$	$1 - \exp(\frac{-0.088d^{3/4}Re(I)^{7/8}L(I)}{U(I)D(I)^2}$

$e = \theta(I)\tau U(I)/D(I)$, $f = t(I)Vcos(\varphi(I))/D(I)$, $K = 4dL(I)/U(I)D(I)^2$

ϕ(I): Inclination of generation I airway with respect to horizontal (°); θ(I): Angle of bend of generation (°); τ: particle relaxation time; G: Gravitational constant=980 cm/s^2; L(I): Length of airway generation I; D(I): Diameter of generation I; U(I): mean air velocity in generation I; Re(I): Airflow Reynolds number in generation I; d: particle diffusion coefficient; t(I): residence time of particle in generation I; V: particle Stroke terminal settling speed. Reprinted with permission from Martonen etal. *Adv Eng Softw* 28, 359-364 (1997).

Table 1.5 List of input and output parameters for aerosol deposition models.

Input parameters	Output parameters
	Images:
Subject characteristics:	Planar gamma camera lungs
height, weight, age	Planar gamma camera oropharynx
Functional Residual Capacity(FRC)	SPECT/CT of lungs
Forced expiratoryvolumein1s(FEV1)	SPECT/CT of lungs with partial volume correction
	SPECT/CT of oropharynx
Ventilatory parameters:	Percentage of inhaled deposition by airway section:
Tidal volume	Extrathoracic
Inhalation time	Trachea/bronchi
Breath hold time	Right lung
Exhalation time	Left lung
Posture	Exhaled
Aerosol characteristics:	
Mass median aerodynamic diameter	Spatial measures of deposition:
Geometric standard deviation	One dimensional curves of variation of deposition with shell number
Particle size distribution curve	2D c/p ratio (absolute and volume normalized)
Humidity	3D c/p ratio (absolute and volume normalized)
Carrier gas	
	Airway measures of deposition:
Airway morphology:	One dimensional curves of variation of deposition with generation number
Images of segmented airway	24 h clearance
	Conducting airways deposition fraction

Adapted with permission from Conway et al. *J Aerosol Sci* 52: 1–17 (2013).

Table 1.6 Breathing pattern of adults at two different conditions, sedentary and light activity.

	Tidal volume (ml)	Frequency (breaths/min)	Minute volume (L)	Inspiratory flow rate (L/min)
Sedentary	500	14	7	14
Light Activity	1291	15.5	20	40

Adapted with permission from Martonen et al. *Pharm Res* 12, 96-102 (1995)

Table 1.7 The impact of lung diseases on the fate of inhaled medicines for each of these processes.

Processes involved in the fate of inhaled medicines	The impact of lung diseases on these different processes
Deposition	For obstructive lung diseases, deposition on the diseased sites ↑ and deposition in the alveoli ↓ For pulmonary fibrosis, deposition ↓ in the whole lung, and heterogeneity ↑
Absorption	For obstructive lung diseases including lung cancer, systemic absorption ↓ For pulmonary vascular diseases, systemic absorption ↓ For pulmonary fibrosis, both pulmonary and systemic absorption ↓ For chronic airway inflammations and pulmonary edema, systemic absorption ↑ Caveolae mediated transcytosis impacted by different lung diseases
Clearance	For COPD, asthma and CF, mucociliary clearance (MCC) rate ↓ For pneumonia and influenza, MCC rate↓ For bronchiectasis, chronic rhinosinusitis and pulmonary edema, MCC rate↓ For chronic bronchitis, cough clearance ↑ Airway macrophage phagocytosis ↑ for asthma Mild to moderate asthma, alveolar macrophage (AMs) phagocytosis unchanged; for severe asthma, AMs impaired For COPD, AMs phagocytosis ↓

Table 2.1 Specific surface area (SSA), geometric particle size distribution of micronized TACMAN (1:1) and TFF TACMAN (1:1). Values are expressed as mean±SD (n=3).

Formulation	TAC potency (%)	SSA (m^2/g)	Calculated particle diameter (μm)	Geometric Particle Size (μm)		
				D10	D50	D90
Micronized TACMAN (1:1)	49.7	2.87±0.16	2.09	0.93±0.03	1.92±0.05	4.82±0.08
TFF TACMAN (1:1)	50.3	32.45±3.28	0.18	4.39±0.21	17.84±0.57	64.49±2.89

Table 2.2 Lung pharmacokinetic parameters of TFF TACMAN (1:1) and micronized TACMAN (1:1) following single dose exposure to dry powder aerosols generated from a rotating brush generator. All the parameters were calculated based on average lung concentration (n=5).

Pharmacokinetic parameters	TFF TACMAN (1:1)	Micronized TACMAN (1:1)
$AUC_{0\text{-}24h}$(ng*hr/g)	1707.47	729.53
K10 (h^{-1})	0.56	2.64
K12 (h^{-1})	2.16	1.70
K21 (h^{-1})	0.20	0.45
C_{max} (ng/g)	948.20	1924.83
CL (ng/(hr*ng/g)	2.93	6.85
MRT (hr)	21.18	1.82
Model fit (R^2)	0.9985	0.9999

Table 3.1 Physicochemical properties of TFF RHOMAN (-140°C), TFF RHOMAN (-50°C) and shelf lyophilized RHOMAN.

Freezing process	Cooling time (ms)	Cooling rate (K/s)	SSA (m^2/g)	Bulk Density ($10^{-3}g/cm^3$)	Porosity (%)
TFF at -140°C, then lyophilized	106	2.36×10^2	77.4±2.5	10.42±0.68	6.8
TFF at -50°C, then lyophilized	148	1.69×10^2	38.6±1.7	12.31±1.12	4.2
Shelf lyophilized, precool to -50°C	$>10^6$	$<2.5\times10^{-5}$	0.8±0.0	26.84±2.53	Undetectable

Table 3.2 Bulk density and calculated aerosolized particle density based on measured geometric and aerodynamic diameters of TFF RHOMAN prepared by different freezing processes.

Formulations	Bulk Density ($10^{-3}g/cm^3$)	MMAD (μm)	D50 (μm)	Dynamic shape factor (X)	Calculated density ($10^{-3}g/cm^3$)
TFF at -140°C	10.42±0.68	2.47	33.46	1.50	8.17
TFF at -50°C	12.31±1.12	3.29	39.84	1.50	10.23
Shelf lyophilized	26.84±2.53	6.34	49.85	1.50	24.26

Table 3.3 Bulk density and calculated aerosolized particle density based on measured geometric and aerodynamic diameters of TFF RHOMAN prepared at different solid concentrations (0.5%, 1%, 5% and 10%).

Solid Concentration (w/v) of TFF RHOMAN	Theoretical Bulk Density (mg/cm^3)	Measured Bulk Density (mg/cm^3)
0.5	5	6.84±0.68
1	10	12.31±1.12
5	50	48.75±4.64
10	100	100.64±9.61

Table A.1 Summary of prior arts of inhaled Tacrolimus.

Formulations, Delivery Systems	Animal Model	Results	references
Inhaled TAC aerosol puffs (50 μg/puff), oral TAC (1 mg/kg)	Inhibits Antigen-Induced Airway Inflammation in Guinea Pigs	Suppress airway inflammation in guinea pigs; effect of 3 inhaled puffs was almost equal to that of 1 mg/kg administered by the oral route. Following inhalation of 3 puffs, TAC concentration in blood was about 1/21 of that following oral FK506 (1 mg/kg).	Morishita et al. 2005
Inhaled TAC (5, 10, 20 puffs per day), IM TAC (0.05, 0.1 or 1.0 mg/kg/day)	Rat Orthotopic Lung Transplantation Model	Inhaled TAC enhances acute lung allograft survival with lower blood concentrations than when using comparable intramuscular administration. (10 puff/day vs 0.1 mg/kg/day). Trough concentrations of TAC in blood were detectable with 0.1 mg/kg/day of intramuscular FK 506, but not with 10 puffs/day.	Ingu et al. 2005
Inhaled TAC (6, 12 puffs 3 times per day), IM TAC (0.3, 0.5 or 1.0 mg/kg/day)	Rat Orthotopic Lung Transplantation Model	Similar histologic grade of the graft, lower blood and allograft concentration, less severe weight loss and diarrhea.	Ide et al. 2007
Aerosolized TAC gengrated by nebulizer for 20min once daily (4 mg/kg, dissolved in 70% ethanol), oral TAC (4mg/kg) once daily	Rat Orthotopic Lung Transplantation Model and in vitro cell culture	Similar tracheal tissue level of TAC with higher lung-tissue concentrations and blood level approximately (5.5-11 times) lower, similar histology grade of grafts, far less effective in systemic cellular immune activation. No airway toxicity, decreases more effectively inflammatory airway cytokine production, and inhibits NFkB activation.	Schrepfer et al. 2007 Deuse et al. 2010
Nebulized TAC nanoparticle dispersions, single dose and 28 days continous dosing	Transplanted and nontransplanted rats	High lung concentration and low blood level of TAC, non-toxic, inhaled TAC providing therapeutic concentrations locally while not be expected to induce toxic side effects.	Watts et al. 2010 Watts et al. 2011

Table B.1 Aerodynamic parameters of TFF TACMAN before and after acoustic mixing.

Samples	TFF TACMAN (1:1)				
	Original	10%, 60s	30%, 60s	50%, 60s	50%,5min
MMAD (μm)	5.05±0.33	5.49	5.53	6.08	7.37
GSD (μm)	2.18±0.14	2.09	2.13	2.02	2.01
FPF (%)	49.4±3.2	45.17	44.97	39.73	31.64
TFD (%)	96.8±1.0	97.45	97.81	97.98	98.33

Table C.1 Aerodynamic parameters of TFF TACMAN (1:1) using three different DPIs, Handihaler®, Aerolizer® and Miat® monodose inhaler.

DPIs	Handihaler®	Aerolizer®	Miat monodose inhaler®
Flow Rate (L/min)	51	90	90
MMAD (μm)	4.52±0.22	2.28±0.19	2.26±0.13
GSD (μm)	2.03±0.09	2.11±0.13	2.08±0.10
FPF (%)	54.6±2.2	83.1±1.9	83.3±1.7
TFD (%)	96.5±1.4	95.0±1.1	94.2±0.7

Table C.2 Aerodynamic parameters of TFF TACMAN (1:1) using three different DPIs, Handihaler®, Aerolizer® and Miat® monodose inhaler at low, medium and high flow rate that generated by patients clinically.

DPIs	Handihaler®			Aerolizer®			Miat® monodose inhaler		
Flow rate (L/min)	20	30	45	60	90	120	60	90	120
MMAD (um)	8.3	5.5	4.9	4.5	2.3	1.8	4.6	2.3	1.9
GSD (um)	1.8	2.1	2.1	2.2	2.1	2.0	2.1	2.1	2.0
FPF (%)	24.5	44.9	51.6	55.6	83.1	87.4	53.5	83.3	88.8
TED (%)	95.2	94.5	93.2	95.9	95.0	96.8	95.6	94.2	95.2

All the experiments have been conducted triply, values in the tables are average, RSD was less than 5%.

Table E. 1 Residual solvent amount of TFF processed powders immediately after preparation, stored for a week in a desiccator at room temperature (25°C, <15% RH) and in a humidity chamber placed in a heated oven (40°C, >90%RH).

Samples	Residual solvent amount (%)		
	Initial	25°C, <15% RH	40°C, >90% RH
Bulk TAC	2.19%	1.60%	
Bulk Lac Mono	5%	4.70%	N/A
Bulk MAN	0%	0%	
TFF TAC only	0%	0%	0%
TFF TACLAC	1.89%	2.24%	2.62%
TFF TACMAN	0%	0%	0%

Table J.1 Density and thermal properties used to calculated thermal diffusivity (α) for water and ice.

Properties	Water	Ice
k (W/mK)	0.6072	2.22
ρ (g/cm^3)	0.9998	0.9162
Cp (J/gK)	4.200	2.116
α (m^2/s)	0.144×10^{-6}	1.145×10^{-6}
Average α (m^2/s)		0.6445×10^{-6}

Figures

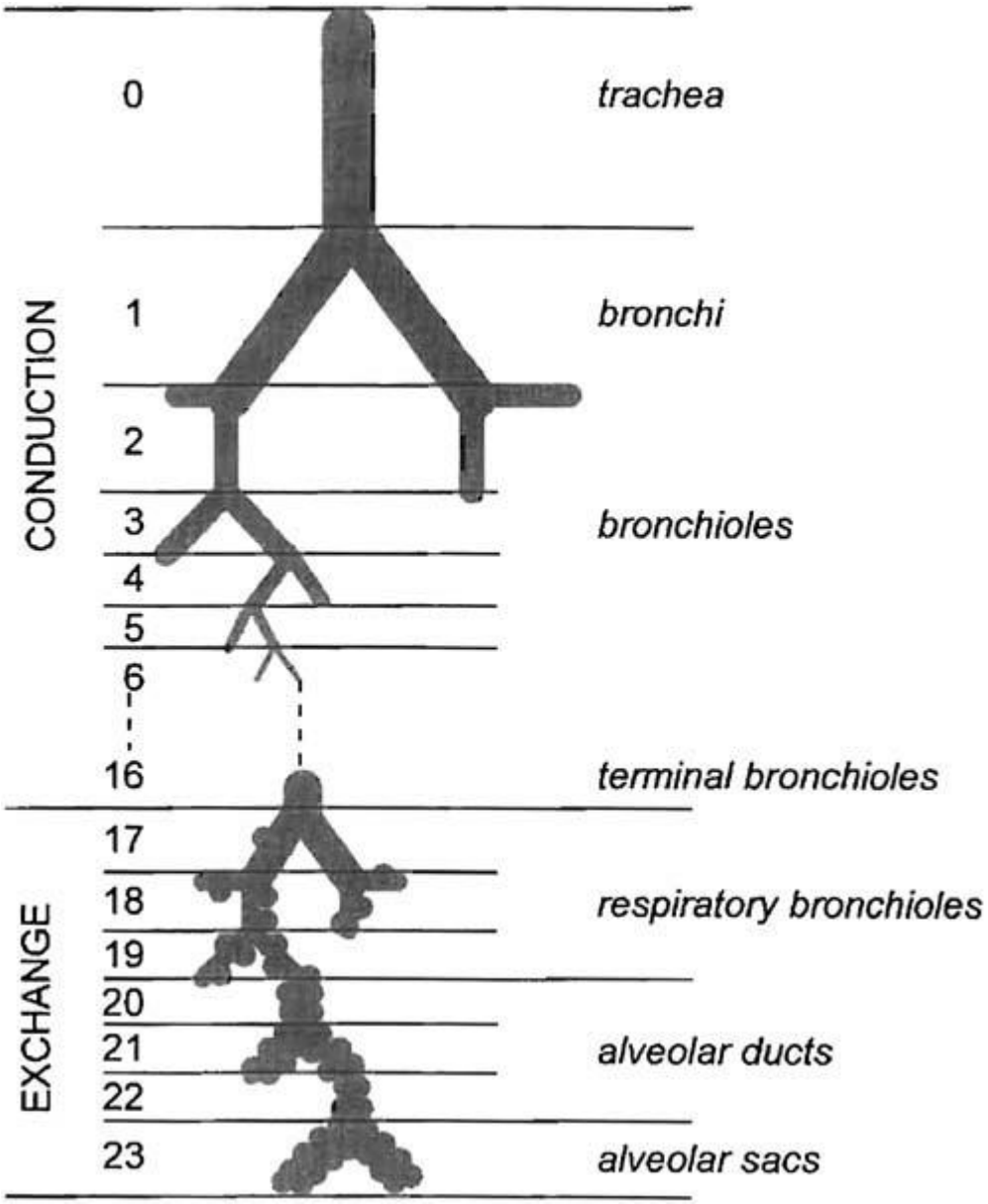

Figure 1.1 Model of airways described by Weibel. Reprinted with permission from Lee et al. AAPS J 11, 414-423 (2009).

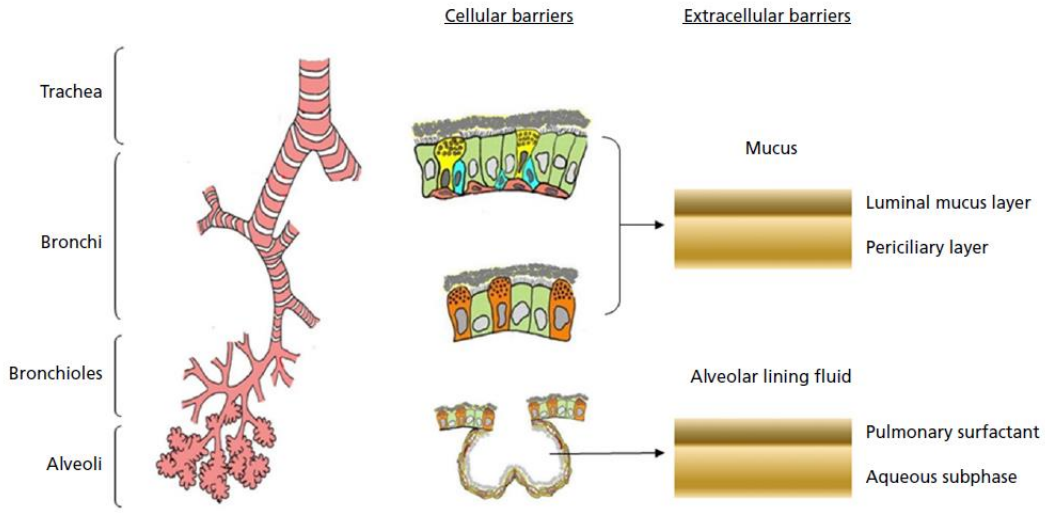

Figure 1.2 Schematic illustration of lung physiology at cellular and extra-cellular levels. Reprinted with permission from Ungaro et al. *J Pharm Pharmacol* 64, 1217-1235 (2012).

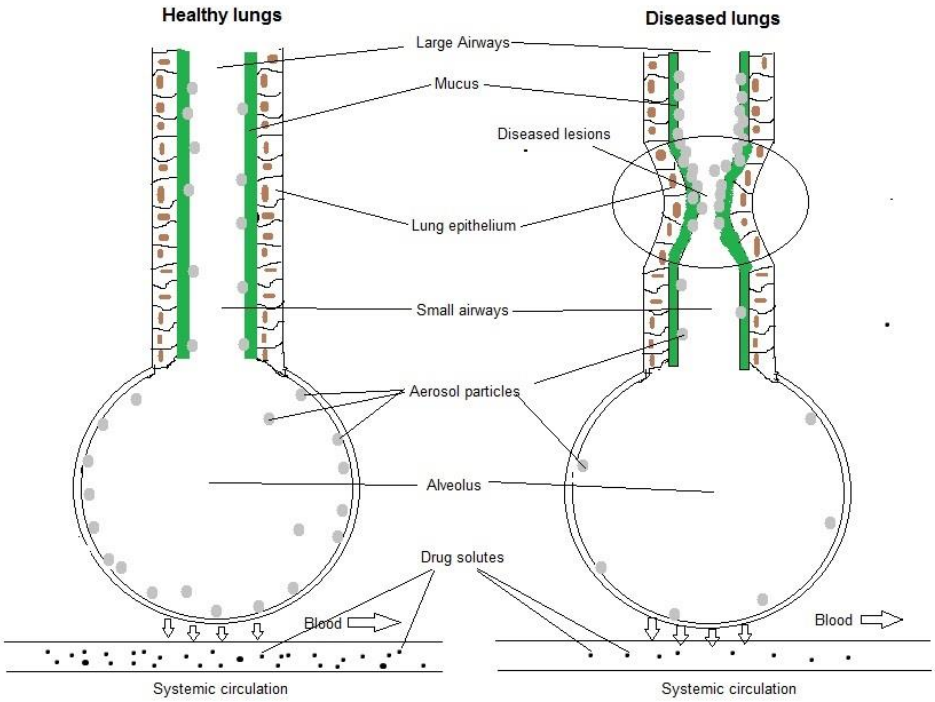

Figure 1.3 The impact of lung diseases on aerosol particle depostion and absorption.

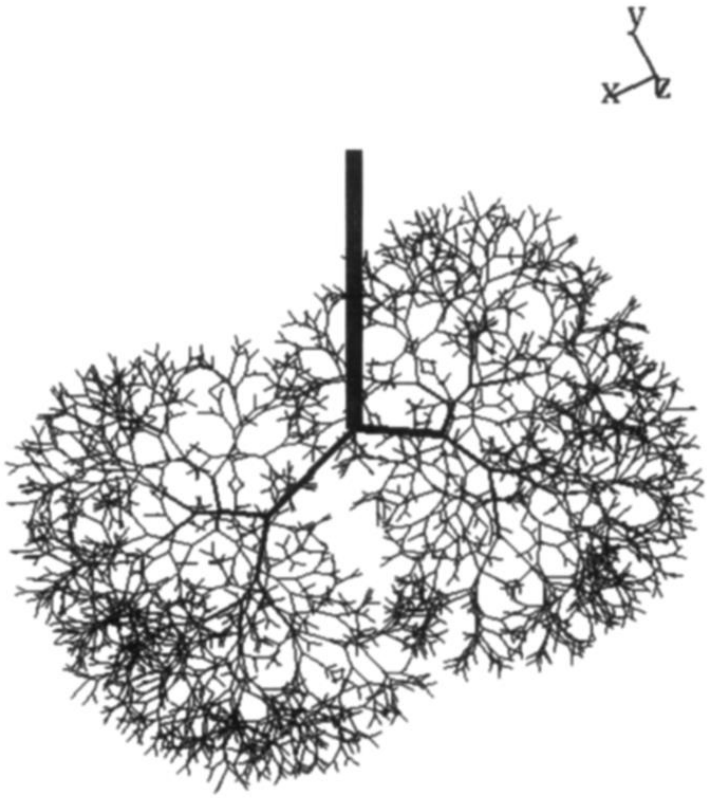

Figure 1.4 Computational modeling of the branching network of airways in the human lung. Only generations 0 (trachea) to 12 are illustrated. Reprinted with permission from Martonen etal. *Adv Eng Softw* 28, 359-364 (1997).

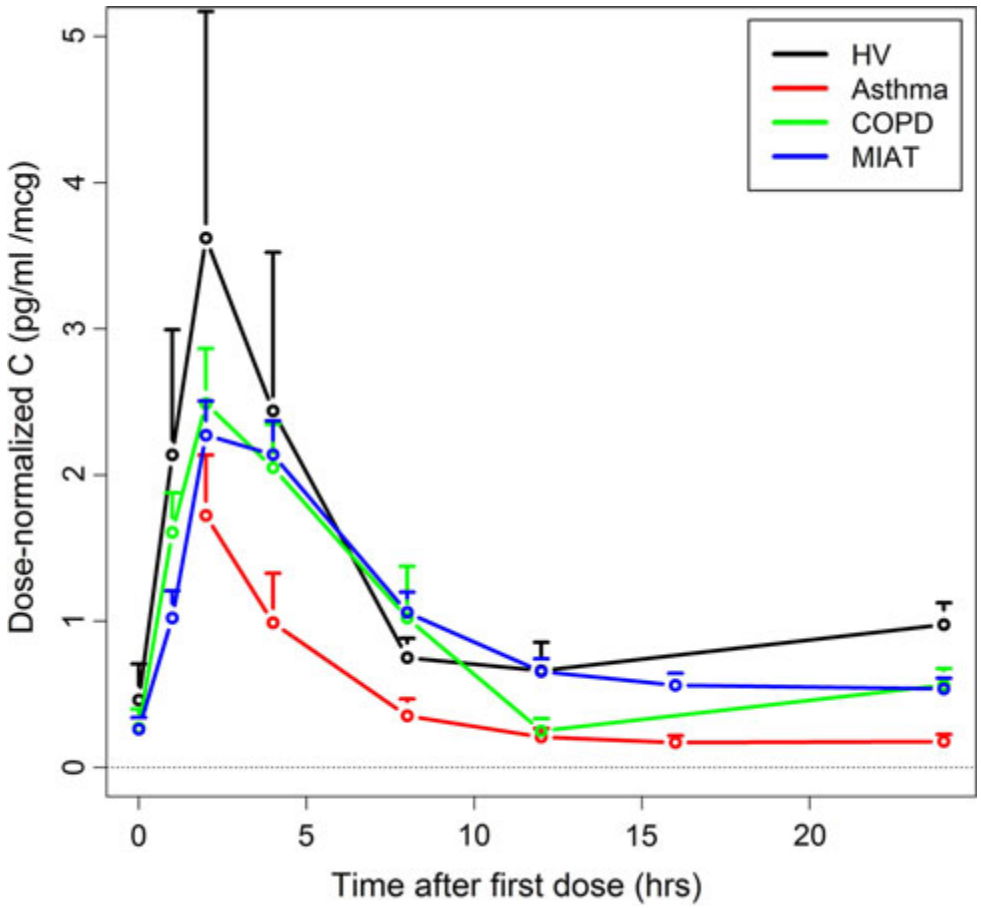

Figure 1.5 Dose-normalized PF-00610355 concentration (C)-time profile following the first inhalation dose in healthy volunteers (HV), patients with asthma and COPD (chronic obstructive pulmonary disease). Reprinted with permission from Diderichsen et al. *Clin Pharmacokinet* 52, 443-452 (2013).

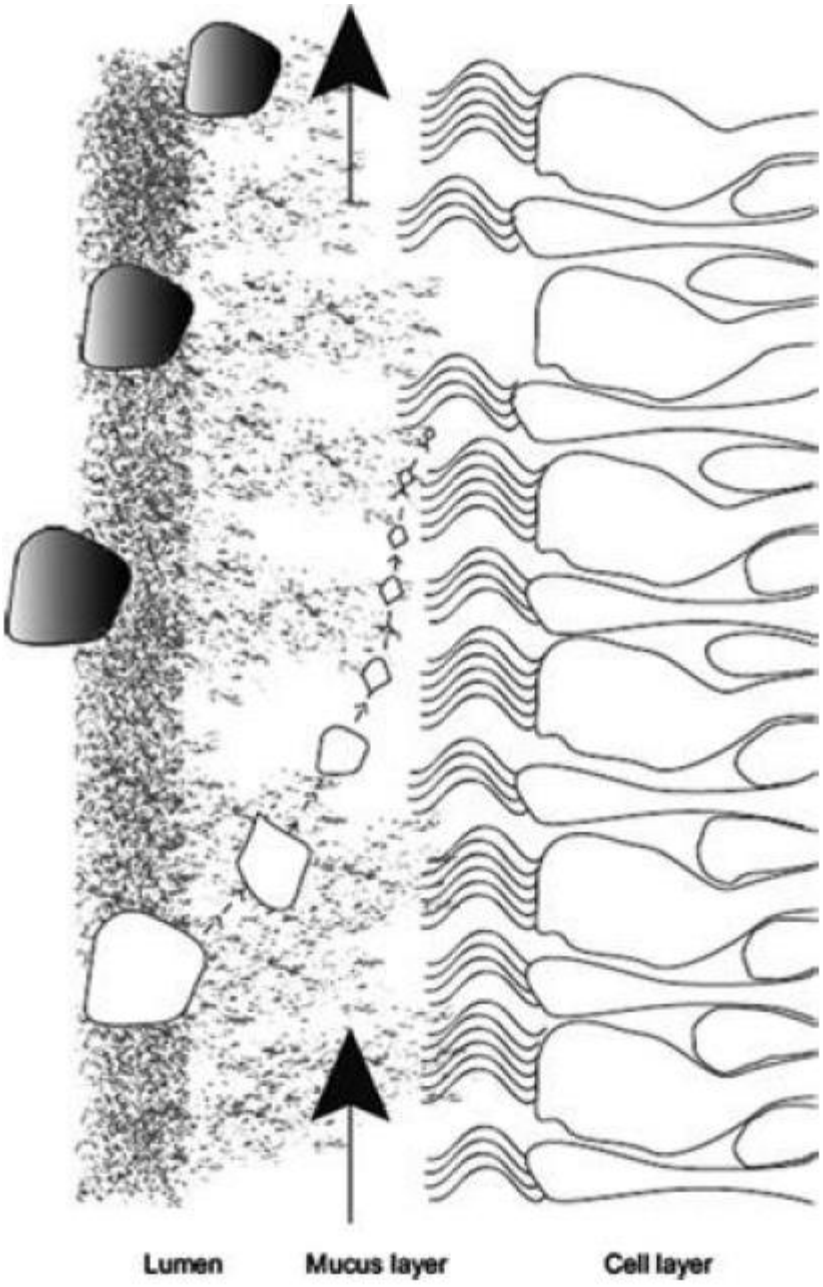

Figure 1.6 Aerosol particles subject to dissolution, absorption and mucociliary clearance spontaneously. Reprinted with permission from Edsbacker et al. *Pulmonary Pharmacology & Therapeutics* 21, 247–258 (2008).

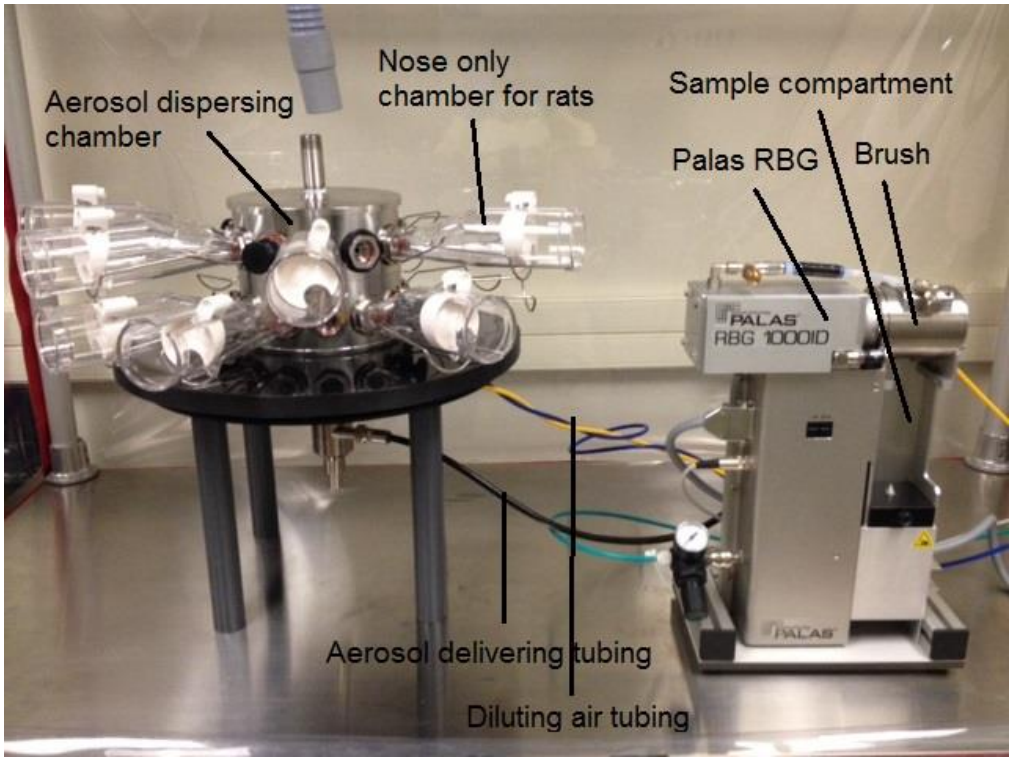

Figure 2.1 Illustration of RBG and nose-only dosing apparatus for rats.

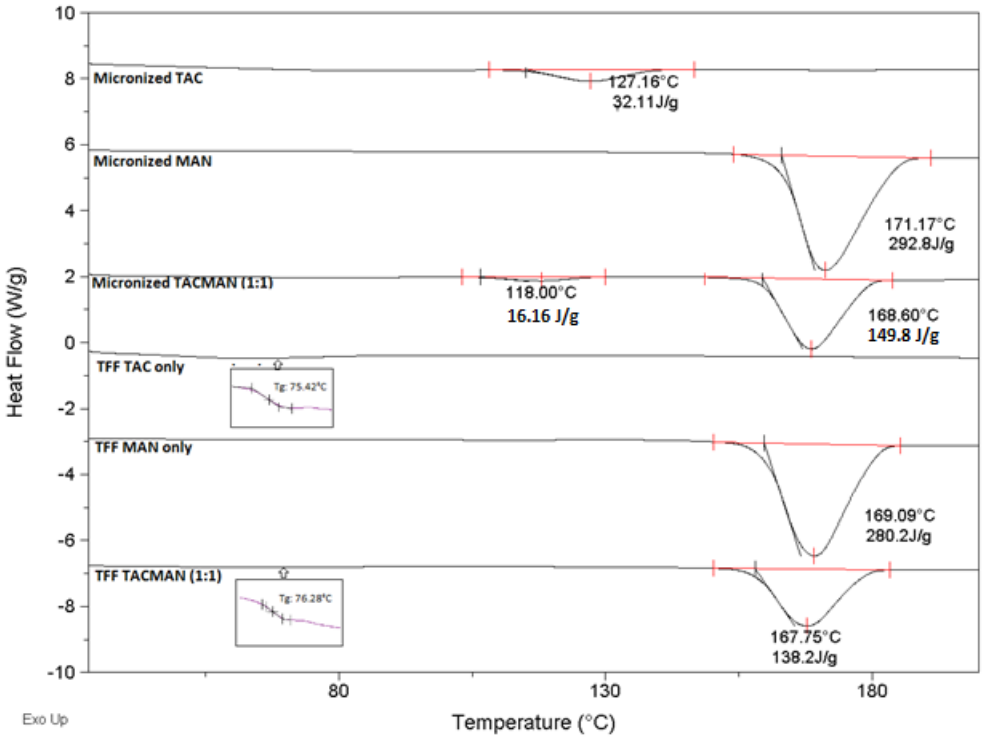

Figure 2.2 DSC profiles of (from top to bottom) micronized bulk TAC, micronized bulk MAN, physical mixture of micronized TAC and MAN (1:1), TFF TAC only, TFF MAN only and TFF TACMAN (1:1).

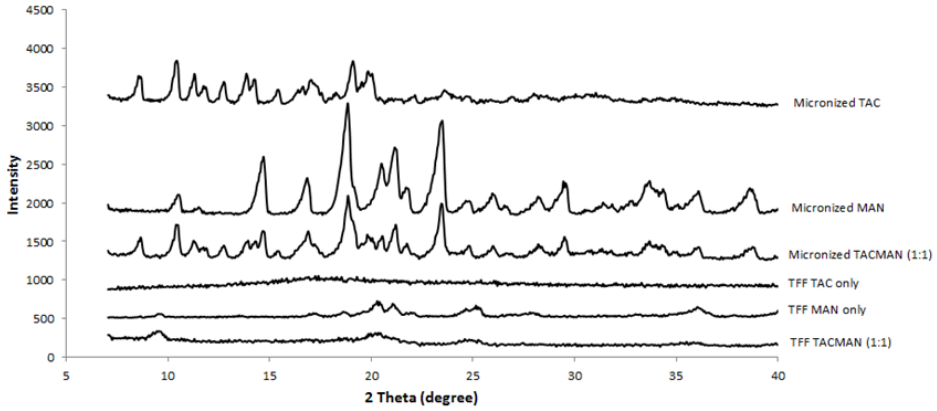

Figure 2.3 X-ray powder diffraction patterns (from the top to bottom): micronized bulk TAC, micronized bulk MAN, physical mixture of micronized TAC and MAN (1:1), TFF TAC only, TFF MAN only and TFF TACMAN (1:1).

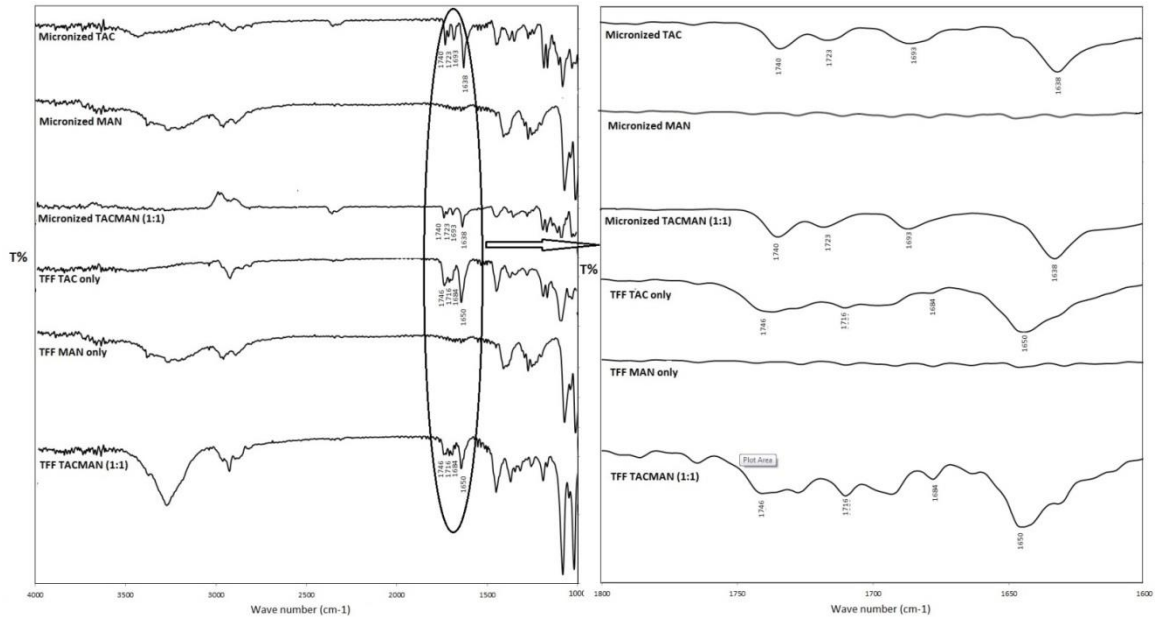

Figure 2.4 Attenuated total reflectance Fourier transform infrared spectroscopy of (from the top to bottom): micronized bulk TAC, micronized bulk MAN, physical mixture of micronized TAC and MAN (1:1), TFF TAC only, TFF MAN only and TFF TACMAN (1:1).

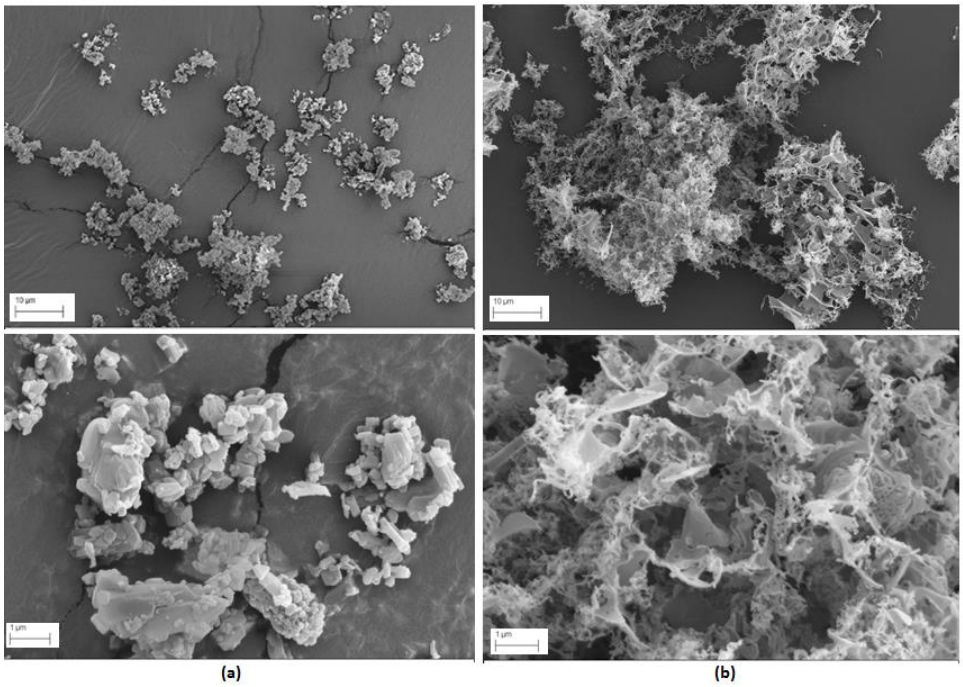

Figure 2.5 SEM images of micronized TACMAN (a) and TFF TACMAN (b) under different magnification: top (2.70KX, scale bar=10 µm) and bottom (25.00KX, scale bar=1 µm).

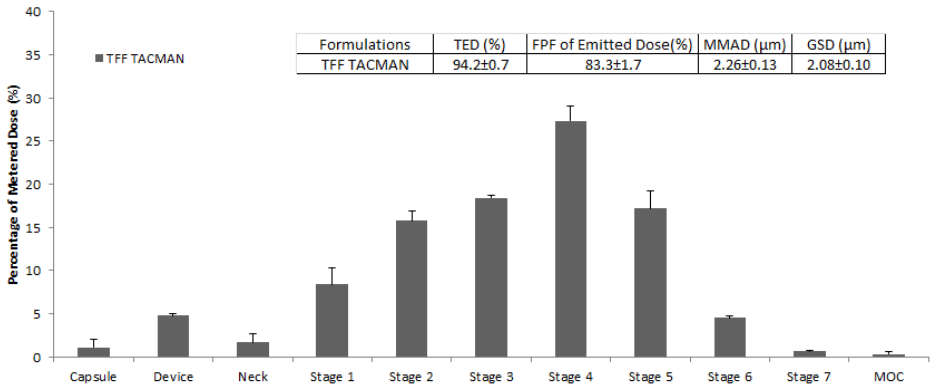

Figure 2.6 Aerodynamic diameter distribution of TFF TACMAN when emitted from a Miat® monodose inhaler at a flow rate of 90 L/min.

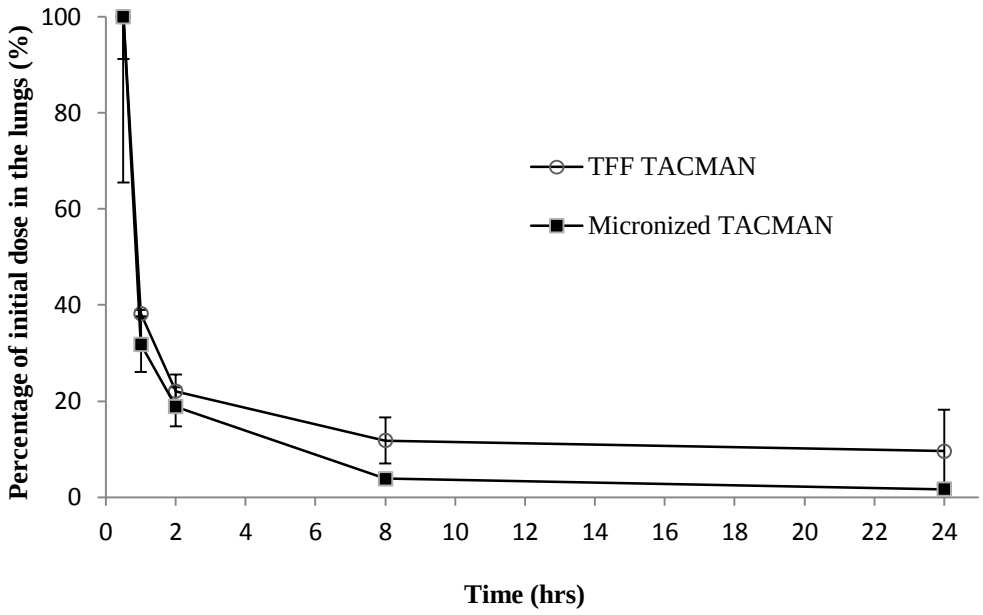

Figure 2.7 TAC concentration in the rat lungs plotted as percentage of initial dose following exposure to dry powder aerosols generated from a rotating brush generator. TFF TACMAN (open cycle) and Micronized TACMAN (solid square).

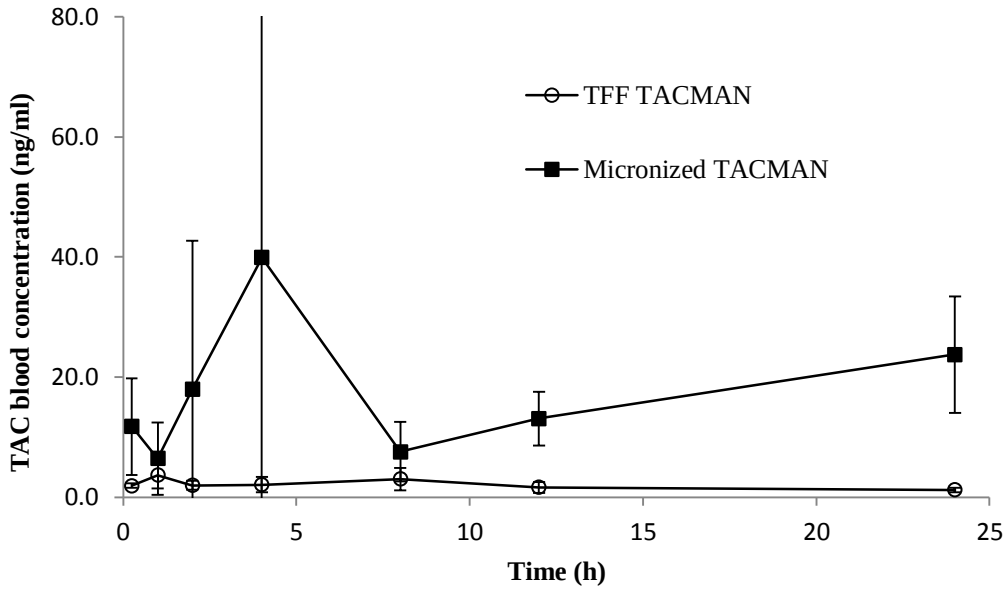

Figure 2.8 TAC concentration in whole blood following single dose exposure to dry powder aerosols generated from a rotating brush generator. TFF TACMAN (open cycle) and Micronized TACMAN (solid square).

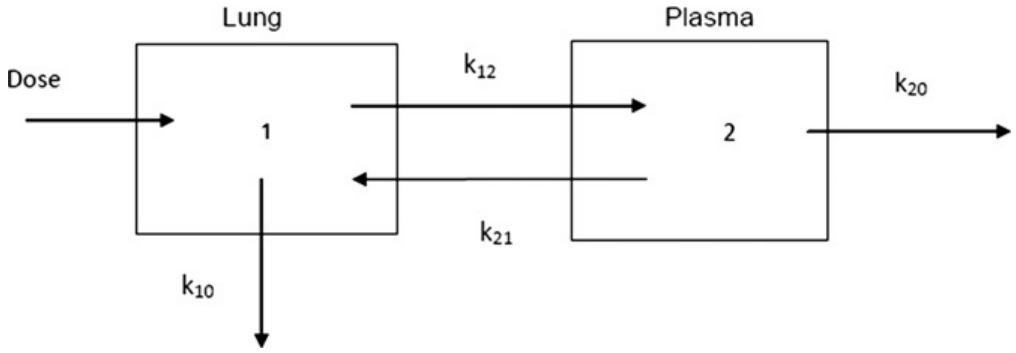

Figure 2.9 Two compartment model for determination of lung pharmacokinetics parameters.

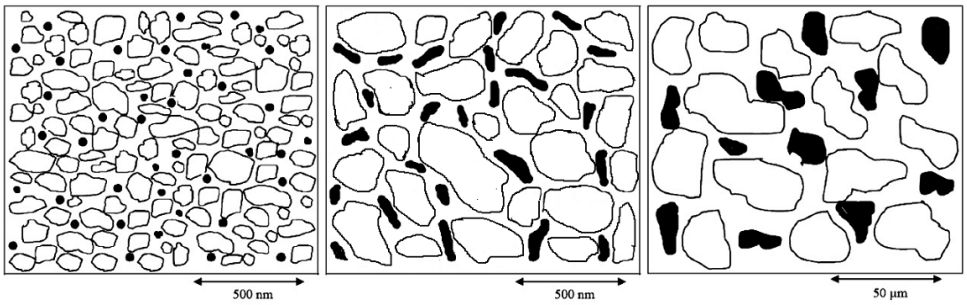

Figure 3.1 Nucleation and growth of particles between frozen ice chips with high cooling rate in thin film freezing (TFF) formulation frozen at -140°C (left); with medium cooling rate in TFF formulation frozen at -50°C (middle); with low cooling rate in shelf lyophilized formulation (right). Amorphous ice particles are represented as white domains and solute precipitate as solid dots or gray regions. Adapted with permission from Engstrom et al. *Eur J Pharm Biopharm* 65 (2007) 149–162.

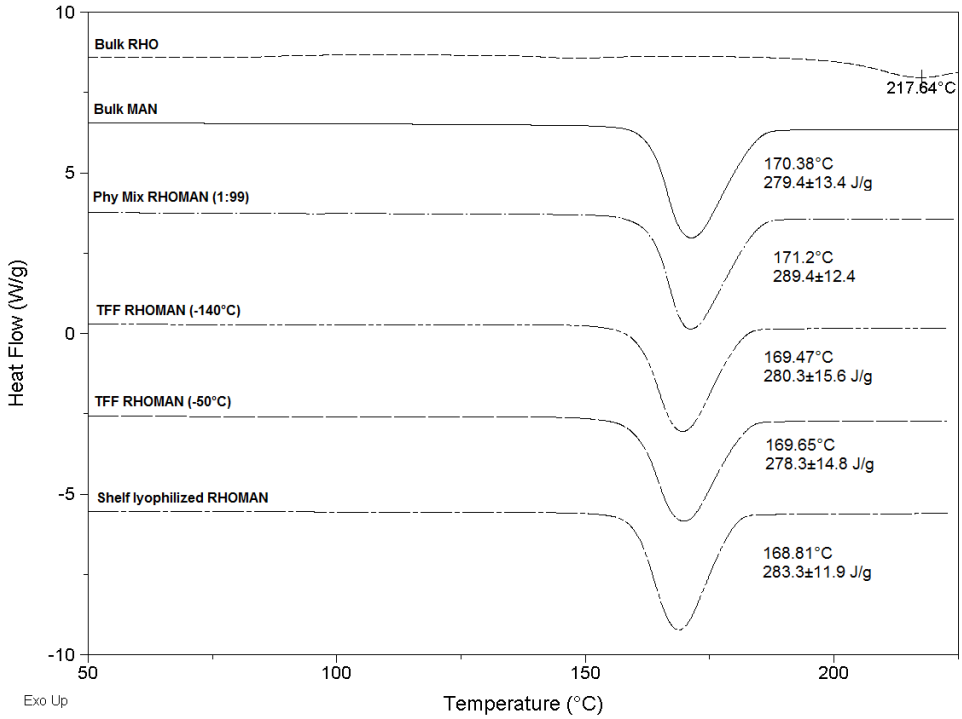

Figure 3.2 DSC of bulk Rhodamine B, bulk mannitol, Physical Mixture of RHOMAN (1:99), TFF RHOMAN (-140°C), TFF RHOMAN (-50°C) and shelf lyophilized RHOMAN.

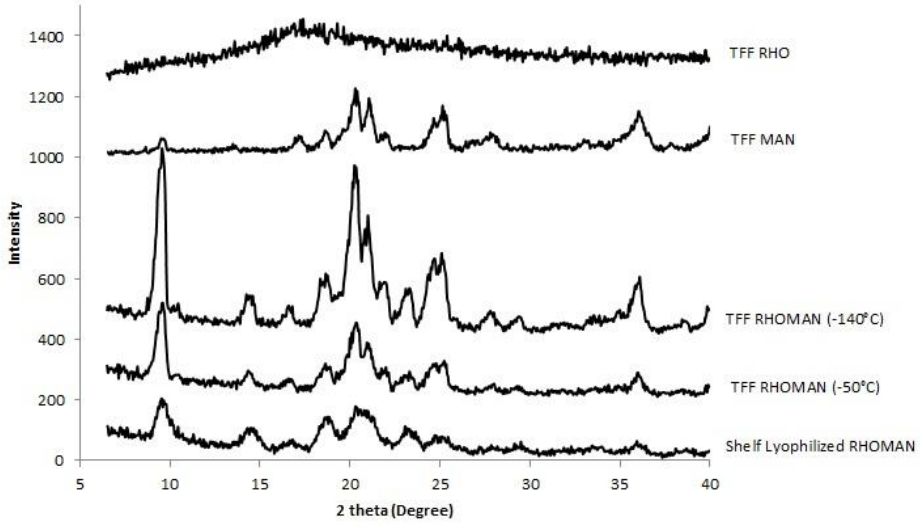

Figure 3.3 X-Ray Diffraction of TFF RHO, TFF MAN, TFF RHOMAN (-140°C), TFF RHOMAN (-50°C) and shelf lyophilized RHOMAN.

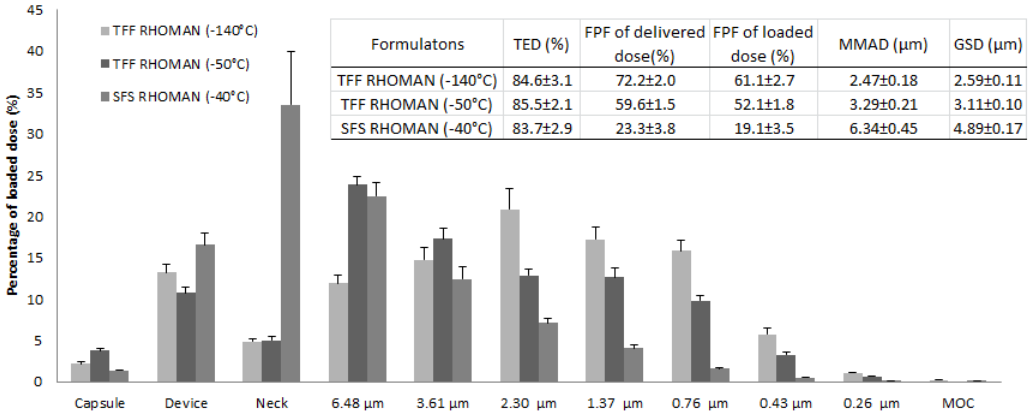

Formulatons	TED (%)	FPF of delivered dose(%)	FPF of loaded dose (%)	MMAD (µm)	GSD (µm)
TFF RHOMAN (-140°C)	84.6±3.1	72.2±2.0	61.1±2.7	2.47±0.18	2.59±0.11
TFF RHOMAN (-50°C)	85.5±2.1	59.6±1.5	52.1±1.8	3.29±0.21	3.11±0.10
SFS RHOMAN (-40°C)	83.7±2.9	23.3±3.8	19.1±3.5	6.34±0.45	4.89±0.17

Figure 3.4 Aerodynamic properties of TFF RHOMAN (-140°C), TFF RHOMAN (-50°C) and shelf lyophilized RHOMAN determined by Next Generation Impactor (NGI) equipped with Miat Monodose Inhaler at flow rate of 90 L/min.

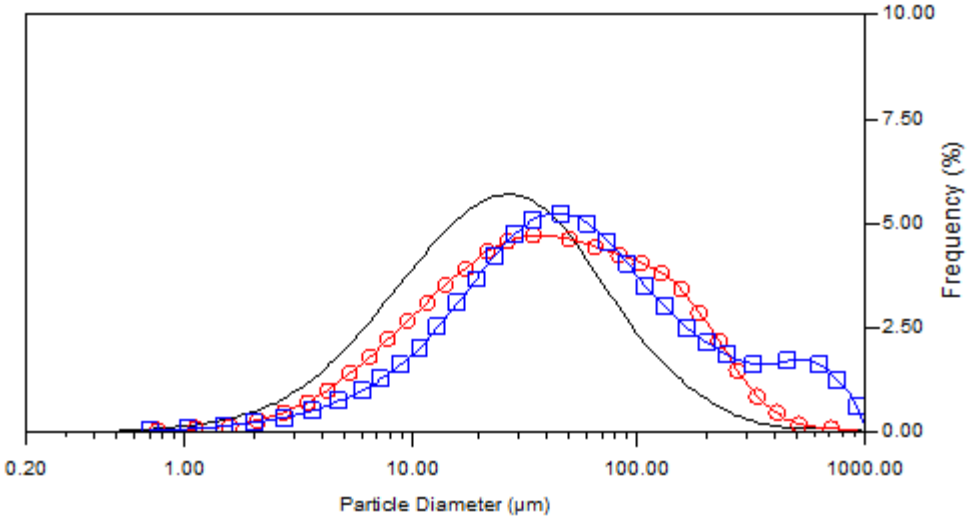

Lables	Formulations	D10 (µm)	D50 (µm)	D90 (µm)
Black line	TFF RHOMAN (-140°C)	5.74	33.46	93.9
Red cycle	TFF RHOMAN (-50°C)	9.32	39.84	184.26
Blue square	Shelf lyophilized RHOMAN	10.74	49.85	339.64

Figure 3.5 Geometric particle size distribution of aerosolized TFF RHOMAN (-140°C), TFF RHOMAN (-50°C) and shelf lyophilized RHOMAN powders determined by Sparytac® equipped with Miat Monodose Inhaler at flow rate of 90 L/min.

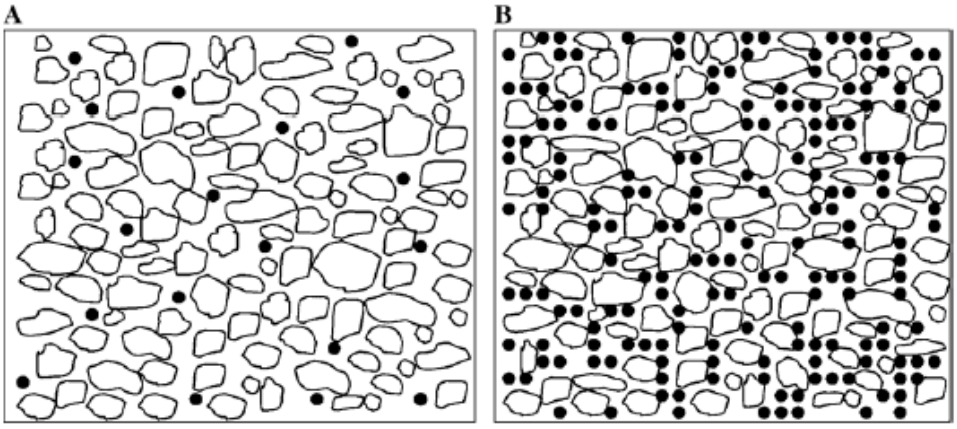

Figure 3.6 Nucleation and growth of particles between frozen ice chips with low solid concentration in TFF formulations (A); with high solid concentration in TFF formulations. Amorphous ice particles are represented as white domains and solute precipitate as solid dots or gray regions. Reprinted with permission from Engstrom et al. *Eur J Pharm Biopharm* 65 (2007) 149–162.

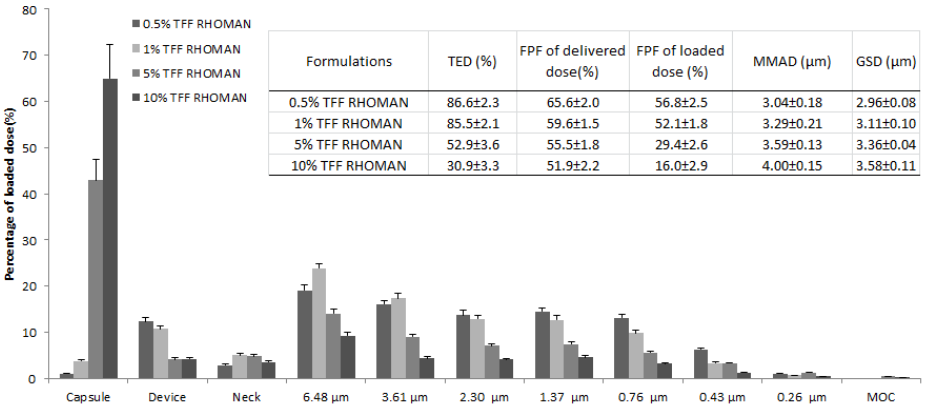

Formulations	TED (%)	FPF of delivered dose(%)	FPF of loaded dose (%)	MMAD (µm)	GSD (µm)
0.5% TFF RHOMAN	86.6±2.3	65.6±2.0	56.8±2.5	3.04±0.18	2.96±0.08
1% TFF RHOMAN	85.5±2.1	59.6±1.5	52.1±1.8	3.29±0.21	3.11±0.10
5% TFF RHOMAN	52.9±3.6	55.5±1.8	29.4±2.6	3.59±0.13	3.36±0.04
10% TFF RHOMAN	30.9±3.3	51.9±2.2	16.0±2.9	4.00±0.15	3.58±0.11

Figure 3.7 Aerodynamic properties of TFF RHOMAN prepared at different solid concentrations (0.5%, 1%, 5% and 10%) determined by Next Generation Impactor (NGI) equipped with Miat Monodose Inhaler at flow rate of 90 L/min.

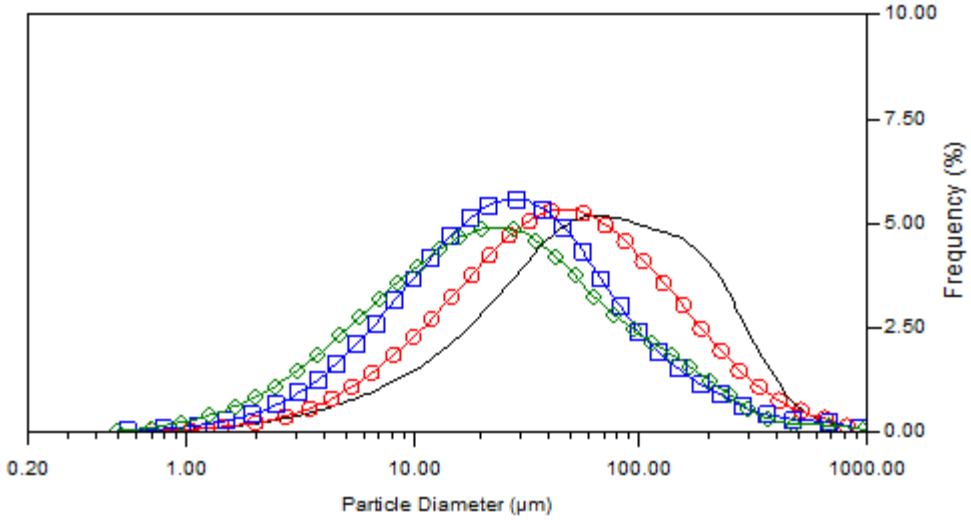

Lables	Formulations	D10 (µm)	D50 (µm)	D90 (µm)
Black line	0.5% TFF RHOMAN	12.02	59.82	240.42
Red cycle	1% TFF RHOMAN	9.32	40	184.26
Blue square	5% TFF RHOMAN	6	28.11	112.49
Green diamond	10% TFF RHOMAN	4.31	22.18	117.25

Figure 3.8 Geometric particle size distribution of aerosolized TFF powders prepared at different solid concentrations (0.5%, 1%, 5% and 10%) determined by Sparytac® equipped with Miat Monodose Inhaler at flow rate of 90 L/min.

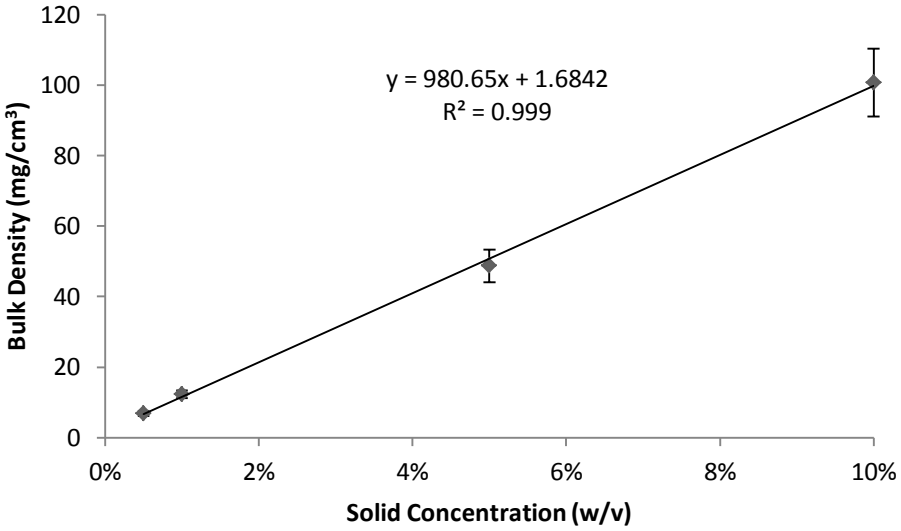

Figure 3.9 Linear regression of the resulting bulk density of TFF powders to initial solid concentrations.

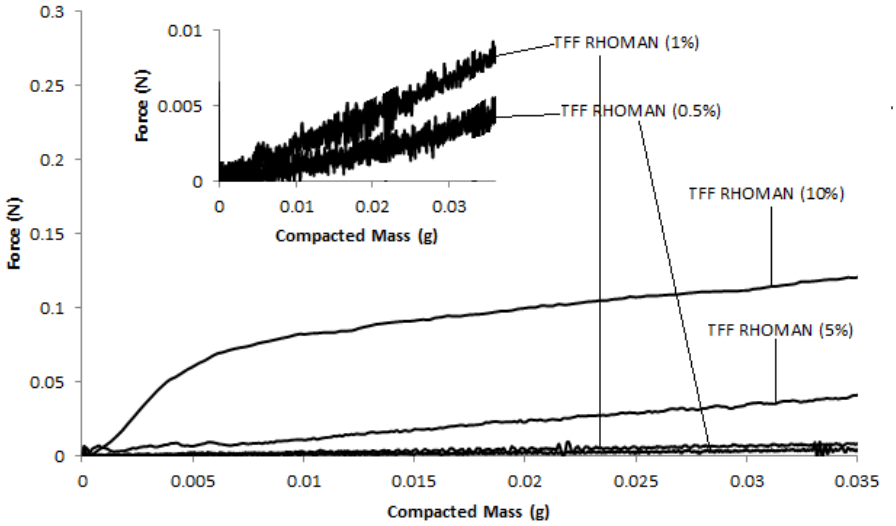

Figure 3.10 Mechanical testing of TFF RHOMAN prepared at different solid concentrations (0.5%, 1%, 5% and 10%) determined by Texture Analyzer.

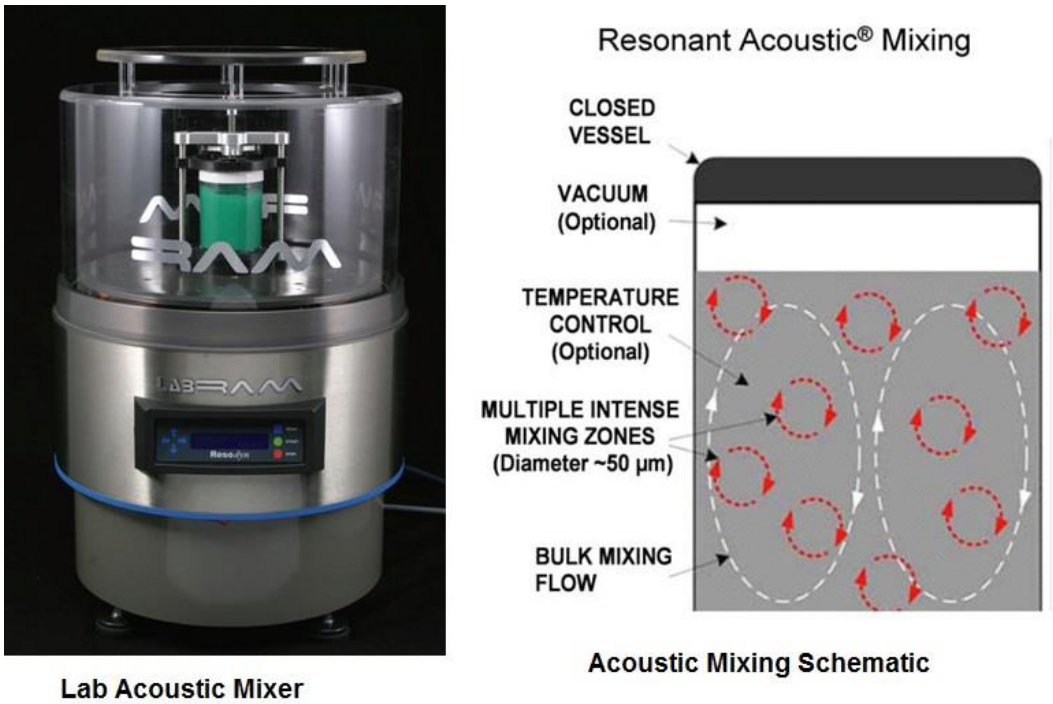

Figure B.1 Acoustic mixer and mixing mechanisms.

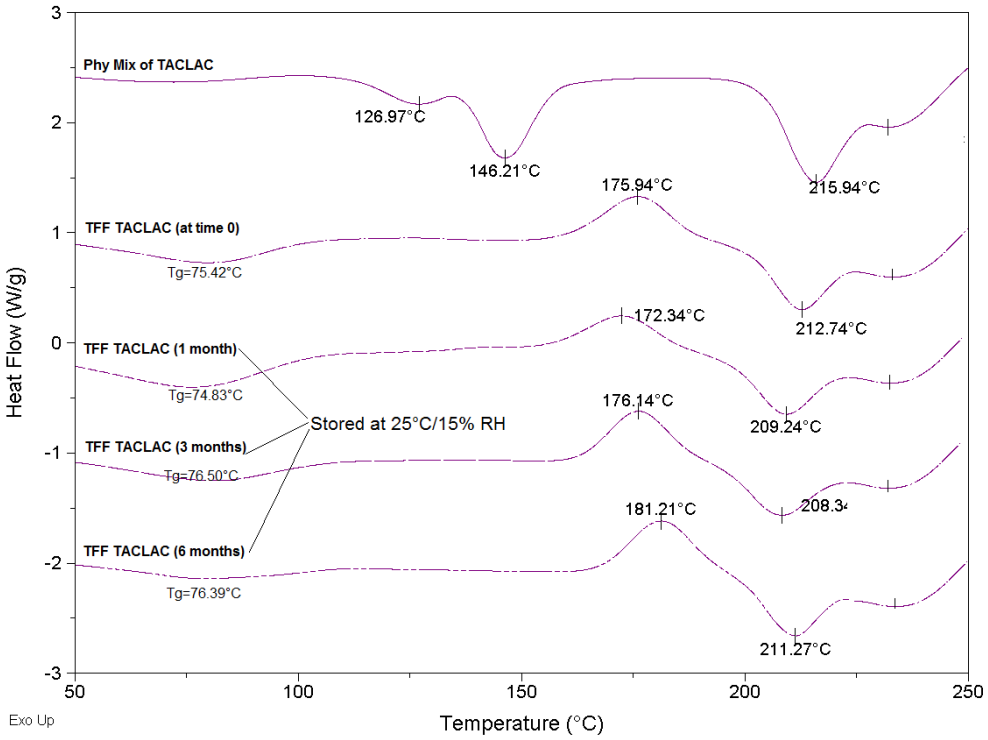

Figure D.1 DSC of TFF TACLAC stored at 25°C/15%RH at time 0, 1 month, 3 months and 6 months.

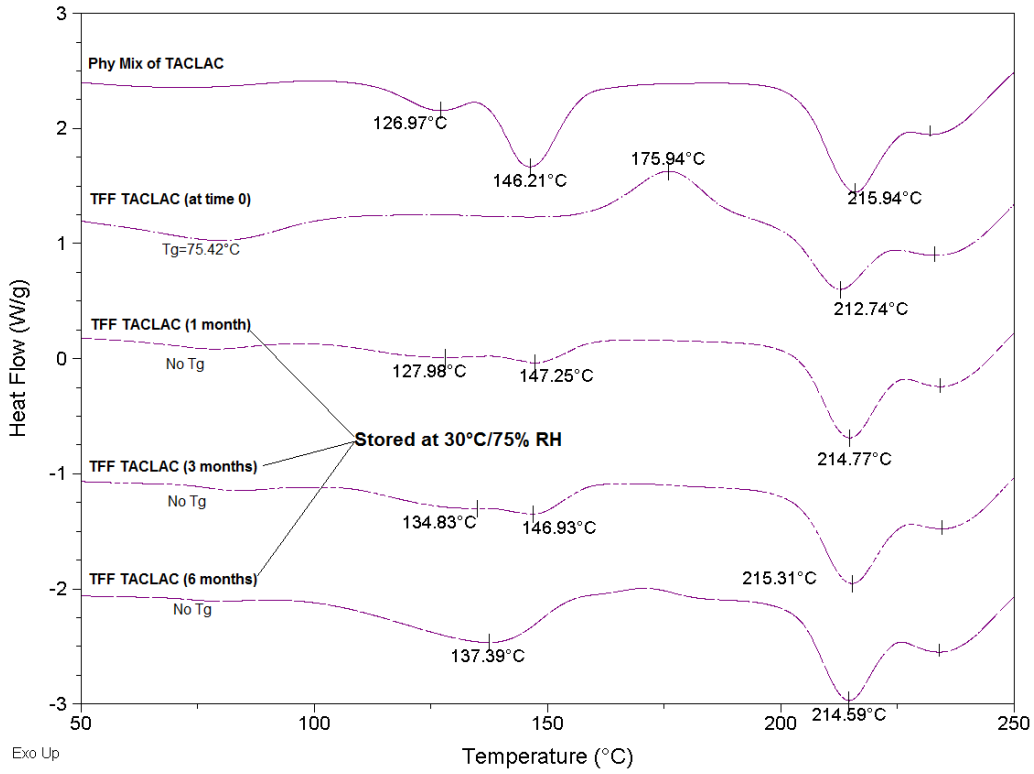

Figure D.2 DSC of TFF TACLAC stored at 30°C/75%RH at time 0, 1 month, 3 months and 6 months.

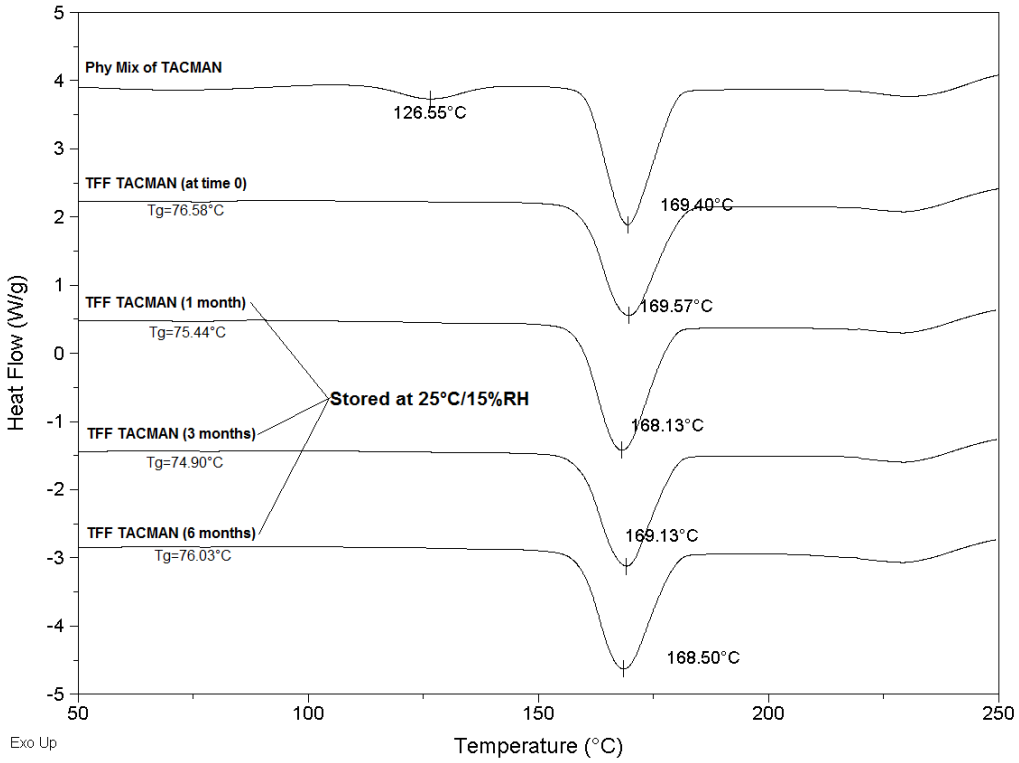

Figure D.3 DSC of TFF TACMAN stored at 25°C/15%RH at time 0, 1 month, 3 months and 6 months.

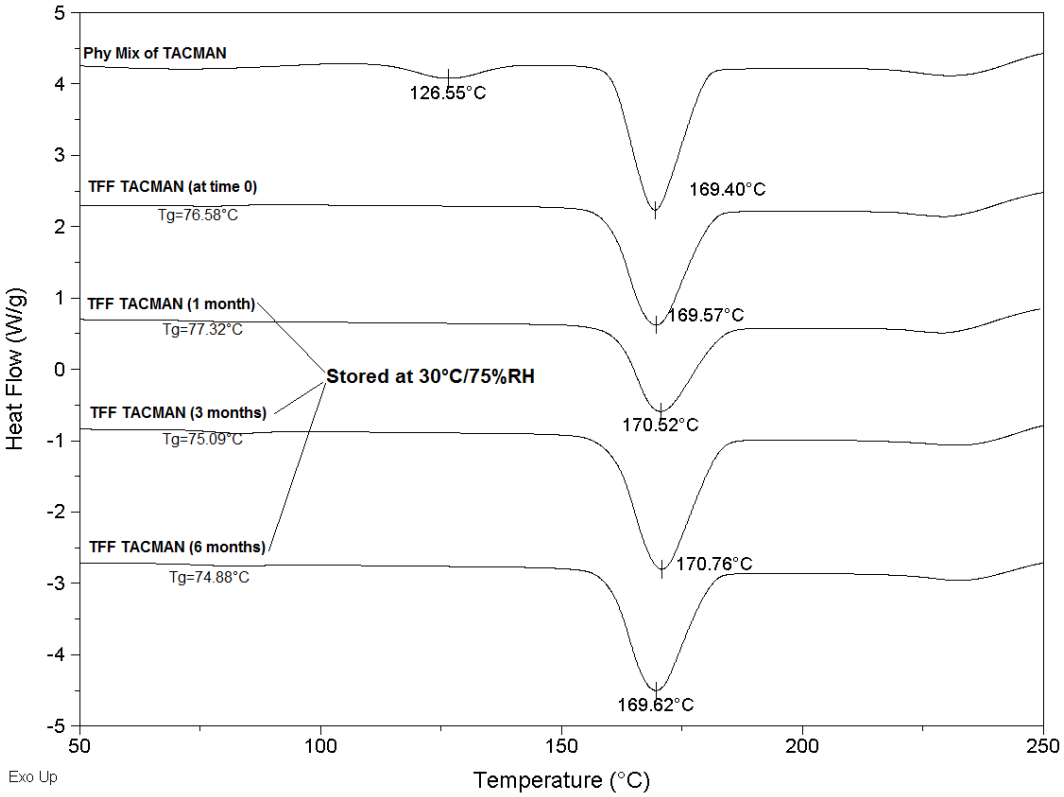

Figure D.4 DSC of TFF TACLAC stored at 30°C/75%RH at time 0, 1 month, 3 months and 6 months.

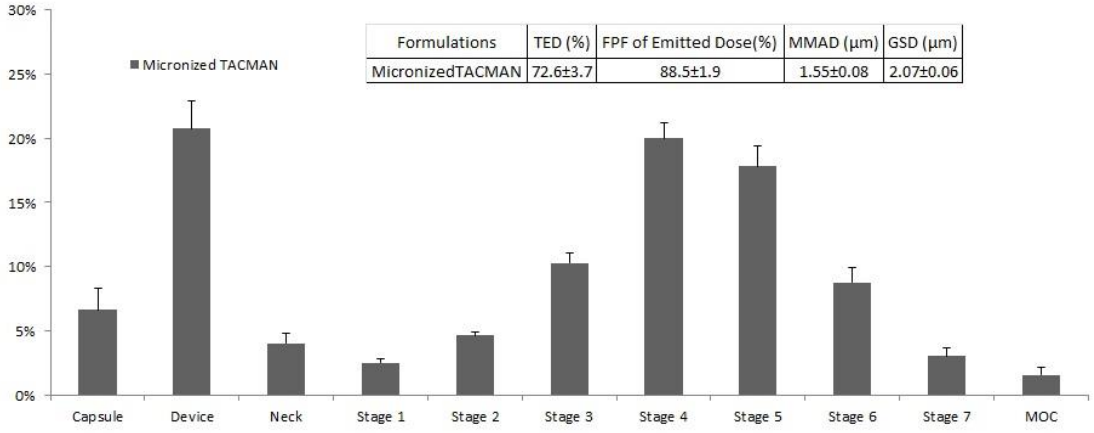

Formulations	TED (%)	FPF of Emitted Dose(%)	MMAD (μm)	GSD (μm)
MicronizedTACMAN	72.6±3.7	88.5±1.9	1.55±0.08	2.07±0.06

Figure F. 1 Aerodynamic properties of micronized TACMAN when emitted from a Miat® monodose inhaler at a flow rate of 90 L/min.

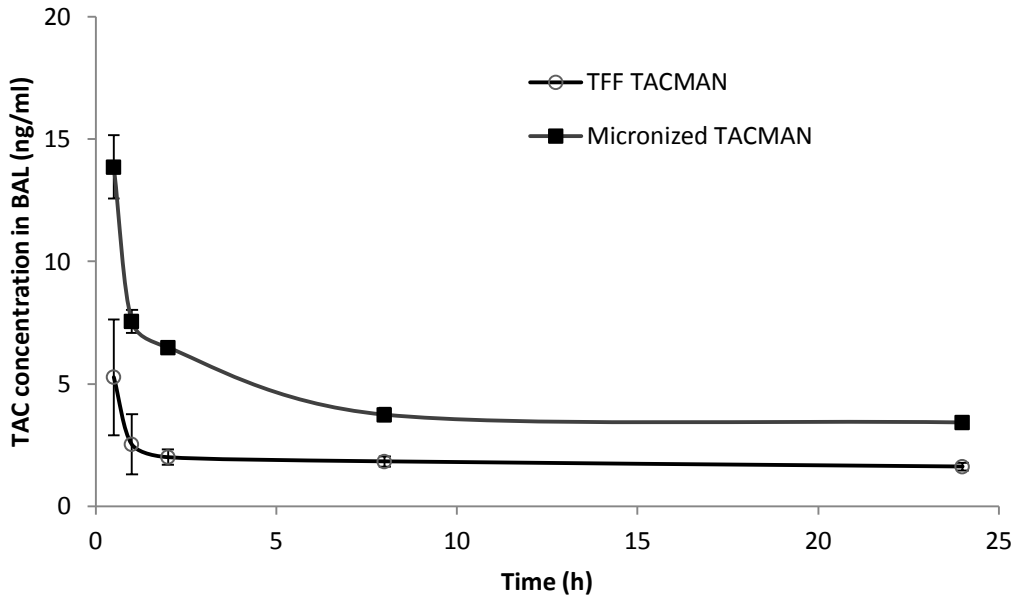

Figure G.1 TAC concentration in the BAL fluid following single dose exposure to dry powder aerosols generated from a rotating brush generator. TFF TACMAN (open cycle) and Micronized TACMAN (solid square).

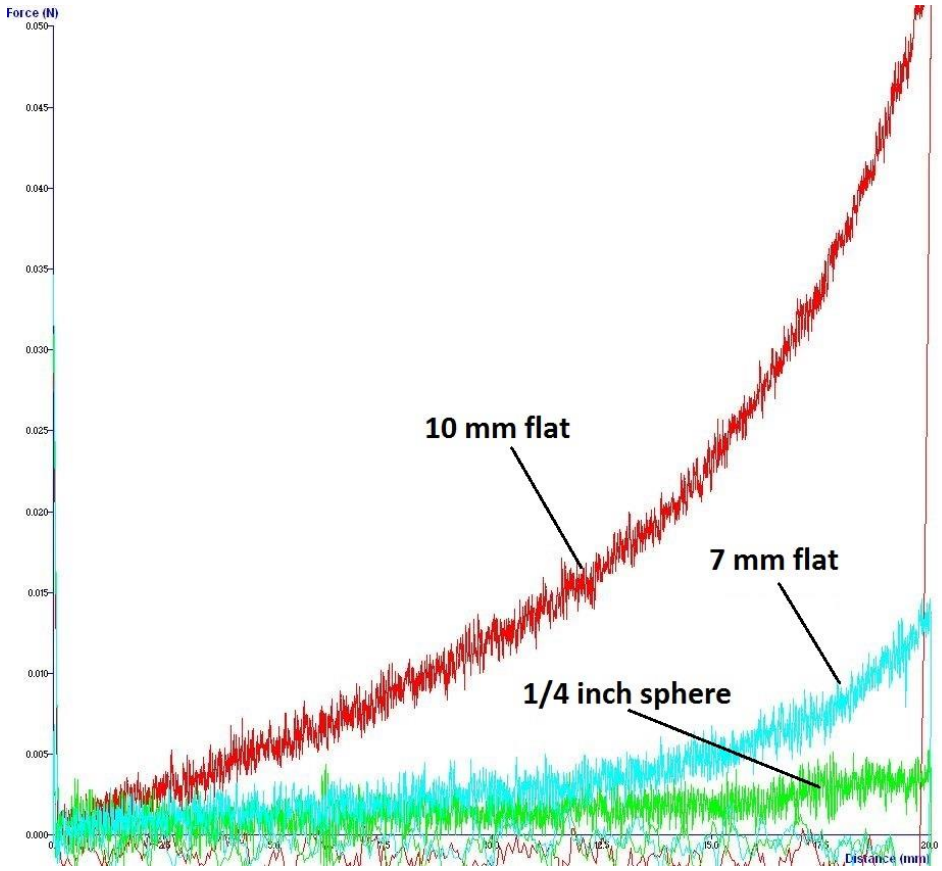

Figure H. 1 Immersion-force-curve of TFF RHOMAN (1%) determined by texture analyzer using different testing probes.

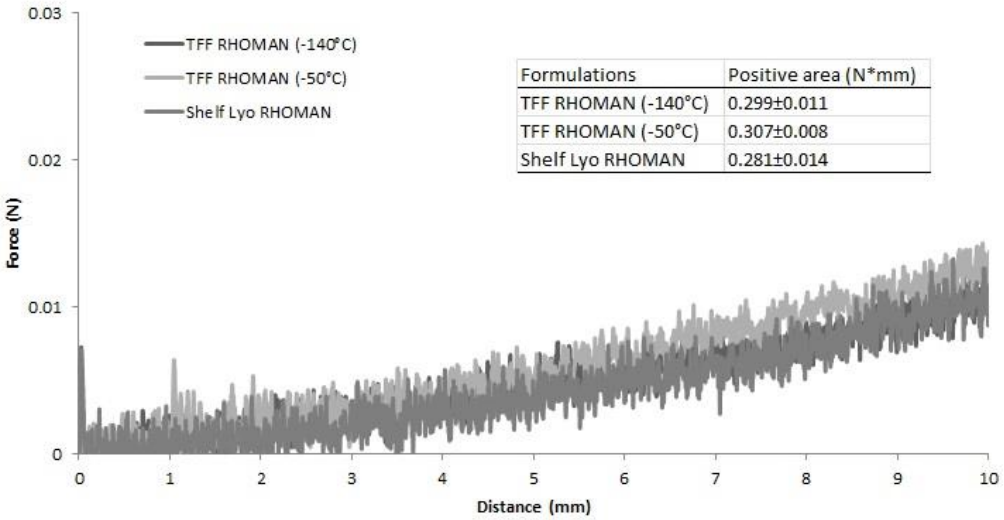

Figure I.1 Mechanical testing of TFF RHOMAN (-140°C), TFF RHOMAN (-50°C) and slow shelf frozen RHOMAN powders determined by Texture Analyzer.

Appendices

Appendix A: Prior Arts for Inhaled Tacrolimus

A.1 Purposes

The objective of this inquiry is to determine the journal history of the active pharmaceutical ingredient, Tacrolimus (TAC), and its potential use in pulmonary delivery.

A.2 Methods

Journal searches were conducted using the online databases Web of Science (Thomson Reuters Web of Knowledge) available from the University of Texas Libraries. Keyword used in the search was “inhaled tacrolimus”, references were chosen based on relevance.

A.3 Results

Table A.1 summarized the journal history of inhaled TAC. The formulations and delivery systems, animal models, results, references are demonstrated in the table.

Appendix B: Optimization of Fine Particle Fraction (FPF) of TFF TACMAN (1:1) by Acoustic Mixing

B.1 Purposes

The purpose of this study was to optimize the FPF of TFF TACMAN using acoustic mixing to uniformly break down the "large flocs" of TFF processed brittle matrix powders prior to cascade impaction testing, which can benefit for aerodynamic properties and future handling and packaging of TFF powders.

B.2 Methods

TFF TACMAN (1:1) was prepared as described in Section 2.3.2. The lab acoustic mixer and mixing schematic were illustrated in Fig.B.1. The two controllable parameters on the acoustic mixer are the mixing intensity and mixing time. TFF TACMAN was mixed for 60s at 10% intensity, 60s at 30% intensity, 60s at 50% intensity and 300s at 50% intensity, respectively. A Next Generation Pharmaceutical Impactor (NGI) was used to evaluate the aerodynamic performance of TFF TACMAN after different mixing time and intensity. Handihaler® (loaded with size 3 HPMC capsules containing approximately 3 mg of formulation was secured to the induction port by a silicone adapter. Aerosols were generated over 4s at a flow rate of 51 L/min. Prior to actuation, surfaces of collection stages were coated with 1% polysorbate 80 in enthanol (v/v) and allowed to completely dry. The cut-off size for each stages were calculated to be 8.80, 4.85, 3.06, 1.79, 1.02, 0.61 and 0.38 μm from stages 1 to 7 and micro-orifice collector (MOC), respectively. Following actuation, the deposited powders in the capsule, inhaler, adaptor, induction

port, stage 1 to 7 and MOC was collected by rinsing with 10 mL of methanol:water (90:10 v/v), which is then quantified by the TAC HPLC method described in Section 2.3.9. Total emitted dose (TED), mass median aerodynamic diameter (MMAD), geometric standard deviation (GSD) and fine particle fraction (FPF) of delivered dose were calculated as described in Section 2.3.9.

B.3 Results

Aerodynamic parameters of TFF TACMAN after mixing at different mixing time and intensity were shown in Table B.1. A decreasing trend of FPF was observed when increased the mixing intensity and prolonged the mixing time, correlated with an increasing MMAD. The reason can be attributed to the mixing principal illustrated in Fig.B.1, which shows a vessel being subjected to a low frequency acoustic field in the axial direction resulting in second order bulk motion of the fluid, known as acoustic streaming, which in turn causes a multitude of micro-mixing cells throughout the vessel. The characteristic mixing lengths for the RAM technology, operating at 60 Hz, is nominally 50 microns. The mixing phenomena in solid-solid systems do not rely upon acoustic streaming, but upon particle collisions. For the solid-solid mixing, particles in the container are excited by collisions with the vessel base and collisions with other particles in the container that can result in harmonic vibrations of the vessel with the granular material. The particle-particle or particle-wall collisions caused the TFF processed matrix particles to collapse instead of breakage. Accordingly impacted the low-

density, porous and brittle characteristics of the TFF process powders, further hindering the aerosolization process of the TFF brittle matrix powders.

Appendix C: Determination of Patient and Device Dependence of TFF TACMAN (1:1)

C.1 Purposes

The objective of this study is to determine the patients and devices dependence of TFF processed brittle matrix powders based on their aerodynamic performance.

C.2 Methods

TFF TACMAN (1:1) was prepared as described in Section 2.3.2. To evaluate the device dependence, three different dry powder inhalers (DPIs) were selected for aerosol testing, Handihaler®, Aerolizer® and Miat® monodose inhaler. The flow rate (L/min) that can achieve a 4 kPa pressure drop across the device was pre-determined for each DPI (Table C.1). Aerosol testing was carried out using a Next Generation Pharmaceutical Impactor (NGI) at the pre-determined flow rate for each DPI. A 4L inhalation volume was fixed to calculate the inhalation time for different flow rates. For patient dependence investigation, three different flow rates were chosen for each DPI, which represented low, medium and high flow rate that a patient can generate clinically (Table C.2). Size 3 HPMC capsules containing approximately 3 mg of formulation was used for all tests. A more detailed NGI testing was described in Section 2.3.9 and all the aerodynamic parameters (MMAD, GSD, FPF and TED) were calculated as well.

C.3 Results

As shown in Table C.1, the flow rate used that can achieve 4 kPa pressure drop across Handihaler®, Aerolizer® and Miat® monodose inhaler were 51, 90 and 90 L/min, respectively. Aerolizer® and Miat® monodose inhaler have similar design, thereby their specific resistance are comparable, hence the same flow rate are required to achieve 4 kPa pressure drop across them. However, the specific resistance of Handihaler® is much higher than the other two DPIs; therefore a lower flow rate is needed to achieve the same pressure drop across it [1]. Identical aerodynamic parameters are observed for TFF TACMAN using Aerolizer® and Miat® monodose inhaler, because they have similar design, leading to similar particle de-agglomeration mechanisms upon actuation with the same shear and impaction forces. For Handihaler®, device design is different and the low flow rate might generate shear and impaction energy for particle de-agglomeration, leading to a lower FPF, larger MMAD and GSD compared to the other two DPIs. There's no significant difference in term of TED for all the three DPIs that have been tested, probably because the flow rate used in this study was able to shear the TFF TACMAN particles apart and form respirable low-density particles that are small enough to exit from the punctured holes on the capsule and enter into the impactor. The flow rates chosen to represent low, medium and high for Handihaler® were 20, 30 and 45 L/min; for Aerolizer® and Miat® monodose inhaler were the same, 60, 90 and 120 L/min [2-4]. For all the three DPIs that have been tested, there was a significant increasing trend in term of FPF of TFF TACMAN when the flow rate was increased, correlated with a

decreasing trend of MMAD (Table C.2). No significant difference was observed in term of TED for all the three DPIs and no matter what flow rate was used (around 95%), indicating that even with the very low energy input from the device, the brittle nature of TFF processed powders make it possible to emit more than 90% of the TFF powders. In summary, the aerodynamic performance of TFF processed powders is dependent of the selected DPI device and patients' inspiratory flow rate.

C.4 References

[1] S.L. Lee, W.P. Adams, B.V. Li, D.P. Conner, B.A. Chowdhury, L.X. Yu, In vitro considerations to support bioequivalence of locally acting drugs in dry powder inhalers for lung diseases, AAPS J, 11 (2009) 414-423.

[2] SPIRIVA® HandiHaler® (tiotropium bromide inhalation powder), Academy of Managed Care Pharmacy (AMCP), Formulary Dossier.

[3] D.J. Ball, P.H. Hirst, S.P. Newman, B. Sonet, B. Streel, F. Vanderbist, Deposition and pharmacokinetics of budesonide from the Miat Monodose inhaler, a simple dry powder device, Int J Pharm, 245 (2002) 123-132.

[4] K.G. Nielsen, M. Skov, B. Klug, M. Ifversen, H. Bisgaard, Flow-dependent effect of formoterol dry-powder inhaled from the Aerolizer, Eur Respir J, 10 (1997) 2105-2109.

Appendix D: Physical Stability of TFF processed powders

D.1 Purposes

The purpose of this study was to assess the physical stability of TFF TACLAC (1:1) and TFF TACMAN (1:1) over time storage at room temperature in a dessicator and accelerated temperature and relative humidity (RH).

D.2 Methods

The TFF processed powders, TFF TACLAC (1:1) and TFF TACMAN (1:1), were stored in a vacuum desiccator (25°C /15%RH) at room temperature and in a humidity chamber placed in a heated oven (30°C/75% RH), respectively. Crystallinity was evaluated by DSC (30 to 250 °C, ramp rate: 10 °C/min, modulation temperature amplitude: 1°C/60 s, nitrogen gas purge flow rate: 40 mL/min) at time 0, 1 month, 3 months and 6 months.

D.3 Results

For physical mixture of TACLAC (Fig.D.1 and D.2), TAC melts around 127°C; the endothermic peak around 146°C is the crystal water in the lactose molecule lattice and the melting peak of LAC is around 210°C. TFF TACLAC exhibited a Tg of TAC around 75 °C and recrystallization peak and the melting peak corresponding to LAC, no melting of TAC was detected indicating that both TAC and LAC are amorphous. When stored at room temperature and less than 15% RH in a desicctor, no significant change in terms of thermal properties was observed (Fig.D.1), indicating that TAC and LAC are still

amorphous up to 6 months storage at 25°C /15%RH. However, when TFF TACLAC was stored at accelerated condition (30°C/75% RH), TAC and LAC started to crystallize around 127°C and 210°C, respectively. Moisture was absorbed into the crystal lattice of LAC, showing an endothermic peak around 147°C. After 6 months storage, the melting peak of TAC and this crystal water peak combined to a broader peak at 137°C (Fig.D.2). No recrystallization peaks and no glass transition temperature were detected upon storage, indicating that TAC and LAC were no longer amorphous. For TACMAN (Fig.D.3), TAC and MAN melt at 127°C and 169°C, respectively. TFF TACMAN exhibited a Tg around 75°C, corresponding to TAC; MAN only displayed a melting peak, indicating that TAC is amorphous and MAN is crystalline in TFF TACMAN. Whether stored at 25°C /15%RH or 30°C/75% RH, no significant change was observed in the DSC profiles, meaning that TFF TACMAN was robust to moisture. To sum up, TFF TACMAN is physically more stable than TFF TACLAC.

Appendix E: Residual Solvent Analysis of TFF-processed Powders by Thermogravimetric Analysis (TGA)

E.1 Purposes

The objective of this study was to determine the amount of the residual solvent in the TFF processed powders stored at room temperature in a desiccator and at accelerated conditions.

E.2 Methods

Three TFF processed powders were subjected to TGA testing, TFF TAC only, TFF TACLAC and TFF TACMAN. They were prepared by using a co-solvent system containing acetonitrile (CAN) and water (60:40, v/v) and the detailed description can be found in Section 2.3.2. After prepared, TFF processed powders were stored for a week in a desiccator at room temperature (25°C, <15% RH) and in a humidity chamber placed in a heated oven (40°C, >90%RH). Then residual solvent content was determined using a Mettler-Toledo TGA/DSC 1. TFF-processed powders and their individual components were accurately weighed to 10-15 mg into 100 μL aluminum pans. The samples were ramped from 25 to 180°C at 10°C/minute then held at 180°C for 30 minutes. The difference between the final sample weight and the initial sample weight was used to calculate the percentage of residual solvent lost on drying.

E.3 Results

As shown in Table E.1, bulk TAC and bulk LAC were both monohydrate forms, therefore the theoretical water amount in them are 2.19% and 5%, respectively. The

measured water amount of bulk TAC and bulk LAC were 1.6% and 4.7%. It has been reported by Watts et al. that no detectable amount of ACN was measured in 50 mg of TFF processed powders [1]; therefore, we can assume that the measured residual solvent by TGA is mainly water. Because of the hydrophobic nature of TAC molecules, TFF TAC only did not absorb any moisture immediately after preparation, or stored after a week under two different conditions. For TFF TACLAC, immediately after preparation, the residual solvent was 1.89%; upon storage in a desiccator at room temperature (25°C, <15% RH), the residual solvent increased to 2.24%; when stored in accelerated condition (40°C, >90%RH), the residual solvent amount increased to 2.62%. Because of the amorphous nature of LAC in TFF TACLAC, it tends to absorb moisture upon storage. For TFF TACMAN, the residual solvent remained at 0% for a week no matter what storage conditions was used. In TFF TACMAN, TAC is hydrophobic and MAN is crystalline, which attributes to the robust characteristic to moisture.

E.4 References

[1] A.B. Watts, J.I. Peters, R.L. Talbert, K.P. O'Donnell, J.J. Coalson, R.O. Williams, 3rd, Preclinical evaluation of tacrolimus colloidal dispersion for inhalation, Eur J Pharm Biopharm, 77 (2011) 207-215.

Appendix F: Aerodynamic properties of micronized TACMAN (1:1)

F.1 Purposes

This appendix is intended to supplement the study conducted in Chapter 2 Section 2.3.9. The objective is to determine the aerodynamic properties of micronized TACMAN (1:1).

F.2 Methods

Micronized TACMAN (1:1) was prepared according to the description in Section 2.3.2. The aerodynamic properties of micronized TACMAN were investigated by a NGI similar to the set up for testing TFF TACMAN in Section 2.3.9. Miat monodose inhaler® loaded with size 3 HPMC capsules containing approximately 3 mg of micronized TACMAN was secured to the induction port by a silicone adapter. Aerosols were generated over 2.7 s at a flow rate of 90 L/min to achieve an inhalation volume of 4 L. Prior to actuation, surfaces of collection stages were coated with 1% polysorbate 80 in enthanol (v/v) and allowed to completely dry. Following actuation, the deposited powders in the capsule, inhaler, adaptor, induction port, stage 1 to 7 and MOC was collected by rinsing with 10 mL of methanol:water (90:10 v/v) and subjected to TAC quantification (Section 2.3.9). Aerodynamic parameters were calculated according to the description in Section 2.3.9 as well.

F.3 Results

As demonstrated in Fig.F.1, micronized TACMAN (1:1) exhibited excellent aerodynamic properties when actuated from a commercially available DPI. The FPF of emitted dose of micronized TACMAN reached up to 88.5%, the MMAD and GSD of micronized TACMAN were 1.55 and 2.07 μm, respectively and the TED was 72.6%.

Appendix G: Determination of Tacrolimus Concentrations in the Bronchoalveolar Lavage (BAL) Fluid

G.1 Purposes

This appendix is designated to supplement the study conducted in Section 2.3.10. The purpose is to measure the TAC concentrations in BAL fluid and assist in pharmacokinetic analysis.

G.2 Methods

Rats BAL fluid was collected as described in Section 2.3.10. Briefly, the trachea was exposed by blunt dissection of the sternohyoideus muscle and a small incision in the middle was made to insert the lavage needle outfitted with a 5 mL BD syringe. Approximately 3 mL of sterile phosphate buffered saline (PBS) was slowly injected to fill the lungs and the BAL fluid was withdrawn by gentle aspiration. This procedure was conducted twice so the total yield of BAL was between 4-5 mL. Then the BAL fluid was stored in a -80℃ freezer prior to analysis. TAC was quantified in BAL fluid according to the following protocol. Briefly, 100 μL of calibrator, control, and unknown samples

were mixed by vortexing with 10 µL of 0.5 µg/mL Ascomycin (ASCO, internal standard) and 200 µL of a solution containing 0.1% formic acid and 10 mM ammonium formate dissolved in 95% HPLC grade methanol for 2 min. After vortexing the samples were transferred to 1.5 ml microfilterfuge tubes and then centrifuged at 15,000 *g* for 1 min at 23^{o}C. Filtrates were transferred to autosampler tubes and 40 µL of the final extracts were injected into the LC/MS/MS (same system used in Section 2.3.11). The ratio of the peak area of TAC to that of the internal standard ASCO (response ratio) for each unknown sample was compared against a linear regression of calibrator response ratios at 0, 1, 2.5, 10, 20, 40 and 160 ng/mL to quantify TAC. The concentration of TAC was expressed as ng/mL in BAL fluid.

G.3 Results

As shown in Fig.G.1, TAC concentrations in the BAL fluid of TFF TACMAN were higher than that of micronized TACMAN. The reason can be attributed to the faster dissolution rate of amorphous TFF TACMAN, compared to crystalline micronized TACMAN [1, 2]. For amorphous TFF TACMAN, the rapidly dissolved TAC molecules immediately became available for absorption into either the lung tissue or the systemic blood circulation. It has been reported by Patton et al. that hydrophobic small molecules can be absorbed into the blood stream extremely fast, approximately 1 to 2 minutes [3]. In this study, once TAC is dissolved in lung lining fluid, the absorption into the lung tissue and blood circulation is pretty fast. For crystalline micronized TACMAN, the slow

dissolving TAC particles acted as a reservoir and continuously released TAC molecules into the lung lining fluid, leading to a higher TAC concentrations in the BAL fluid.

G.4 References

[1] P. Sinswat, K.A. Overhoff, J.T. McConville, K.P. Johnston, R.O. Williams, 3rd, Nebulization of nanoparticulate amorphous or crystalline tacrolimus--single-dose pharmacokinetics study in mice, Eur J Pharm Biopharm, 69 (2008) 1057-1066.

[2] A.B. Watts, J.I. Peters, R.L. Talbert, K.P. O'Donnell, J.J. Coalson, R.O. Williams, 3rd, Preclinical evaluation of tacrolimus colloidal dispersion for inhalation, Eur J Pharm Biopharm, 77 (2011) 207-215.

[3] J.S. Patton, C.S. Fishburn, J.G. Weers, The Lungs as a Portal of Entry for Systemic Drug Delivery, Proc Am Thorac Soc, 1 (2004) 338-344.

Appendix H: Mechanical Testing of TFF Processed Powders by Texture Analyzer using Different Selection of Probes

H.1 Purposes

The objective of this appendix is to select the appropriate probe to carry out mechanical testing for TFF processed powders by texture analyzer.

H.2 Methods

TFF RHOMAN (1% solid concentration) was prepared as described in Section 3.3.2 and used for the test. The mechanical properties of TFF processed powders were evaluated using a Texture Analyzer (TA.XT.plus, Stable micro Systems, Godalming, United Kingdom) equipped with a 5 kg load cell. Three different probes were used in the study, a 1/4 inch sphere probe, a 7 mm flat probe and a 10 mm stainless steel probe. Test was conducted at a speed of 1 mm/s and a maximal immersion into the bulk powders of 20 mm. Compression mode was applied in the test. The probe compressed the bulk powders by proceeding at constant speed and the force needed for the immersion was recorded. The resulting immersion force represents the force requires for breakage of TFF processed powders. At the end of the immersion, the probe returned to its original height.

H.3 Results

As shown in Fig.H.1, when immersed into the 1% TFF RHOMAN at the same depth, the 10 mm flat probe detected greater immersion forces than the 7 mm flat probe and the

1/4 inch sphere probe sensed the smallest immersion forces due to their surface differences when contacting with the bulk powders. Therefore, the 10 mm flat probe is the most sensitive probe and will be used for future mechanical testing of TFF processed powders.

Appendix I: Mechanical Testing of TFF Processed Powders Prepared at Different Freezing Rates by Texture Analyzer

I.1 Purposes

The aim of this study is to evaluate the mechanical properties of TFF processed powders prepared at different freezing rates.

I.2 Methods

As described in Section 3.3.2, a solution of RHO and MAN (1:99 w/w, solid concentration:1% w/v) was rapidly frozen on a on a cryogenically cooled rotating stainless steel surface (−50°C or -140°C). The resulting thin film was removed from the surface by a scraper and maintained in the frozen state in liquid nitrogen. Solvents were sublimated by lyophilization over 48 hours at pressures less than 200mTorr while the shelf temperature was gradually ramped from −40°C to 25°C. For the slow shelf freezing RHOMAN, solution of RHO and MAN was slowly frozen in a freezer (-80°C) and then subject to lyophilization. The mechanical properties of TFF processed powders prepared at different freezing rate were evaluated using a Texture Analyzer equipped with a 5 kg load cell and a 10 mm cylindrical probe. Test was conducted at a speed of 1 mm/s and a maximal immersion into the bulk powders of 10 mm. Compression mode was applied in the test. The probe compressed the bulk powders by proceeding at constant speed and the force needed for the immersion was recorded. The resulting immersion force represents the force requires for breakage of TFF processed powders.

I.3 Results

As illustrated in Fig.I.1, by immersing 10 mm in the bulk powders, none of the formulations exhibited immersion forces greater than 0.01 N. No significant difference in term of positive area under the curve was observed for the three formulations prepared by different freezing processes, indicating that there's no significant difference in term of mechanical properties between formulations prepared by different freezing process.

Appendix J: Theoretical Modeling of the Freezing Rate of Formulations Prepared by Different Freezing Processes

J.1Purposes

The objective this appendix is to calculate the freezing rate of formulations prepared by different freezing processes according to theoretical modeling.

J.2 Methods

Three different freezing processes were applied to a solution of RHO and MAN (1:99, w/w) in water (1%, w/v). TFF process with cryogenic surface temperature at −50°C, -140°C and a slow freezing on the shelf (-40°C) process. Following the freezing process, solvent was sublimated by lyophilization over 48 hours at pressures less than 200mTorr while the shelf temperature was gradually ramped from −40°C to 25°C. Calculation of the freezing rate was based on the theoretical model reported by Overhoff et al. and Engstrom et al. [1, 2].

J.3 Results

The phenomena of droplet spreading and freezing upon impinging with a cryogenic solid substrate have been previously studied [1, 2]. The fact of whether the droplet will first spread or solidify to form thin films upon impact with the cryogenic surface has been described in terms of the Weber number, $We=\rho V^2 D/\gamma$ (inertial to interfacial forces) where ρ is the liquid droplet density; V is the impact velocity; D is the droplet diameter and γ is the droplet interfacial tension in air. For We>30, droplets spread immediately

upon impacting the cryogenic solid substrate and deformed into cylindrical thin films before solidifying; for low We<1, impacting droplets solidified as spherical domes with minimal spreading [3-6]. In this study, water was used as a solvent in the TFF process, γ (air–water) =0.072 N/m; droplets were falling from a height of 10 cm, $V= (2gH)^{1/2}$ =1.414 m/s; ρ=1000 kg/m^3 for water droplets; the volume of the water droplet was determined by dropping 20 droplets into a graduated cylinder to measure the volume (the volume of 20 droplets was about 1.6 mL, thereby the volume of one drop is approximately 0.08 mL) and the diameter $D =2(3Volume/4\pi)^{1/3}$ =0.0053 m. Therefore, the calculated We= 147, which is >30, and means that the water droplets will spread on the surface and deform into cylindrical thin films prior to being frozen. This correlated with the observed formation of thin cylindrical disks.

The diameter of the frozen cylindrical disks were measured across two directions and averaged for 10 droplets. The thickness of the frozen cylindrical disks was then calculated by assuming that a droplet impacting on the cryogenic substrate will deform into a cylindrical disk with the same volume as the original droplet. In this study, no significant difference was observed for the diameter of the frozen cylindrical disks between the two TFF formulations prepared at different freezing temperatures (-50°C and -140°C). The measured diameters for both TFF formulations were 12 mm. It has been reported by Fukai et al. that the diameter of the thin films depends on the Weber number and the surface temperature of the cryogenic substrate, and the diameter increases as the Weber number increases [3]. On a stainless steel surface, for a relatively large Weber number (200-600), higher surface temperature (523 K) results in larger diameters of the

thin films (usually ranging from 4-6 times the original droplet diameter), compared to the diameters (usually ranging from 3-4 times the original droplet diameter) resulting from a lower surface temperature (300 K); For an intermediate Weber number (30-200), the diameter of the resulting thin films typically ranges from 1.5-3 times the original droplet diameter and the surface temperature does not significantly impact the diameter; for a small Weber number (<30), no deformation is expected to occur and the droplets are frozen as spherical domes with minimal spreading [3]. In this study, the Weber number was 147 and the measured diameter of the thin films (12mm) is approximately 2.3 times the original droplet diameter (5.3mm). Therefore, the surface temperature difference did not impact the resulting diameter of the frozen cylindrical disks. The thickness of the frozen disks was calculated to be 176.8 μm for both TFF formulations.

It was previously demonstrated with infrared imaging of cooling thin films that the water droplets' spreading occurred within the first 10 milliseconds upon impact with the cryogenic surface, which is much shorter than the freezing time (hundred to thousand milliseconds) [2]. The cooling rate of the thin films can be predicted with a simplified analytical heat transfer model, which was validated with experimental IR data [1]. Briefly, a few assumptions are made based on the theoretical model. The first assumption is that the spreading of water droplets happens in a very short time scale compared to the freezing time so no heat transfer occurs during the spreading process. The second assumption is that since the thickness of the thin films was relatively small (176.8 μm) compared to its large diameter (12mm), heat transfer only occurs in the z-direction and the heat transfer paralleled to the surface is negligible. The last assumption is that the

thermal diffusivity, $\alpha=k/\rho\times C_p$ (where k is the thermal conductivity, ρ is the density, and C_p is the heat capacity) is constant over the entire temperature range and stays unchanged during the freezing process. For the case of freezing water the density and thermal properties were determined from the DIPPR database (Brigham Young University, Provo, UT) at the initial temperatures of 298 and 273K for water and ice, respectively (Table J.1). The average thermal diffusivity of water and ice was used for the mathematical model. Two boundary conditions were fit into the model, the air is acted as an insulator so the heat transfer from the top surface of the thin film to the exposed air is negligible; the cryogenic surface temperature remains constant so there is no heat transfer resistance between the cryogenic substrate and the water droplets. Therefore, a one-dimensional heat transfer for a finite slab according to the two boundary conditions above is described by the following equation:

$$T(x,t) = T_{cryo} + \frac{2}{L}\sum_{n=0}^{\infty} e^{-\alpha(2n+1)^2\pi^2 t/4L^2} \times \cos\frac{(2n+1)\pi x}{2L}\left\{\frac{2L(-1)^{n+1}T_{cryo}}{(2n+1)\pi} + \int_0^L T_i \frac{\cos(2n+1)\pi x'}{2L}\,dx'\right\}$$

where x is the distance from the top of the spread droplet, T(x,t) is the temperature in the film reaching distance x and at time t, T_{cryo} is the temperature of the cryogenic substrate in contact with the bottom thin film surface, and L is the film thickness [7]. Then the cooling time (ms) was calculated by determining the time t, it takes for the top surface of the thin film at x=0 with thickness L to reach a given temperature T (freezing

point of water, 273.15K). The cooling rate (K/s) was determined by dividing the temperature change at the top surface of the thin film (from room temperature to freezing point of water) by the cooling time. As shown in Table 1, the calculated cooling time for TFF process at -140°C and -50°C were 106ms (cooling rate 2.36×10^{2} K/s) and 148ms (cooling rate 1.69×10^{2} K/s), respectively. For the sample frozen directly on the tray of the lyophilizer, the observed cooling time was more than 10^{6}ms with a very slow cooling rate ($<2.5\times10^{-5}$ K/s).

J.4 References

[1] K.A. Overhoff, J.D. Engstrom, B. Chen, B.D. Scherzer, T.E. Milner, K.P. Johnston, R.O. Williams, 3rd, Novel ultra-rapid freezing particle engineering process for enhancement of dissolution rates of poorly water-soluble drugs, Eur J Pharm Biopharm, 65 (2007) 57-67.

[2] J.D. Engstrom, E.S. Lai, B.S. Ludher, B. Chen, T.E. Milner, R.O. Williams, 3rd, G.B. Kitto, K.P. Johnston, Formation of stable submicron protein particles by thin film freezing, Pharm Res, 25 (2008) 1334-1346.

[3] J. Fukai, T. Ozaki, H. Asami, M. O., Numerical simulation of liquid droplet solidification on substrates., J. Chem. Eng. Jpn., 33 (2000) 630-637.

[4] M. Pasandideh-Fard, S. Chandra, J. Mostaghimi, A three-dimensional model of droplet impact and solidification., Int. J. Heat Mass Transfer, 45 (2002) 2229–2242.

[5] D. Sivakumar, H. Nishiyama, Numerical analysis on the impact behavior of molten metal droplets using a modified splat-quench solidification model., J. Heat Transf.-Trans. ASME, 126 (2004) 1014-1022.

[6] B. Kang, Z. Zhao, D. Poulikakos, Solidification of liquid metal droplets impacting sequentially on a solid surface., J. Heat Transfer, 116 (1994) 436-445.

[7] H.S. Carslaw, J.C. Jaeger, Conduction of heat in solids, 2d ed., Clarendon Press, Oxford,, 1973.

Bibliography

Aalbers, R., Ayres, J., Backer, V., Decramer, M., Lier, P.A., Magyar, P., Malolepszy, J., Ruffin, R., Sybrecht, G.W., 2002. Formoterol in patients with chronic obstructive pulmonary disease: a randomized, controlled, 3-month trial. Eur Respir J 19, 936-943.

Accurso, F.J., 2006. Update in cystic fibrosis 2005. Am J Respir Crit Care Med 173, 944-947.

Aikawa, T., Shimura, S., Sasaki, H., Takishima, T., Yaegashi, H., Takahashi, T., 1989. Morphometric analysis of intraluminal mucus in airways in chronic obstructive pulmonary disease. Am Rev Respir Dis 140, 477-482.

Alexander, D.J., Collins, C.J., Coombs, D.W., Gilkison, I.S., Hardy, C.J., Healey, G., Karantabias, G., Johnson, N., Karlsson, A., Kilgour, J.D., McDonald, P., 2008. Association of Inhalation Toxicologists (AIT) working party recommendation for standard delivered dose calculation and expression in non-clinical aerosol inhalation toxicology studies with pharmaceuticals. Inhalation toxicology 20, 1179-1189.

Alexis, N.E., Soukup, J., Nierkens, S., Becker, S., 2001. Association between airway hyperreactivity and bronchial macrophage dysfunction in individuals with mild asthma. Am J Physiol Lung Cell Mol Physiol 280, L369-375.

Anderson, P.J., Blanchard, J.D., Brain, J.D., Feldman, H.A., McNamara, J.J., Heyder, J., 1989. Effect of cystic fibrosis on inhaled aerosol boluses. Am Rev Respir Dis 140, 1317-1324.

Anderson, P.J., Gann, L.P., Walls, R.C., Tennal, K.B., Hiller, F.C., 1994. Utility of aerosol bolus behavior as a diagnostic index of asthma during bronchoprovocation. Am. J. Respir. Crit. Care Med. 149, A1047.

Anderson, P.J., Wilson, J.D., Hiller, F.C., 1990. Respiratory tract deposition of ultrafine particles in subjects with obstructive or restrictive lung disease. Chest 97, 1115-1120.

Annapragada, A., Mishchiy, N., 2007. In silico modeling of aerosol deposition in lungs. Drug Discovery Today: Disease Models. Respiratory diseases 4, 155-161.

Antunes, M.B., Cohen, N.A., 2007. Mucociliary clearance--a critical upper airway host defense mechanism and methods of assessment. Current opinion in allergy and clinical immunology 7, 5-10.

Apiou-Sbirlea, G., Katz, I.M., Martonen, T.B., 2010. The effects of simulated airway diseases and affected flow distributions on aerosol deposition. Respir Care 55, 707-718.

Ari, A., Restrepo, R.D., American Association for Respiratory, C., 2012. Aerosol delivery device selection for spontaneously breathing patients: 2012. Respir Care 57, 613-626.

Armengot, M., Escribano, A., Carda, C., Sanchez, C., Romero, C., Basterra, J., 1997. Nasal mucociliary transport and ciliary ultrastructure in cystic fibrosis. A comparative study with healthy volunteers. Int J Pediatr Otorhinolaryngol 40, 27-34.

Bailey, M.M., Berkland, C.J., 2009. Nanoparticle formulations in pulmonary drug delivery. Medicinal research reviews 29, 196-212.

Baker, S.E., Hockman, R.H., 2005. Inhaled iloprost in pulmonary arterial hypertension. Ann Pharmacother 39, 1265-1274.

Ball, D.J., Hirst, P.H., Newman, S.P., Sonet, B., Streel, B., Vanderbist, F., 2002. Deposition and pharmacokinetics of budesonide from the Miat Monodose inhaler, a simple dry powder device. Int J Pharm 245, 123-132.

Bateman, J.R., Pavia, D., Sheahan, N.F., Agnew, J.E., Clarke, S.W., 1983. Impaired tracheobronchial clearance in patients with mild stable asthma. Thorax 38, 463-467.

Bayram, H., Rusznak, C., Khair, O.A., Sapsford, R.J., Abdelaziz, M.M., 2002. Effect of ozone and nitrogen dioxide on the permeability of bronchial epithelial cell cultures of non-asthmatic and asthmatic subjects. Clinical and experimental allergy : journal of the British Society for Allergy and Clinical Immunology 32, 1285-1292.

Behr, J., Zimmermann, G., Baumgartner, R., Leuchte, H., Neurohr, C., Brand, P., Herpich, C., Sommerer, K., Seitz, J., Menges, G., Tillmanns, S., Keller, M., Munich Lung Transplant, G., 2009. Lung deposition of a liposomal cyclosporine A inhalation solution in patients after lung transplantation. Journal of aerosol medicine and pulmonary drug delivery 22, 121-130.

Bennett, W.D., 2002. Effect of beta-adrenergic agonists on mucociliary clearance. J Allergy Clin Immunol 110, S291-297.

Berenson, C.S., Garlipp, M.A., Grove, L.J., Maloney, J., Sethi, S., 2006. Impaired phagocytosis of nontypeable Haemophilus influenzae by human alveolar

macrophages in chronic obstructive pulmonary disease. J Infect Dis 194, 1375-1384.

Bhaskar, K.R., O'Sullivan, D.D., Opaskar-Hincman, H., Reid, L.M., Coles, S.J., 1986. Density gradient analysis of secretions produced in vitro by human and canine airway mucosa: identification of lipids and proteoglycans in such secretions. Exp Lung Res 10, 401-422.

Boehler, A., Estenne, M., 2000. Obliterative bronchiolitis after lung transplantation. Curr Opin Pulm Med 6, 133-139.

Bondesson, E., Bengtsson, T., Nilsson, L.E., Wollmer, P., 2007. Site of deposition and absorption of an inhaled hydrophilic solute. Br J Clin Pharmacol 63, 722-731.

Boucher, R.C., Stutts, M.J., Knowles, M.R., Cantley, L., Gatzy, J.T., 1986. Na+ transport in cystic fibrosis respiratory epithelia. Abnormal basal rate and response to adenylate cyclase activation. J Clin Invest 78, 1245-1252.

Brain, J.D., Sweeney, T.D., Tryka, A.F., Skornik, W.A., Godleski, J.J., 1984. Effects of pulmonary fibrosis on aerosol deposition in hamsters. J Aerosol Sci. 15, 217-218.

Brand, P., Friemel, I., Meyer, T., Schulz, H., Heyder, J., Haubetainger, K., 2000. Total deposition of therapeutic particles during spontaneous and controlled inhalations. J Pharm Sci 89, 724-731.

Brennan, S., Sly, P.D., Gangell, C.L., Sturges, N., Winfield, K., Wikstrom, M., Gard, S., Upham, J.W., Arest, C.F., 2009. Alveolar macrophages and CC chemokines are increased in children with cystic fibrosis. Eur Respir J 34, 655-661.

Brown, J.S., Zeman, K.L., Bennett, W.D., 2001. Regional deposition of coarse particles and ventilation distribution in healthy subjects and patients with cystic fibrosis. J Aerosol Med 14, 443-454.

Brown, J.S., Zeman, K.L., Bennett, W.D., 2002. Ultrafine particle deposition and clearance in the healthy and obstructed lung. Am J Respir Crit Care Med 166, 1240-1247.

Bruewer, M., Luegering, A., Kucharzik, T., Parkos, C.A., Madara, J.L., Hopkins, A.M., Nusrat, A., 2003. Proinflammatory cytokines disrupt epithelial barrier function by apoptosis-independent mechanisms. J Immunol 171, 6164-6172.

Burke, J.M., Zufall, M.J., Ozkaynak, H., 2001. A population exposure model for particulate matter: case study results for PM(2.5) in Philadelphia, PA. Journal of exposure analysis and environmental epidemiology 11, 470-489.

Byron, P.R., 1986. Prediction of drug residence times in regions of the human respiratory tract following aerosol inhalation. J Pharm Sci 75, 433-438.

Camner, P., Jarstrand, C., Philipson, K., 1973a. Tracheobronchial clearance in patients with influenza. Am Rev Respir Dis 108, 131-135.

Camner, P., Mossberg, B., Philipson, K., 1973b. Tracheobronchial clearance and chronic obstructive lung disease. Scandinavian journal of respiratory diseases 54, 272-281.

Carslaw, H.S., Jaeger, J.C., 1973. Conduction of heat in solids, 2d ed. Clarendon Press, Oxford,.

Chambers, C.E., Corrigan, B., Newhouse, M.T., 1999. Salmeterol speeds mucociliary transport in healthy subjects. Am J Respir Crit Care Med 159, A636.

Champion, J.A., Mitragotri, S., 2006. Role of target geometry in phagocytosis. Proc Natl Acad Sci U S A 103, 4930-4934.

Chiou, H., Li, L., Hu, T., Chan, H.K., Chen, J.F., Yun, J., 2007. Production of salbutamol sulfate for inhalation by high-gravity controlled antisolvent precipitation. Int J Pharm 331, 93-98.

Chougule, M., Padhi, B., Misra, A., 2007a. Nano-liposomal dry powder inhaler of tacrolimus: preparation, characterization, and pulmonary pharmacokinetics. International journal of nanomedicine 2, 675-688.

Chougule, M.B., Padhi, B.K., Jinturkar, K.A., Misra, A., 2007b. Development of dry powder inhalers. Recent patents on drug delivery & formulation 1, 11-21.

Chow, A.H., Tong, H.H., Chattopadhyay, P., Shekunov, B.Y., 2007. Particle engineering for pulmonary drug delivery. Pharm Res 24, 411-437.

Christie, J.D., Edwards, L.B., Aurora, P., Dobbels, F., Kirk, R., Rahmel, A.O., Taylor, D.O., Kucheryavaya, A.Y., Hertz, M.I., 2008. Registry of the International Society for Heart and Lung Transplantation: twenty-fifth official adult lung and heart/lung transplantation report--2008. J Heart Lung Transplant 27, 957-969.

Clark, A., Kuo, M.C., Newman, S., Hirst, P., Pitcairn, G., Pickford, M., 2008. A comparison of the pulmonary bioavailability of powder and liquid aerosol formulations of salmon calcitonin. Pharm Res 25, 1583-1590.

Claus, S., Weiler, C., Schiewe, J., Friess, W., 2013. Optimization of the fine particle fraction of a lyophilized lysozyme formulation for dry powder inhalation. Pharm Res 30, 1698-1713.

Cloutier, M.M., Guernsey, L., Wu, C.A., Thrall, R.S., 2004. Electrophysiological properties of the airway: epithelium in the murine, ovalbumin model of allergic airway disease. Am J Pathol 164, 1849-1856.

Conway, J., Fleming, J., Bennett, M., Havelock, T., 2013. The co-imaging of gamma camera measurements of aerosol deposition and respiratory anatomy. Journal of aerosol medicine and pulmonary drug delivery 26, 123-130.

Corcoran, T.E., 2006. Inhaled delivery of aerosolized cyclosporine. Adv Drug Deliv Rev 58, 1119-1127.

Coyne, C.B., Vanhook, M.K., Gambling, T.M., Carson, J.L., Boucher, R.C., Johnson, L.G., 2002. Regulation of airway tight junctions by proinflammatory cytokines. Molecular biology of the cell 13, 3218-3234.

Crampton, M., Kinnersley, R., Ayres, J., 2004. Sub-micrometer particle production by pressurized metered dose inhalers. J Aerosol Med 17, 33-42.

Crandall, E.D., Matthay, M.A., 2001. Alveolar epithelial transport. Basic science to clinical medicine. Am J Respir Crit Care Med 163, 1021-1029.

Crowder, T.M., Rosati, J.A., Schroeter, J.D., Hickey, A.J., Martonen, T.B., 2002. Fundamental effects of particle morphology on lung delivery: predictions of Stokes' law and the particular relevance to dry powder inhaler formulation and development. Pharm Res 19, 239-245.

Crystal, R.G., 1997. The lung : scientific foundations, 2nd ed. Lippincott-Raven, Philadelphia.

Culpitt, S.V., Rogers, D.F., Shah, P., De Matos, C., Russell, R.E., Donnelly, L.E., Barnes, P.J., 2003. Impaired inhibition by dexamethasone of cytokine release by alveolar macrophages from patients with chronic obstructive pulmonary disease. Am J Respir Crit Care Med 167, 24-31.

Dalby, C., Polanowski, T., Larsson, T., Borgstrom, L., Edsbacker, S., Harrison, T.W., 2009. The bioavailability and airway clearance of the steroid component of budesonide/formoterol and salmeterol/fluticasone after inhaled administration in patients with COPD and healthy subjects: a randomized controlled trial. Respir Res 10, 104.

Davies, J.R., Hovenberg, H.W., Linden, C.J., Howard, R., Richardson, P.S., Sheehan, J.K., Carlstedt, I., 1996. Mucins in airway secretions from healthy and chronic bronchitic subjects. Biochem J 313 (Pt 2), 431-439.

Daviskas, E., Anderson, S.D., Eberl, S., Chan, H.K., Bautovich, G., 1999. Inhalation of dry powder mannitol improves clearance of mucus in patients with bronchiectasis. Am J Respir Crit Care Med 159, 1843-1848.

Daviskas, E., Anderson, S.D., Eberl, S., Chan, H.K., Young, I.H., 2001. The 24-h effect of mannitol on the clearance of mucus in patients with bronchiectasis. Chest 119, 414-421.

Daviskas, E., Anderson, S.D., Shaw, J., Eberl, S., Seale, J.P., Yang, I.A., Young, I.H., 2005. Mucociliary clearance in patients with chronic asthma: effects of beta agonists. Respirology 10, 426-435.

Dawson, M., Wirtz, D., Hanes, J., 2003. Enhanced viscoelasticity of human cystic fibrotic sputum correlates with increasing microheterogeneity in particle transport. J Biol Chem 278, 50393-50401.

de Villiers, M.M., 1995. Influence of cohesive properties of micronized drug powders on particle size analysis. J Pharm Biomed Anal 13, 191-198.

Del Donno, M., Bittesnich, D., Chetta, A., Olivieri, D., Lopez-Vidriero, M.T., 2000. The effect of inflammation on mucociliary clearance in asthma: an overview. Chest 118, 1142-1149.

Dellamary, L.A., Tarara, T.E., Smith, D.J., Woelk, C.H., Adractas, A., Costello, M.L., Gill, H., Weers, J.G., 2000. Hollow porous particles in metered dose inhalers. Pharm Res 17, 168-174.

Deng, Z., Xu, S., Li, S., 2008. Understanding a relaxation behavior in a nanoparticle suspension for drug delivery applications. Int J Pharm 351, 236-243.

Deuse, T., Blankenberg, F., Haddad, M., Reichenspurner, H., Phillips, N., Robbins, R.C., Schrepfer, S., 2010. Mechanisms behind local immunosuppression using inhaled tacrolimus in preclinical models of lung transplantation. Am J Respir Cell Mol Biol 43, 403-412.

Devalia, J.L., Sapsford, R.J., Rusznak, C., Toumbis, M.J., Davies, R.J., 1992. The effects of salmeterol and salbutamol on ciliary beat frequency of cultured human bronchial epithelial cells, in vitro. Pulmonary pharmacology 5, 257-263.

Diderichsen, P.M., Cox, E., Martin, S.W., Cleton, A., Ribbing, J., 2013. Characterizing systemic exposure of inhaled drugs: application to the long-acting beta2-agonist PF-00610355. Clin Pharmacokinet 52, 443-452.

Dixit, S., Khanna, S.K., Das, M., 2011. A simple method for simultaneous determination of basic dyes encountered in food preparations by reversed-phase HPLC. J AOAC Int 94, 1874-1881.

Duchateau, G.S., Zuidema, J., Merkus, F.W., 1986. The in vitro and in vivo effect of a new non-halogenated corticosteroid - budesonide - aerosol on human ciliary epithelial function. Allergy 41, 260-265.

Duddu, S.P., Sisk, S.A., Walter, Y.H., Tarara, T.E., Trimble, K.R., Clark, A.R., Eldon, M.A., Elton, R.C., Pickford, M., Hirst, P.H., Newman, S.P., Weers, J.G., 2002. Improved lung delivery from a passive dry powder inhaler using an Engineered PulmoSphere powder. Pharm Res 19, 689-695.

Dugas, H.L., Peters, J.I., Williams, R.O., 3rd, 2013. Nebulization of mycophenolate mofetil inhalation suspension in rats: comparison with oral and pulmonary administration of Cellcept(R). Int J Pharm 441, 19-29.

Edwards, D.A., Ben-Jebria, A., Langer, R., 1998a. Recent advances in pulmonary drug delivery using large, porous inhaled particles. J Appl Physiol 85, 379-385.

Edwards, D.A., Ben-Jebria, A., Langer, R., 1998b. Recent advances in pulmonary drug delivery using large, porous inhaled particles. Journal of applied physiology 85, 379-385.

Edwards, D.A., Hanes, J., Caponetti, G., Hrkach, J., Ben-Jebria, A., Eskew, M.L., Mintzes, J., Deaver, D., Lotan, N., Langer, R., 1997. Large porous particles for pulmonary drug delivery. Science 276, 1868-1871.

Effros, R.M., Mason, G.R., 1983. Measurements of pulmonary epithelial permeability in vivo. Am Rev Respir Dis 127, S59-65.

El-Sherbiny, I.M., McGill, S., Smyth, H.D., 2010. Swellable microparticles as carriers for sustained pulmonary drug delivery. J Pharm Sci 99, 2343-2356.

Engstrom, J.D., Lai, E.S., Ludher, B.S., Chen, B., Milner, T.E., Williams, R.O., 3rd, Kitto, G.B., Johnston, K.P., 2008. Formation of stable submicron protein particles by thin film freezing. Pharm Res 25, 1334-1346.

Engstrom, J.D., Tam, J.M., Miller, M.A., Williams, R.O., 3rd, Johnston, K.P., 2009. Templated open flocs of nanorods for enhanced pulmonary delivery with pressurized metered dose inhalers. Pharm Res 26, 101-117.

EPA., U., 2008a. Total Risk Integrated Methodology (TRIM) Air Pollutants Exposure Model Documentation (TRIM.Expo/APEX, Version 4.3). Office of Air Quality

Planning and Standards, Research Triangle Park, NC., p. http://www.epa.gov/ttn/fera/human_apex.html.

EPA., U.S., Exposure Model for Individuals., p. http://www.epa.gov/heasd/products/emi/emi.html.

Evans, S.M., Blyth, D.I., Wong, T., Sanjar, S., West, M.R., 2002. Decreased distribution of lung epithelial junction proteins after intratracheal antigen or lipopolysaccharide challenge: correlation with neutrophil influx and levels of BALF sE-cadherin. Am J Respir Cell Mol Biol 27, 446-454.

Evora, C., Soriano, I., Rogers, R.A., Shakesheff, K.N., Hanes, J., Langer, R., 1998. Relating the phagocytosis of microparticles by alveolar macrophages to surface chemistry: the effect of 1,2-dipalmitoylphosphatidylcholine. J Control Release 51, 143-152.

Falcoz, C., Oliver, R., McDowall, J.E., Ventresca, P., Bye, A., Daley-Yates, P.T., 2000. Bioavailability of orally administered micronised fluticasone propionate. Clin Pharmacokinet 39 Suppl 1, 9-15.

Farkas, A., Balásházy, I., 2007. Simulation of the effect of local obstructions and blockage on airflow and aerosol deposition in central human airways. Aerosol Science 38, 865-884.

Fitzpatrick, A.M., Holguin, F., Teague, W.G., Brown, L.A., 2008. Alveolar macrophage phagocytosis is impaired in children with poorly controlled asthma. J Allergy Clin Immunol 121, 1372-1378, 1378 e1371-1373.

Fleming, J., Conway, J., Majoral, C., Tossici-Bolt, L., Katz, I., Caillibotte, G., Perchet, D., Pichelin, M., Muellinger, B., Martonen, T., Kroneberg, P., Apiou-Sbirlea, G., 2011. The use of combined single photon emission computed tomography and X-ray computed tomography to assess the fate of inhaled aerosol. Journal of aerosol medicine and pulmonary drug delivery 24, 49-60.

Forbes, B., Asgharian, B., Dailey, L.A., Ferguson, D., Gerde, P., Gumbleton, M., Gustavsson, L., Hardy, C., Hassall, D., Jones, R., Lock, R., Maas, J., McGovern, T., Pitcairn, G.R., Somers, G., Wolff, R.K., 2011. Challenges in inhaled product development and opportunities for open innovation. Adv Drug Deliv Rev 63, 69-87.

Foster, W.M., Langenback, E., Bergofsky, E.H., 1980. Measurement of tracheal and bronchial mucus velocities in man: relation to lung clearance. J Appl Physiol 48, 965-971.

Foster, W.M., Langenback, E.G., Bergofsky, E.H., 1982. Lung mucociliary function in man: interdependence of bronchial and tracheal mucus transport velocities with lung clearance in bronchial asthma and healthy subjects. Ann Occup Hyg 26, 227-244.

Foster, W.M., Wagner, E.M., 2001. Bronchial edema alters (99m)Tc-DTPA clearance from the airway surface in sheep. J Appl Physiol 91, 2567-2573.

Frizzell, R.A., Rechkemmer, G., Shoemaker, R.L., 1986. Altered regulation of airway epithelial cell chloride channels in cystic fibrosis. Science 233, 558-560.

Fu, J., Fiegel, J., Krauland, E., Hanes, J., 2002. New polymeric carriers for controlled drug delivery following inhalation or injection. Biomaterials 23, 4425-4433.

Fukai, J., Ozaki, T., Asami, H., O., M., 2000. Numerical simulation of liquid droplet solidification on substrates. J. Chem. Eng. Jpn. 33, 630-637.

Geiser, M., 2010. Update on macrophage clearance of inhaled micro- and nanoparticles. Journal of aerosol medicine and pulmonary drug delivery 23, 207-217.

Geiser, M., Kreyling, W.G., 2010. Deposition and biokinetics of inhaled nanoparticles. Part Fibre Toxicol 7, 2.

Geller, D.E., Flume, P.A., Griffith, D.C., Morgan, E., White, D., Loutit, J.S., Dudley, M.N., 2011. Pharmacokinetics and safety of MP-376 (levofloxacin inhalation solution) in cystic fibrosis subjects. Antimicrob Agents Chemother 55, 2636-2640.

Gerrity, T.R., Garrard, C.S., Yeates, D.B., 1983. A mathematical model of particle retention in the air-spaces of human lungs. Br J Ind Med 40, 121-130.

Gill, K.K., Nazzal, S., Kaddoumi, A., 2011. Paclitaxel loaded PEG(5000)-DSPE micelles as pulmonary delivery platform: formulation characterization, tissue distribution, plasma pharmacokinetics, and toxicological evaluation. Eur J Pharm Biopharm 79, 276-284.

GINA, 2012. Global Strategy for Asthma Management and Prevention. [Global Initiative for Asthma (GINA) web site]. Available at: http://www.ginasthma.org/.

GOLD, 2012. Global Strategy for the Diagnosis, Management and Prevention of COPD. [Global Initiative for Chronic Obstructive Lung Disease (GOLD) web site]. Available at: http://www.goldcopd.org/.

Gombás, A., Szabó-Révész, P., Kata, M., G., R.J., Erõs, I., 2002. QUANTITATIVE DETERMINATION OF CRYSTALLINITY OF a-LACTOSE

MONOHYDRATE BY DSC. Journal of Thermal Analysis and Calorimetry 68, 503-510.

Grisedale, L.C., Jamieson, M.J., Belton, P.S., Barker, S.A., Craig, D.Q., 2011. Characterization and quantification of amorphous material in milled and spray-dried salbutamol sulfate: a comparison of thermal, spectroscopic, and water vapor sorption approaches. J Pharm Sci 100, 3114-3129.

Groves, S., Galazka, M., Johnson, B., Corcoran, T., Verceles, A., Britt, E., Todd, N., Griffith, B., Smaldone, G.C., Iacono, A., 2010. Inhaled cyclosporine and pulmonary function in lung transplant recipients. Journal of aerosol medicine and pulmonary drug delivery 23, 31-39.

Gumbleton, M., 2001. Caveolae as potential macromolecule trafficking compartments within alveolar epithelium. Adv Drug Deliv Rev 49, 281-300.

Han, X., Fink, M.P., Delude, R.L., 2003. Proinflammatory cytokines cause NO*-dependent and -independent changes in expression and localization of tight junction proteins in intestinal epithelial cells. Shock 19, 229-237.

Hariharan, S., Peddi, V.R., Munda, R., Demmy, A.M., Schroeder, T.J., Alexander, J.W., First, M.R., 1997. Long-term renal and pancreas function with tacrolimus rescue therapy following kidney/pancreas transplantation. Transplant Proc 29, 652-653.

Hasani, A., Pavia, D., Rotondetto, S., Clarke, S.W., Spiteri, M.A., Agnew, J.E., 1998. Effect of oral antibiotics on lung mucociliary clearance during exacerbation of chronic obstructive pulmonary disease. Respir Med 92, 442-447.

Henry, R.R., Mudaliar, S.R., Howland, W.C., 3rd, Chu, N., Kim, D., An, B., Reinhardt, R.R., 2003. Inhaled insulin using the AERx Insulin Diabetes Management System in healthy and asthmatic subjects. Diabetes Care 26, 764-769.

Heyder, J., Gebhart, J., Rudolf, G., Schiller, C.F., Stahlhofen, W., 1986. Deposition of particles in the human respiratory-tract in the size range 0.005-15 μm. Journal of Aerosol Science 17, 811-825.

Hilden, L.R., Morris, K.R., 2004. Physics of amorphous solids. J Pharm Sci 93, 3-12.

Hodge, S., Hodge, G., Scicchitano, R., Reynolds, P.N., Holmes, M., 2003. Alveolar macrophages from subjects with chronic obstructive pulmonary disease are deficient in their ability to phagocytose apoptotic airway epithelial cells. Immunol Cell Biol 81, 289-296.

Hofmann, W., Ménache, M.G., Martonen, T.B., 1989. Age-dependent lung dosimetry of radon progeny, in: Crapo, J.D., Smolko, E.D., Miller, F.J., Graham, J.A., Hayes,

A.W. (Eds.), Extrapolation of Dosimetric Relationships for Inhaled Particles and Gases. Academic Press, San Diego.

Huynh, M.L., Malcolm, K.C., Kotaru, C., Tilstra, J.A., Westcott, J.Y., Fadok, V.A., Wenzel, S.E., 2005. Defective apoptotic cell phagocytosis attenuates prostaglandin E2 and 15-hydroxyeicosatetraenoic acid in severe asthma alveolar macrophages. Am J Respir Crit Care Med 172, 972-979.

Iacono, A.T., Johnson, B.A., Grgurich, W.F., Youssef, J.G., Corcoran, T.E., Seiler, D.A., Dauber, J.H., Smaldone, G.C., Zeevi, A., Yousem, S.A., Fung, J.J., Burckart, G.J., McCurry, K.R., Griffith, B.P., 2006. A randomized trial of inhaled cyclosporine in lung-transplant recipients. N Engl J Med 354, 141-150.

Ide, N., Nagayasu, T., Matsumoto, K., Tagawa, T., Tanaka, K., Taguchi, T., Sumida, Y., Nakashima, M., 2007. Efficacy and safety of inhaled tacrolimus in rat lung transplantation. J Thorac Cardiovasc Surg 133, 548-553.

Ingu, A., Komatsu, K., Ichimiya, S., Sato, N., Hirayama, Y., Morikawa, M., Abe, T., 2005. Effects of inhaled FK 506 on the suppression of acute rejection after lung transplantation: use of a rat orthotopic lung transplantation model. J Heart Lung Transplant 24, 538-543.

Izutsu, K., Kojima, S., 2002. Excipient crystallinity and its protein-structure-stabilizing effect during freeze-drying. J Pharm Pharmacol 54, 1033-1039.

Izutsu, K., Yoshioka, S., Terao, T., 1994. Effect of mannitol crystallinity on the stabilization of enzymes during freeze-drying. Chem Pharm Bull (Tokyo) 42, 5-8.

Jarstrand, C., Camner, P., Philipson, K., 1974. Mycoplasma pneumoniae and tracheobronchial clearance. Am Rev Respir Dis 110, 415-419.

Kang, B., Zhao, Z., Poulikakos, D., 1994. Solidification of liquid metal droplets impacting sequentially on a solid surface. J. Heat Transfer 116, 436-445.

Kasper, J.C., Friess, W., 2011. The freezing step in lyophilization: physico-chemical fundamentals, freezing methods and consequences on process performance and quality attributes of biopharmaceuticals. Eur J Pharm Biopharm 78, 248-263.

Keenan, R.J., Konishi, H., Kawai, A., Paradis, I.L., Nunley, D.R., Iacono, A.T., Hardesty, R.L., Weyant, R.J., Griffith, B.P., 1995. Clinical trial of tacrolimus versus cyclosporine in lung transplantation. Ann Thorac Surg 60, 580-584; discussion 584-585.

Kelly, H.W., Murphy, S., 1992. Beta-adrenergic agonists for acute, severe asthma. Ann Pharmacother 26, 81-91.

Kim, A.I., Akers, M.J., Nail, S.L., 1998. The physical state of mannitol after freeze-drying: effects of mannitol concentration, freezing rate, and a noncrystallizing cosolute. J Pharm Sci 87, 931-935.

Kim, C.S., Hu, S.C., 2006. Total respiratory tract deposition of fine micrometer-sized particles in healthy adults: empirical equations for sex and breathing pattern. Journal of applied physiology 101, 401-412.

Kim, C.S., Kang, T.C., 1997. Comparative measurement of lung deposition of inhaled fine particles in normal subjects and patients with obstructive airway disease. Am J Respir Crit Care Med 155, 899-905.

Kino, T., Hatanaka, H., Miyata, S., Inamura, N., Nishiyama, M., Yajima, T., Goto, T., Okuhara, M., Kohsaka, M., Aoki, H., et al., 1987. FK-506, a novel immunosuppressant isolated from a Streptomyces. II. Immunosuppressive effect of FK-506 in vitro. J Antibiot (Tokyo) 40, 1256-1265.

Kirch, J., Guenther, M., Doshi, N., Schaefer, U.F., Schneider, M., Mitragotri, S., Lehr, C.M., 2012. Mucociliary clearance of micro- and nanoparticles is independent of size, shape and charge--an ex vivo and in silico approach. J Control Release 159, 128-134.

Knight, D.A., Holgate, S.T., 2003. The airway epithelium: structural and functional properties in health and disease. Respirology 8, 432-446.

Knoop, C., Haverich, A., Fischer, S., 2004. Immunosuppressive therapy after human lung transplantation. Eur Respir J 23, 159-171.

Knoop, C., Thiry, P., Saint-Marcoux, F., Rousseau, A., Marquet, P., Estenne, M., 2005. Tacrolimus pharmacokinetics and dose monitoring after lung transplantation for cystic fibrosis and other conditions. Am J Transplant 5, 1477-1482.

Knowles, M., Gatzy, J., Boucher, R., 1983. Relative ion permeability of normal and cystic fibrosis nasal epithelium. J Clin Invest 71, 1410-1417.

Koblizek, V., Tomsova, M., Cermakova, E., Papousek, P., Pracharova, S., Mandalia, R.A., Ceral, J., Novosad, J., Fila, L., Sedlak, V., Ruta, J., Bartos, V., Salajka, F., Hrnciarik, M., 2011. Impairment of nasal mucociliary clearance in former smokers with stable chronic obstructive pulmonary disease relates to the presence of a chronic bronchitis phenotype. Rhinology 49, 397-406.

Koo, S., Kubiak, D.W., Issa, N.C., Dietzek, A., Boukedes, S., Camp, P.C., Goldberg, H.J., Baden, L.R., Fuhlbrigge, A.L., Marty, F.M., 2012. A targeted peritransplant

antifungal strategy for the prevention of invasive fungal disease after lung transplantation: a sequential cohort analysis. Transplantation 94, 281-286.

Kreyling, W.G., Semmler-Behnke, M., Moller, W., 2006. Ultrafine particle-lung interactions: does size matter? J Aerosol Med 19, 74-83.

Kuehl, P.J., Anderson, T.L., Candelaria, G., Gershman, B., Harlin, K., Hesterman, J.Y., Holmes, T., Hoppin, J., Lackas, C., Norenberg, J.P., Yu, H., McDonald, J.D., 2012. Regional particle size dependent deposition of inhaled aerosols in rats and mice. Inhalation toxicology 24, 27-35.

Kuiper, L., Ruijgrok, E.J., 2009. A review on the clinical use of inhaled amphotericin B. Journal of aerosol medicine and pulmonary drug delivery 22, 213-227.

Lalloo, U.G., Ainslie, G.M., Abdool-Gaffar, M.S., Awotedu, A.A., Feldman, C., Greenblatt, M., Irusen, E.M., Mash, R., Naidoo, S.S., O'Brien, J., Otto, W., Richards, G.A., Wong, M.L., South African Thoracic, S., 2013. Guideline for the management of acute asthma in adults: 2013 update. S Afr Med J 103, 189-198.

Larhrib, H., Martin, G.P., Marriott, C., Prime, D., 2003. The influence of carrier and drug morphology on drug delivery from dry powder formulations. Int J Pharm 257, 283-296.

Latimer, P., Menchaca, M., Snyder, R.M., Yu, W., Gilbert, B.E., Sanders, B.G., Kline, K., 2009. Aerosol delivery of liposomal formulated paclitaxel and vitamin E analog reduces murine mammary tumor burden and metastases. Exp Biol Med (Maywood) 234, 1244-1252.

Lay, J.C., Alexis, N.E., Zeman, K.L., Peden, D.B., Bennett, W.D., 2009. In vivo uptake of inhaled particles by airway phagocytes is enhanced in patients with mild asthma compared with normal volunteers. Thorax 64, 313-320.

Lee, K.C., Chae, S.Y., Kim, T.H., Lee, S., Lee, E.S., Youn, Y.S., 2009a. Intrapulmonary potential of polyethylene glycol-modified glucagon-like peptide-1s as a type 2 anti-diabetic agent. Regul Pept 152, 101-107.

Lee, S.L., Adams, W.P., Li, B.V., Conner, D.P., Chowdhury, B.A., Yu, L.X., 2009b. In vitro considerations to support bioequivalence of locally acting drugs in dry powder inhalers for lung diseases. AAPS J 11, 414-423.

Lehnert, B.E., Morrow, P.E., 1985. Association of 59iron oxide with alveolar macrophages during alveolar clearance. Exp Lung Res 9, 1-16.

Lenney, W., Edenborough, F., Kho, P., Kovarik, J.M., 2011. Lung deposition of inhaled tobramycin with eFlow rapid/LC Plus jet nebuliser in healthy and cystic fibrosis subjects. J Cyst Fibros 10, 9-14.

Lindberg, S., Khan, R., Runer, T., 1995. The effects of formoterol, a long-acting beta 2-adrenoceptor agonist, on mucociliary activity. Eur J Pharmacol 285, 275-280.

Lopez-Vidriero, M.T., Reid, L., 1978. Chemical markers of mucous and serum glycoproteins and their relation to viscosity in mucoid and purulent sputum from various hypersecretory diseases. Am Rev Respir Dis 117, 465-477.

Love, R.G., Muir, D.C., 1976. Aerosol deposition and airway obstruction. Am Rev Respir Dis 114, 891-897.

Mahler, D.A., Donohue, J.F., Barbee, R.A., Goldman, M.D., Gross, N.J., Wisniewski, M.E., Yancey, S.W., Zakes, B.A., Rickard, K.A., Anderson, W.H., 1999. Efficacy of salmeterol xinafoate in the treatment of COPD. Chest 115, 957-965.

Marple, V.A., Olson, B.A., Santhanakrishnan, K., Mitchell, J.P., Murray, S.C., Hudson-Curtis, B.L., 2003. Next generation pharmaceutical impactor (a new impactor for pharmaceutical inhaler testing). Part II: Archival calibration. J Aerosol Med 16, 301-324.

Martonen, T., Fleming, J., Schroeter, J., Conway, J., Hwang, D., 2003. In silico modeling of asthma. Adv Drug Deliv Rev 55, 829-849.

Martonen, T., Katz, I., Cress, W., 1995. Aerosol deposition as a function of airway disease: cystic fibrosis. Pharm Res 12, 96-102.

Martonen, T.B., 1982. Analytical model of hygroscopic particle behavior in human airways. Bull Math Biol 44, 425-442.

Martonen, T.B., Guan, X., 2001a. Effects of tumors on inhaled pharmacologic drugs: I. Flow patterns. Cell biochemistry and biophysics 35, 233-243.

Martonen, T.B., Guan, X., 2001b. Effects of tumors on inhaled pharmacologic drugs: II. Particle motion. Cell biochemistry and biophysics 35, 245-253.

Martonen, T.B., Hofmann, W., 1991. Dosimetry of localised accumulations of cigarette smoke and radon progeny at bifurcations. Radiat Prot Dosim 38, 81.

Martonen, T.B., Hwang, D., Katz, I., Yang, Y., Guan, X., 1997. Cystic fibrosis: treatment with a supercomputer drug delivery model. Advances in Engineering Software 28, 359-364.

Martonen, T.B., Rosati, J.A., Isaacs, K.K., 2013. Modeling Deposition of Inhaled Particles, in: Ruzer, L.S., Harley, N.H. (Eds.), Aerosols handbook measurement, dosimetry, and health effects, 2nd ed. CRC Press,, Boca Raton.

Matsui, H., Grubb, B.R., Tarran, R., Randell, S.H., Gatzy, J.T., Davis, C.W., Boucher, R.C., 1998. Evidence for periciliary liquid layer depletion, not abnormal ion composition, in the pathogenesis of cystic fibrosis airways disease. Cell 95, 1005-1015.

Medicine, S.S.o.C., 1990. High-dose inhaled versus intravenous salbutamol combined with theophylline in severe acute asthma. Swedish Society of Chest Medicine. Eur Respir J 3, 163-170.

Melloni, B., Germouty, J., 1992. [The influence of a new beta agonist: formoterol on mucociliary function]. Revue des maladies respiratoires 9, 503-507.

Mitchell, J.P., 2003. Practices of coating collection surfaces of cascade impactors: a survey of members of the european pharmaceutical aerosol group (EPAG). Drug Deliv Lung 14, 75-78.

Morishita, Y., Hirayama, Y., Miyayasu, K., Tabata, K., Kawamura, A., Ohkubo, Y., Mutoh, S., 2005. FK506 aerosol locally inhibits antigen-induced airway inflammation in Guinea pigs. International archives of allergy and immunology 136, 372-378.

Mortensen, J., Lange, P., Nyboe, J., Groth, S., 1994. Lung mucociliary clearance. European journal of nuclear medicine 21, 953-961.

Moyano, M.A., Simionato, L.D., Pizzorno, M.T., Segall, A.I., 2006. Validation of a liquid chromatographic method for determination of tacrolimus in pharmaceutical dosage forms. J AOAC Int 89, 1547-1551.

Mulligan, C., Beghetti, M., 2012. Inhaled iloprost for the control of acute pulmonary hypertension in children: a systematic review. Pediatr Crit Care Med 13, 472-480.

Newhouse, M.T., Hirst, P.H., Duddu, S.P., Walter, Y.H., Tarara, T.E., Clark, A.R., Weers, J.G., 2003. Inhalation of a dry powder tobramycin PulmoSphere formulation in healthy volunteers. Chest 124, 360-366.

Nielsen, K.G., Skov, M., Klug, B., Ifversen, M., Bisgaard, H., 1997. Flow-dependent effect of formoterol dry-powder inhaled from the Aerolizer. Eur Respir J 10, 2105-2109.

Niven, R.W., 2011. Toward managing chronic rejection after lung transplant: the fate and effects of inhaled cyclosporine in a complex environment. Adv Drug Deliv Rev 63, 88-109.

O'Grady, J.G., Burroughs, A., Hardy, P., Elbourne, D., Truesdale, A., Uk, Republic of Ireland Liver Transplant Study, G., 2002. Tacrolimus versus microemulsified ciclosporin in liver transplantation: the TMC randomised controlled trial. Lancet 360, 1119-1125.

Oberdörster, G., 1988. Lung clearance of inhaled insoluble and soluble particles. J Aerosol Med 1, 289.

Oberdörster, G., 2007. Biokinetics and effects of nanoparticles, in: Simeonova, P.P., Opopol, N., Luster, M.I. (Eds.), Nanotechnology--toxicological issues and environmental safety. Springer, Dordrecht, Netheralnds, pp. 15-51.

Olsson, B., Bondesson, E., Borgstrom, L., 2011. Pulmonary Drug Metabolism, Clearance, and Absorption, in: Smyth, H.D.C., Hickey, A.J. (Eds.), Controlled Pulmonary Drug Delivery, 1. ed. Springer, New York, NY.

Onoue, S., Sato, H., Kawabata, Y., Mizumoto, T., Hashimoto, N., Yamada, S., 2009. In vitro and in vivo characterization on amorphous solid dispersion of cyclosporine A for inhalation therapy. J Control Release 138, 16-23.

Onoue, S., Sato, H., Ogawa, K., Kojo, Y., Aoki, Y., Kawabata, Y., Wada, K., Mizumoto, T., Yamada, S., 2012. Inhalable dry-emulsion formulation of cyclosporine A with improved anti-inflammatory effects in experimental asthma/COPD-model rats. Eur J Pharm Biopharm 80, 54-60.

Overhoff, K.A., Engstrom, J.D., Chen, B., Scherzer, B.D., Milner, T.E., Johnston, K.P., Williams, R.O., 3rd, 2007. Novel ultra-rapid freezing particle engineering process for enhancement of dissolution rates of poorly water-soluble drugs. Eur J Pharm Biopharm 65, 57-67.

Palmer, L.B., Smaldone, G.C., Chen, J.J., Baram, D., Duan, T., Monteforte, M., Varela, M., Tempone, A.K., O'Riordan, T., Daroowalla, F., Richman, P., 2008. Aerosolized antibiotics and ventilator-associated tracheobronchitis in the intensive care unit. Crit Care Med 36, 2008-2013.

Pasandideh-Fard, M., Chandra, S., Mostaghimi, J., 2002. A three-dimensional model of droplet impact and solidification. Int. J. Heat Mass Transfer 45, 2229–2242.

Patton, J.S., Brain, J.D., Davies, L.A., Fiegel, J., Gumbleton, M., Kim, K.J., Sakagami, M., Vanbever, R., Ehrhardt, C., 2010. The particle has landed--characterizing the

fate of inhaled pharmaceuticals. Journal of aerosol medicine and pulmonary drug delivery 23 Suppl 2, S71-87.

Patton, J.S., Bukar, J.G., Eldon, M.A., 2004a. Clinical pharmacokinetics and pharmacodynamics of inhaled insulin. Clin Pharmacokinet 43, 781-801.

Patton, J.S., Byron, P.R., 2007. Inhaling medicines: delivering drugs to the body through the lungs. Nat Rev Drug Discov 6, 67-74.

Patton, J.S., Fishburn, C.S., Weers, J.G., 2004b. The Lungs as a Portal of Entry for Systemic Drug Delivery. Proc Am Thorac Soc 1, 338-344.

Pavia, D., 1984. Lung mucociliary clearance, in: Clarke, S.W., Pavia, D. (Eds.), Aerosols and the lung : clinical and experimental aspects. Butterworths, London ; Boston, p. 275.

Pavia, D., Agnew, J.E., Sutton, P.P., Lopez-Vidriero, M.T., Clay, M.M., Killip, M., Clarke, S.W., 1987. Effect of terbutaline administered from metered dose inhaler (2 mg) and subcutaneously (0.25 mg) on tracheobronchial clearance in mild asthma. British journal of diseases of the chest 81, 361-370.

Pavia, D., Bateman, J.R., Sheahan, N.F., Agnew, J.E., Clarke, S.W., 1985. Tracheobronchial mucociliary clearance in asthma: impairment during remission. Thorax 40, 171-175.

Phipps, R.J., Williams, I.P., Richardson, P.S., Pell, J., Pack, R.J., Wright, N., 1982. Sympathomimetic drugs stimulate the output of secretory glycoproteins from human bronchi in vitro. Clin Sci (Lond) 63, 23-28.

Pilcer, G., Goole, J., Van Gansbeke, B., Blocklet, D., Knoop, C., Vanderbist, F., Amighi, K., 2008. Pharmacoscintigraphic and pharmacokinetic evaluation of tobramycin DPI formulations in cystic fibrosis patients. Eur J Pharm Biopharm 68, 413-421.

Plumley, C., Gorman, E.M., El-Gendy, N., Bybee, C.R., Munson, E.J., Berkland, C., 2009. Nifedipine nanoparticle agglomeration as a dry powder aerosol formulation strategy. Int J Pharm 369, 136-143.

Predescu, S.A., Predescu, D.N., Malik, A.B., 2007. Molecular determinants of endothelial transcytosis and their role in endothelial permeability. Am J Physiol Lung Cell Mol Physiol 293, L823-842.

Prescott, E., Lange, P., Vestbo, J., 1995. Chronic mucus hypersecretion in COPD and death from pulmonary infection. Eur Respir J 8, 1333-1338.

Puchelle, E., Zahm, J.M., Girard, F., Bertrand, A., Polu, J.M., Aug, F., Sadoul, P., 1980. Mucociliary transport in vivo and in vitro. Relations to sputum properties in chronic bronchitis. European journal of respiratory diseases 61, 254-264.

Rasenack, N., Muller, B.W., 2004. Micron-size drug particles: common and novel micronization techniques. Pharm Dev Technol 9, 1-13.

Regnis, J.A., Robinson, M., Bailey, D.L., Cook, P., Hooper, P., Chan, H.K., Gonda, I., Bautovich, G., Bye, P.T., 1994. Mucociliary clearance in patients with cystic fibrosis and in normal subjects. Am J Respir Crit Care Med 150, 66-71.

Richardson, P.C., Boss, A.H., 2007. Technosphere insulin technology. Diabetes Technol Ther 9 Suppl 1, S65-72.

Robinson, M., Eberl, S., Tomlinson, C., Daviskas, E., Regnis, J.A., Bailey, D.L., Torzillo, P.J., Menache, M., Bye, P.T., 2000. Regional mucociliary clearance in patients with cystic fibrosis. J Aerosol Med 13, 73-86.

Rogers, D.F., 2000. Mucus pathophysiology in COPD: differences to asthma, and pharmacotherapy. Monaldi Arch Chest Dis 55, 324-332.

Rogers, D.F., 2005. Mucociliary dysfunction in COPD: effect of current pharmacotherapeutic options. Pulmonary pharmacology & therapeutics 18, 1-8.

Rogueda, P.G., Traini, D., 2007a. The nanoscale in pulmonary delivery. Part 1: deposition, fate, toxicology and effects. Expert Opin Drug Deliv 4, 595-606.

Rogueda, P.G., Traini, D., 2007b. The nanoscale in pulmonary delivery. Part 2: formulation platforms. Expert Opin Drug Deliv 4, 607-620.

Russell, R.E., Culpitt, S.V., DeMatos, C., Donnelly, L., Smith, M., Wiggins, J., Barnes, P.J., 2002. Release and activity of matrix metalloproteinase-9 and tissue inhibitor of metalloproteinase-1 by alveolar macrophages from patients with chronic obstructive pulmonary disease. Am J Respir Cell Mol Biol 26, 602-609.

Sackner, M.A., 1978. Effect of respiratory drugs on mucociliary clearance. Chest 73, 958-966.

Sakagami, M., 2004. Insulin disposition in the lung following oral inhalation in humans : a meta-analysis of its pharmacokinetics. Clin Pharmacokinet 43, 539-552.

Salathe, M., 2002. Effects of beta-agonists on airway epithelial cells. J Allergy Clin Immunol 110, S275-281.

Saleem, I.Y., Smyth, H.D., 2010. Micronization of a soft material: air-jet and micro-ball milling. AAPS PharmSciTech 11, 1642-1649.

Sanchis, J., Dolovich, M., Chalmers, R., Newhouse, M., 1972. Quantitation of regional aerosol clearance in the normal human lung. J Appl Physiol 33, 757-762.

Sanders, N.N., De Smedt, S.C., Van Rompaey, E., Simoens, P., De Baets, F., Demeester, J., 2000. Cystic fibrosis sputum: a barrier to the transport of nanospheres. Am J Respir Crit Care Med 162, 1905-1911.

Sbirlea-Apiou, G., Lemaire, M., Katz, I., Conway, J., Fleming, J., Martonen, T., 2004. Simulation of the regional manifestation of asthma. J Pharm Sci 93, 1205-1216.

Scheuch, G., Heyder, J., 1990. Dynamic Shape Factor of Nonspherical Aerosol Particles in the Diffusion Regime. Aerosol Science and Technology 12, 270-277.

Schmid, O., Moller, W., Semmler-Behnke, M., Ferron, G.A., Karg, E., Lipka, J., Schulz, H., Kreyling, W.G., Stoeger, T., 2009. Dosimetry and toxicology of inhaled ultrafine particles. Biomarkers : biochemical indicators of exposure, response, and susceptibility to chemicals 14 Suppl 1, 67-73.

Schrepfer, S., Deuse, T., Reichenspurner, H., Hoffmann, J., Haddad, M., Fink, J., Fischbein, M.P., Robbins, R.C., Pelletier, M.P., 2007. Effect of inhaled tacrolimus on cellular and humoral rejection to prevent posttransplant obliterative airway disease. Am J Transplant 7, 1733-1742.

Segal, R.A., Martonen, T.B., Kim, C.S., Shearer, M., 2002. Computer simulations of particle deposition in the lungs of chronic obstructive pulmonary disease patients. Inhalation toxicology 14, 705-720.

Sethi, S., 2000. Bacterial infection and the pathogenesis of COPD. Chest 117, 286S-291S.

Shin, S.B., Cho, H.Y., Kim, D.D., Choi, H.G., Lee, Y.B., 2010. Preparation and evaluation of tacrolimus-loaded nanoparticles for lymphatic delivery. Eur J Pharm Biopharm 74, 164-171.

Siekmeier, R., Schiller-Scotland, C.H.F., Gebhart, J., Kronenberger, H., 1990. Pharmacon-induced airway obstruction in healthy subjects: Dose dependent changes of inspired aerosol boluses. J. Aerosol Sci. 21, S423.

Singh, S.D., Whale, C., Houghton, N., Daley-Yates, P., Kirby, S.M., Woodcock, A.A., 2003. Pharmacokinetics and systemic effects of inhaled fluticasone propionate in chronic obstructive pulmonary disease. Br J Clin Pharmacol 55, 375-381.

Sinswat, P., Overhoff, K.A., McConville, J.T., Johnston, K.P., Williams, R.O., 3rd, 2008. Nebulization of nanoparticulate amorphous or crystalline tacrolimus--single-dose pharmacokinetics study in mice. Eur J Pharm Biopharm 69, 1057-1066.

Sivakumar, D., Nishiyama, H., 2004. Numerical analysis on the impact behavior of molten metal droplets using a modified splat-quench solidification model. J. Heat Transf.-Trans. ASME 126, 1014-1022.

Snider, G.L., Faling, L.J., Rennard, S.I., 1994. Chronic bronchitis and emphysema, in: Murray, J.F., Nadel, J.A. (Eds.), Textbook of respiratory medicine, 2nd ed. Saunders, Philadelphia, pp. 1331-1397.

Snipes, M.B., McClellan, R.O., Mauderly, J.L., Wolff, R.K., 1989. Retention patterns for inhaled particles in the lung: comparisons between laboratory animals and humans for chronic exposures. Health Phys 57 Suppl 1, 69-77; discussion 77-68.

Son, Y.J., McConville, J.T., 2008. Advancements in dry powder delivery to the lung. Drug Dev Ind Pharm 34, 948-959.

Stahlhofen, W., Scheuch, G., 1990. [Measuring human mucociliary clearance]. Pneumologie 44 Suppl 1, 422-423.

Stober, W., McClellan, R.O., 1997. Pulmonary retention and clearance of inhaled biopersistent aerosol particles: data-reducing interpolation models and models of physiologically based systems--a review of recent progress and remaining problems. Critical reviews in toxicology 27, 539-598.

Sweeney, T.D., Brain, J.D., A.F., T., Godleski, J.J., 1983. Deposition of particles in hamsters with pulmonary fibrosis. Am Rev Respir Dis 128, 138-143.

Sweeney, T.D., Brain, J.D., Leavitt, S.A., Godleski, J.J., 1987. Emphysema alters the deposition pattern of inhaled particles in hamsters. Am J Pathol 128, 19-28.

Sweeney, T.D., Skornik, W.A., Brain, J.D., Hatch, V., Godleski, J.J., 1995. Chronic bronchitis alters the pattern of aerosol deposition in the lung. Am J Respir Crit Care Med 151, 482-488.

Tabata, Y., Ikada, Y., 1988. Effect of the size and surface charge of polymer microspheres on their phagocytosis by macrophage. Biomaterials 9, 356-362.

Tamaoki, J., Kondo, M., Takizawa, T., 1989. Effect of cAMP on ciliary function in rabbit tracheal epithelial cells. Journal of applied physiology 66, 1035-1039.

Taylor, A.E., Finney-Hayward, T.K., Quint, J.K., Thomas, C.M., Tudhope, S.J., Wedzicha, J.A., Barnes, P.J., Donnelly, L.E., 2010. Defective macrophage phagocytosis of bacteria in COPD. Eur Respir J 35, 1039-1047.

Telang, C., Yu, L., Suryanarayanan, R., 2003. Effective inhibition of mannitol crystallization in frozen solutions by sodium chloride. Pharm Res 20, 660-667.

Thornton, D.J., Carlstedt, I., Howard, M., Devine, P.L., Price, M.R., Sheehan, J.K., 1996. Respiratory mucins: identification of core proteins and glycoforms. Biochem J 316 (Pt 3), 967-975.

Tiruppathi, C., Shimizu, J., Miyawaki-Shimizu, K., Vogel, S.M., Bair, A.M., Minshall, R.D., Predescu, D., Malik, A.B., 2008. Role of NF-kappaB-dependent caveolin-1 expression in the mechanism of increased endothelial permeability induced by lipopolysaccharide. J Biol Chem 283, 4210-4218.

Todoroff, J., Vanbever, R., 2011. Fate of nanomedicines in the lungs. Current Opinion in Colloid & Interface Science 16, 246-254.

Tolman, J.A., Williams, R.O., 3rd, 2010. Advances in the pulmonary delivery of poorly water-soluble drugs: influence of solubilization on pharmacokinetic properties. Drug Dev Ind Pharm 36, 1-30.

Tomashefski Jr., J.F., Abrmowsky, C.R., Dahms, B.B., 1993. The pathology of cystic fibrosis., in: Davis, P.B. (Ed.), Cystic fibrosis. M. Dekker, New York, pp. 435-489.

Toremalm, N.G., 1960. The daily amoung of tracheo-bronchial secretions in man. A method for continuous tracheal aspiration in laryngectomized and tracheotomized patients. Acta oto-laryngologica. Supplementum 158, 43-53.

Travers, A.H., Jones, A.P., Camargo, C.A., Jr., Milan, S.J., Rowe, B.H., 2012. Intravenous beta(2)-agonists versus intravenous aminophylline for acute asthma. Cochrane Database Syst Rev 12, CD010256.

Tsapis, N., Bennett, D., Jackson, B., Weitz, D.A., Edwards, D.A., 2002. Trojan particles: large porous carriers of nanoparticles for drug delivery. Proc Natl Acad Sci U S A 99, 12001-12005.

Ungaro, F., d'Angelo, I., Miro, A., La Rotonda, M.I., Quaglia, F., 2012. Engineered PLGA nano- and micro-carriers for pulmonary delivery: challenges and promises. J Pharm Pharmacol 64, 1217-1235.

Vanbever, R., Mintzes, J.D., Wang, J., Nice, J., Chen, D., Batycky, R., Langer, R., Edwards, D.A., 1999. Formulation and physical characterization of large porous particles for inhalation. Pharm Res 16, 1735-1742.

Vandivier, R.W., Fadok, V.A., Hoffmann, P.R., Bratton, D.L., Penvari, C., Brown, K.K., Brain, J.D., Accurso, F.J., Henson, P.M., 2002. Elastase-mediated phosphatidylserine receptor cleavage impairs apoptotic cell clearance in cystic fibrosis and bronchiectasis. J Clin Invest 109, 661-670.

Velaga, S.P., Berger, R., Carlfors, J., 2002. Supercritical fluids crystallization of budesonide and flunisolide. Pharm Res 19, 1564-1571.

Venkataramanan, R., Shaw, L.M., Sarkozi, L., Mullins, R., Pirsch, J., MacFarlane, G., Scheller, D., Ersfeld, D., Frick, M., Fitzsimmons, W.E., Virji, M., Jain, A., Brayman, K.L., Shaked, A., 2001. Clinical utility of monitoring tacrolimus blood concentrations in liver transplant patients. J Clin Pharmacol 41, 542-551.

Videira, M.A., Botelho, M.F., Santos, A.C., Gouveia, L.F., de Lima, J.J., Almeida, A.J., 2002. Lymphatic uptake of pulmonary delivered radiolabelled solid lipid nanoparticles. Journal of drug targeting 10, 607-613.

Wagner, K., Webber, S.A., Kurland, G., Boyle, G.J., Miller, S.A., Cipriani, L., Griffith, B.P., Fricker, F.J., 1997. New-onset diabetes mellitus in pediatric thoracic organ recipients receiving tacrolimus-based immunosuppression. J Heart Lung Transplant 16, 275-282.

Wang, T., Noonberg, S., Steigerwalt, R., Lynch, M., Kovelesky, R.A., Rodriguez, C.A., Sprugel, K., Turner, N., 2007. Preclinical safety evaluation of inhaled cyclosporine in propylene glycol. J Aerosol Med 20, 417-428.

Wanner, A., 1985. Effects of methylxanthines on airway mucociliary function. Am J Med 79, 16-21.

Watts, A.B., Cline, A.M., Saad, A.R., Johnson, S.B., Peters, J.I., Williams, R.O., 3rd, 2010. Characterization and pharmacokinetic analysis of tacrolimus dispersion for nebulization in a lung transplanted rodent model. Int J Pharm 384, 46-52.

Watts, A.B., Peters, J.I., Talbert, R.L., O'Donnell, K.P., Coalson, J.J., Williams, R.O., 3rd, 2011. Preclinical evaluation of tacrolimus colloidal dispersion for inhalation. Eur J Pharm Biopharm 77, 207-215.

Watts, A.B., Wang, Y.B., Johnston, K.P., Williams, R.O., 3rd, 2013. Respirable low-density microparticles formed in situ from aerosolized brittle matrices. Pharm Res 30, 813-825.

Weber, B., Hochhaus, G., 2013. A pharmacokinetic simulation tool for inhaled corticosteroids. AAPS J 15, 159-171.

Weibel, E.R., 1963. Morphometry of the human lung. Academic Press, New York,.

West, J.B., 2007. Nomal Physiology: Exercise, Pulmonary physiology and pathophysiology : an integrated, case-based approach, 2nd ed. Wolters Kluwer Health/Lippincott Williams & Wilkins, Philadelphia, pp. vii, 150 p.

West, J.B., 2012. Pulmonary pathophysiology : the essentials, 8th ed. Wolters Kluwer/Lippincott Williams & Wilkins Health, Philadelphia.

Wies, S., Geyer, A., Eysel, W., 1992. The limit of detection in differential scanning calorimetry. J Therm Anal 38, 277-287.

Wine, J.J., 1999. The genesis of cystic fibrosis lung disease. J Clin Invest 103, 309-312.

Wittgen, B.P., Kunst, P.W., van der Born, K., van Wijk, A.W., Perkins, W., Pilkiewicz, F.G., Perez-Soler, R., Nicholson, S., Peters, G.J., Postmus, P.E., 2007. Phase I study of aerosolized SLIT cisplatin in the treatment of patients with carcinoma of the lung. Clin Cancer Res 13, 2414-2421.

Wolff, R.K., Dorato, M.A., 1993. Toxicologic testing of inhaled pharmaceutical aerosols. Critical reviews in toxicology 23, 343-369.

Yang, J.Z., Young, A.L., Chiang, P.C., Thurston, A., Pretzer, D.K., 2008a. Fluticasone and budesonide nanosuspensions for pulmonary delivery: preparation, characterization, and pharmacokinetic studies. J Pharm Sci 97, 4869-4878.

Yang, W., Johnston, K.P., Williams, R.O., 3rd, 2010. Comparison of bioavailability of amorphous versus crystalline itraconazole nanoparticles via pulmonary administration in rats. Eur J Pharm Biopharm 75, 33-41.

Yang, W., Peters, J.I., Williams, R.O., 3rd, 2008b. Inhaled nanoparticles--a current review. Int J Pharm 356, 239-247.

Yeates, D.B., Gerrity, T.R., Garrard, C.S., 1981. Particle deposition and clearance in the bronchial tree. Ann Biomed Eng 9, 577-592.

Yeates, D.B., Spektor, D.M., Pitt, B.R., 1986. Effect of orally administered orciprenaline on tracheobronchial mucociliary clearance. European journal of respiratory diseases 69, 100-108.

Yusen, R.D., Christie, J.D., Edwards, L.B., Kucheryavaya, A.Y., Benden, C., Dipchand, A.I., Dobbels, F., Kirk, R., Lund, L.H., Rahmel, A.O., Stehlik, J., International

Society for, H., Lung, T., 2013. The registry of the international society for heart and lung transplantation: thirtieth adult lung and heart-lung transplant report-2013; focus theme: age. J Heart Lung Transplant 32, 965-978.

Zhang, J., Wu, L., Chan, H.K., Watanabe, W., 2011. Formation, characterization, and fate of inhaled drug nanoparticles. Adv Drug Deliv Rev 63, 441-455.

Zhang, Y., Gilbertson, K., Finlay, W.H., 2007. In vivo-in vitro comparison of deposition in three mouth-throat models with Qvar and Turbuhaler inhalers. J Aerosol Med 20, 227-235.

Zhao, M., Barker, S.A., Belton, P.S., McGregor, C., Craig, D.Q., 2012. Development of fully amorphous dispersions of a low T(g) drug via co-spray drying with hydrophilic polymers. Eur J Pharm Biopharm 82, 572-579.

Zidan, A.S., Rahman, Z., Sayeed, V., Raw, A., Yu, L., Khan, M.A., 2012. Crystallinity evaluation of tacrolimus solid dispersions by chemometric analysis. Int J Pharm 423, 341-350.

Vita

Yi-Bo Wang was born in Tieling, Liaoning province, P.R. China. After he graduated from Liaohe Youtian No. 1 High School in China in 2002, he began his undergraduate education at Peking University Health Science Center, Beijing, China. He received the degree of Bachelor of Science (Pharmacy) in July 2006. He then continued his graduate study in Peking University Health Science Center, and obtained his Master of Science (Pharmaceutics) degree under Dr. Qiang Zhang's supervision in 2008. After graduation, he worked as a quality control internship for 6 months in Beijing Asia East Bio-pharmaceutical Co., Ltd., Beijing, China. In September 2009, he was admitted into the Graduate School in the College of Pharmacy at The University of Texas at Austin to pursue his Ph.D. under the supervision of Dr. Robert O. Williams. During Yi-Bo's graduate career he has presented his research at several scientific conferences in U.S. All the chapters presented in this dissertation have already been submitted for publication in several high impact pharmaceutical journals.

Email: yibo.wang@utexas.edu

This dissertation was typed by Yi-Bo Wang.